

**OPTIMIZATION OF A CO<sub>2</sub> FLOOD DESIGN**

**WASSON FIELD - WEST TEXAS**

A Thesis

by

MARYLENA GARCIA QUIJADA

Submitted to the Office of Graduate Studies of  
Texas A&M University  
in partial fulfillment of the requirements for the degree of

MASTER OF SCIENCE

August 2005

Major Subject: Petroleum Engineering

**OPTIMIZATION OF A CO<sub>2</sub> FLOOD DESIGN**

**WASSON FIELD - WEST TEXAS**

A Thesis

by

MARYLENA GARCIA QUIJADA

Submitted to the Office of Graduate Studies of  
Texas A&M University  
in partial fulfillment of the requirements for the degree of

MASTER OF SCIENCE

Approved by:

Chair of Committee, David Schechter

Committee Members, Walter B. Ayers

Wayne M. Ahr

Head of Department, Stephen A. Holditch

August 2005

Major Subject: Petroleum Engineering

## ABSTRACT

Optimization of a CO<sub>2</sub> Flood Design Wasson Field - West Texas. (August 2005)

Marylena Garcia Quijada, B.S., Universidad de Oriente

Chair of Advisory Committee: Dr. David Schechter

The Denver Unit of Wasson Field, located in Gaines and Yoakum Counties in west Texas, produces oil from the San Andres dolomite at a depth of 5,000 ft. Wasson Field is part of the Permian Basin and is one of the largest petroleum-producing basins in the United States.

This research used a modeling approach to optimize the existing carbon dioxide (CO<sub>2</sub>) flood in section 48 of the Denver Unit by improving the oil sweep efficiency of miscible CO<sub>2</sub> floods and enhancing the conformance control.

A full compositional simulation model using a detailed geologic characterization was built to optimize the injection pattern of section 48 of Denver Unit. The model is a quarter of an inverted nine-spot and covers 20 acres in San Andres Formation of Wasson Field. The Peng-Robinson equation of state (EOS) was chosen to describe the phase behavior during the CO<sub>2</sub> flooding. An existing geologic description was used to construct the simulation grid. Simulation layers represent actual flow units and resemble the large variation of reservoir properties. A 34-year history match was performed to validate the model. Several sensitivity runs were made to improve the CO<sub>2</sub> sweep efficiency and increase the oil recovery.

During this study I found that the optimum CO<sub>2</sub> injection rate for San Andres Formation in the section 48 of the Denver Unit is approximately 300 res bbl (762 Mscf/D) of carbon dioxide. Simulation results also indicate that a water-alternating-gas (WAG) ratio of 1:1 along with an ultimate CO<sub>2</sub> slug of 100% hydrocarbon pore volume (HCPV) will

allow an incremental oil recovery of 18%. The additional recovery increases to 34% if a polymer is injected as a conformance control agent during the course of the WAG process at a ratio of 1:1. According to the results, a pattern reconfiguration change from the typical Denver Unit inverted nine spot to staggered line drive would represent an incremental oil recovery of 26%.

## **DEDICATION**

First to God for so many blessings.

To my beloved husband Sergio, for all his love and encouragement.

To my parents, Juan and Milena, for their unconditional love, caring and support.

## ACKNOWLEDGEMENTS

Reflecting upon my graduate career, I recognize a great faculty and friends deserving of my gratitude. They have provided me extraordinary guidance and support. This work is a reflection of their efforts as much as my own.

I would like to express my sincere gratitude to Dr. David S. Schechter for accepting me in his research group and assisting and supporting this research. His knowledge, support, and friendship have made my work possible and enjoyable.

My appreciation also goes to Dr. Walter Ayers and Dr. Wayne Ahr, my committee members, who were always willing to help me. With their guidance and assistance, I gained a lot of useful geologic knowledge.

I would like to extend my appreciation to Dr. Erwinsyah Putra for his guidance during the development of this research.

I am also thankful to Occidental Oil & Gas for providing the field data for this research.

I cannot fully express my gratitude to my friends, Amara Okeke, Rustam Gasimov and Anar Azimov, for their friendship and for making my days at A&M infinitely more enjoyable with exceptional grace and good humor. We spent quite a great time together.

## TABLE OF CONTENTS

	Page
ABSTRACT.....	iii
DEDICATION.....	v
ACKNOWLEDGEMENTS .....	vi
TABLE OF CONTENTS.....	vii
LIST OF FIGURES .....	ix
LIST OF TABLES.....	xiii
CHAPTER	
I    INTRODUCTION .....	1
1.1    Background .....	1
1.2    Problem Description.....	3
1.3    Objectives .....	3
II   LITERATURE REVIEW.....	4
2.1    CO <sub>2</sub> Flooding Mechanisms .....	4
2.2    Water-Alternating-Gas (WAG) Process .....	5
2.3    WAG Process Classification .....	7
2.4    Design Parameters for a WAG Process .....	7
2.5    Conformance Control .....	15
III  GEOLOGY REVIEW.....	17
3.1    Introduction .....	17
3.2    Structure .....	20
3.3    Stratigraphy .....	22
3.4    Environment of Deposition .....	26
3.5    Reservoir Geology of the Area .....	26
IV  RESERVOIR PERFORMANCE .....	28
4.1    Reservoir Basic Data.....	28
4.2    Reservoir Development (Denver Unit Overview) .....	29
4.3    CO <sub>2</sub> Flood Development .....	31

CHAPTER	Page
V SIMULATION PARAMETERS AND MODEL .....	37
5.1 Numerical Simulator .....	37
5.2 Fluid Properties .....	37
5.3 Equation-of-State Characterization .....	38
5.4 Relative Permeability .....	48
5.5 Reservoir Model.....	52
5.6 Initial Conditions.....	54
5.7 History Match .....	54
VI OPTIMIZATION OF MISCIBLE WAG PROCESS .....	75
6.1 CO <sub>2</sub> Injection Rate Optimization .....	75
6.2 Optimum Water-Alternating-Gas (WAG) Ratio .....	76
6.3 Conformance Control.....	78
6.4 Optimum Well Pattern.....	82
VII CONCLUSIONS .....	85
NOMENCLATURE .....	86
REFERENCES .....	87
VITA .....	93



## LIST OF FIGURES

FIGURE	Page
1.1 Location map of Denver Unit, Wasson San Andres Field.....	2
2.1 One-dimensional schematic showing how CO <sub>2</sub> becomes miscible with crude oil.....	5
2.2 Schematic of the WAG process .....	5
2.3 Effect of gravity during WAG injection .....	8
2.4 Displacement of oil by water in a stratified reservoir .....	9
2.5 Two-phase relative permeability diagram.....	11
2.6 Placement of a blocking agent in a high permeability layer .....	15
3.1 Location of Wasson Field in the Permian Basin.....	17
3.2 Generalized stratigraphic column showing Permian Section at the Wasson Field...	18
3.3 Structural map of top of San Andres Formation in the Wasson Field. ....	21
3.4 North-south cross section showing the distribution of the depositional facies across Denver Unit in Wasson Field.....	23
3.5 Denver Unit type log.....	25
4.1 Denver Unit production performance .....	30
4.2 Denver Unit typical well pattern configuration.....	32
4.3 Continuous CO <sub>2</sub> flood area production performance.....	33
4.4 Continuous CO <sub>2</sub> flood area oil cut vs. cumulative oil.....	34
4.5 WAG area oil production. ....	35
4.6 Cumulative incremental EOR recovery vs. time .....	36
5.1 Preliminary match for the oil FVF .....	40

FIGURE	Page
5.2 Preliminary match for the gas deviation factor (Z).....	40
5.3 Preliminary match for the gas FVF .....	41
5.4 Preliminary match for the oil density ( $\rho_o$ ) .....	41
5.5 Preliminary match for the CO <sub>2</sub> swelling factor .....	42
5.6 Preliminary match for the GOR .....	42
5.7 Comparison of the predicted and observed values for the GOR .....	45
5.8 Comparison of the predicted and observed values for the oil FVF .....	46
5.9 Comparison of the predicted and observed values for the oil density ( $\rho_o$ ) .....	46
5.10 Comparison of the predicted and observed values for the gas deviation factor (Z) .....	47
5.11 Comparison of the predicted and observed values for the gas FVF .....	47
5.12 Comparison of the predicted and observed values for the CO <sub>2</sub> swelling factor	48
5.13 Water and oil relative permeability curves as a function of water saturation .....	49
5.14 Gas and oil relative permeability curves as a function of gas saturation .....	50
5.15 Imbibition and secondary drainage water relative permeability .....	52
5.16 Simulation grid for Denver Unit section 48 .....	53
5.17 Gas production history match. ....	56
5.18 Water production history match.....	56
5.19 Water cut history match.....	57
5.20 Simulated reservoir pressure.....	57
5.21 Diag-Prod well: Gas production rate history match.....	58
5.22 Diag-Prod well: Water production rate history match. ....	58
5.23 NS-Prod well: Gas production rate history match. ....	59

FIGURE	Page
5.24 NS-Prod well: Water production rate history match.....	59
5.25 EW-Prod well: Gas production rate history match.....	60
5.26 EW-Prod well: Water production rate history match.....	60
5.27 Areal view of the oil saturation distribution. Year 0.....	62
5.28 Areal view of the oil saturation distribution. Year 2.....	62
5.29 Areal view of the oil saturation distribution. Year 4.....	63
5.30 Areal view of the oil saturation distribution. Year 6.....	63
5.31 Areal view of the oil saturation distribution. Year 8.....	64
5.32 Areal view of the oil saturation distribution. Year 10.....	64
5.33 Areal view of the oil saturation distribution. Year 12.....	65
5.34 Areal view of the oil saturation distribution. Year 14.....	65
5.35 Areal view of the oil saturation distribution. Year 16.....	66
5.36 Areal view of the oil saturation distribution. Year 18.....	66
5.37 Areal view of the oil saturation distribution. Year 20.....	67
5.38 Areal view of the oil saturation distribution. Year 22.....	67
5.39 Areal view of the oil saturation distribution. Year 24.....	68
5.40 E-W cross section showing oil saturation. Year 0.....	68
5.41 E-W cross section showing oil saturation. Year 2.....	69
5.42 E-W cross section showing oil saturation. Year 4.....	69
5.43 E-W cross section showing oil saturation. Year 6.....	70
5.44 E-W cross section showing oil saturation. Year 8.....	70
5.45 E-W cross section showing oil saturation. Year 10.....	71

FIGURE	Page
5.46 E-W cross section showing oil saturation. Year 12 .....	71
5.47 E-W cross section showing oil saturation. Year 14 .....	72
5.48 E-W cross section showing oil saturation. Year 16 .....	72
5.49 E-W cross section showing oil saturation. Year 18 .....	73
5.50 E-W cross section showing oil saturation. Year 20 .....	73
5.51 E-W cross section showing oil saturation. Year 22 .....	74
5.52 E-W cross section showing oil saturation. Year 24 .....	74
6.1 Oil recovery at a WAG ratio of 1:1 as a function of injection rates .....	75
6.2 Comparison of different WAG ratios in terms of the incremental oil recovery as a function of the CO <sub>2</sub> slug size .....	77
6.3 Comparison of the residual oil saturation for various WAG ratios after injection of 100% HCPV of CO <sub>2</sub> .....	77
6.4 East-West cross section view of the simulation model showing the permeability block by the polymer .....	79
6.5 Injection pressure profile during the viscous water treatment .....	80
6.6 Comparison of conformance control treatments as a function of oil production rate.....	80
6.7 Comparison of conformance control treatments in terms of the incremental oil recovery as a function of the CO <sub>2</sub> slug size.....	81
6.8 (a) Staggered line drive, (b) line drive and (c) nine-spot well patterns .....	82
6.9 Comparison of staggered line drive, line drive and nine-spot well patterns .....	83

**LIST OF TABLES**

TABLE	Page
4.1 Summary of reservoir data.....	29
5.1 Reservoir fluid composition in mole fractions .....	38
5.2 P.V.T experimental data.....	39
5.3 Fluid description for San Andres reservoir fluid .....	48
5.3 Net pay, porosity and permeability distribution in the simulation model.....	53

## CHAPTER I

### INTRODUCTION

#### 1.1 Background

The Denver Unit is the largest unit in Wasson Field and is the world's largest carbon dioxide enhanced oil recovery (EOR) project. The Denver Unit is located in the southern edge of North Basin Platform of the Permian Basin in West Texas (Figure 1.1). Primary depletion drive production began in 1936 with single well production rates greater than of 1500 STB/D. In 1964, the Denver Unit was formed and a waterflooding was initiated. Carbon dioxide (CO<sub>2</sub>) injection began in 1983, when nine inverted nine-spot patterns were placed on CO<sub>2</sub> injection.<sup>1</sup>

The unit produces from the San Andres Formation, a middle Permian-aged dolomite located at subsurface depths ranging approximately from 4,800 to 5,200 ft. The Denver Unit initially contained more than 2 billion bbls of oil in the oil column (OC), which is the interval of the San Andres hydrocarbon accumulation above the producing oil/water contact (OWC). The field's producing oil/water contact (POWC), above which oil is produced water-free during primary recovery, varies from -1,250 ft to -2,050 ft below sea level. Above the POWC, petrophysical data generally show that oil occupies the pore space unsaturated by the reservoir connate water. The San Andres formation contains more than 650 million bbl of oil in a transition zone (TZ), which is the interval between the OWC and the true water level, commonly known as the base of zone (BOZO). The transition zone saturation of 35 to 65% was not effectively recovered by primary and waterflood primary methods. At Denver Unit, the transition oil has been proven to be an economical CO<sub>2</sub> enhanced oil recovery target.<sup>2,3,4</sup>

---

This thesis follows the style of *SPE Reservoir Evaluation and Engineering*.

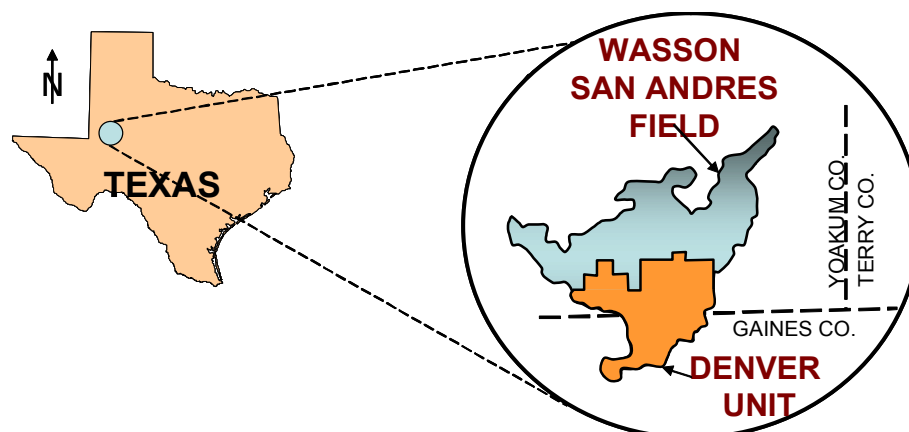


**Figure 1.1- Location map of Denver Unit, Wasson San Andres Field<sup>5</sup>.**

The Wasson San Andres Field contains a primary gas cap. The subsea depth of the initial gas/oil contact (GOC) was estimated to be -1,325 ft when the field was unitized in 1964. Because San Andres Formation in the Denver Unit is stratigraphically highest among all units operating the Wasson Field, more than 90% of the gas cap resides within the western portion on the Denver Unit.<sup>2</sup>

The 27,848-acre Denver Unit was formed for the purpose of implementing a secondary waterflood. In 1984 as the waterflood was maturing, a tertiary enhanced oil recovery project using CO<sub>2</sub> was implemented. CO<sub>2</sub> was initially injected into the eastern half the unit. Flood patterns were regularized with infill drilling to become inverted nine spot patterns. From 1989 to 1991, CO<sub>2</sub> injection was expanded areally to include most of the western half of the field. In 1994, the area of the field with the highest transition zone oil in place also began CO<sub>2</sub> injection.<sup>4</sup>

Today, over 400 million cubic feet per day of CO<sub>2</sub> are injected into 185 injector wells within the 21,000-acre project area, while 38,000 bbl of oil per day are produced.

## **1.2 Problem Description**

This research addresses the effects of heterogeneity on the overall sweep efficiency. The heterogeneity of the formation causes the response to the CO<sub>2</sub> injection to vary across the field, causing poor sweep efficiency and also bypassing a considerable amount of oil.

A reservoir simulation model was used to optimize CO<sub>2</sub> injection rates, evaluate different CO<sub>2</sub> injection patterns, determine the optimum WAG ratio, evaluate the use of a viscous agent in WAG application, and improve conformance control by applying polymer injection via compositional simulations in section 48 of the Wasson San Andres Formation.

## **1.3 Objectives**

The main goal of this work was to provide the best methodology to improve the sweep efficiency of miscible CO<sub>2</sub> floods and enhance the conformance control in section 48 in the San Andres Formation, Wasson Field. The main objectives of this work also include:

- determining the optimum CO<sub>2</sub> injection rates and WAG ratios;
- investigating the effect of conformance control on the ultimate oil recovery;
- studying the effect of pattern changes on the sweep efficiency



## CHAPTER II

### LITERATURE REVIEW

#### 2.1 CO<sub>2</sub> Flooding Mechanisms

CO<sub>2</sub> flooding processes can be classified as immiscible and miscible, even though CO<sub>2</sub> and crude oils are not miscible upon first contact at the reservoir.

Recovery mechanisms in immiscible processes involve reduction in oil viscosity, oil swelling, and dissolved-gas drive.

In miscible process, CO<sub>2</sub> is effective for improving oil recovery for a number of reasons. In general, CO<sub>2</sub> is very soluble in crude oils at reservoir pressures; therefore, it swells the oil and reduces oil viscosity.<sup>6</sup> Miscibility between CO<sub>2</sub> and crude oil is achieved through a multiple-contact miscibility process. Multiple-contact miscibility starts with dense-phase CO<sub>2</sub> and hydrocarbon liquid. The CO<sub>2</sub> first condenses into the oil, making it lighter and often driving methane out ahead of the oil bank. The lighter components of the oil then vaporize into the CO<sub>2</sub>-rich phase, making it denser, more like the oil, and thus more easily soluble in the oil. Mass transfer continues between the CO<sub>2</sub> and the oil until the two mixtures become indistinguishable in terms of fluid properties. Figure 2.1 illustrates the condensing/vaporizing mechanisms for miscibility.<sup>7</sup>

Because of this mechanism, good recovery may occur at pressures high enough to achieve miscibility. In general, the high pressures are required to compress CO<sub>2</sub> to a density at which it becomes a good solvent for the lighter hydrocarbons in the crude oil. This pressure is known as “minimum miscibility pressure” (MMP) and it is the minimum pressure at which miscibility between CO<sub>2</sub> and crude oil can occur.<sup>6</sup>

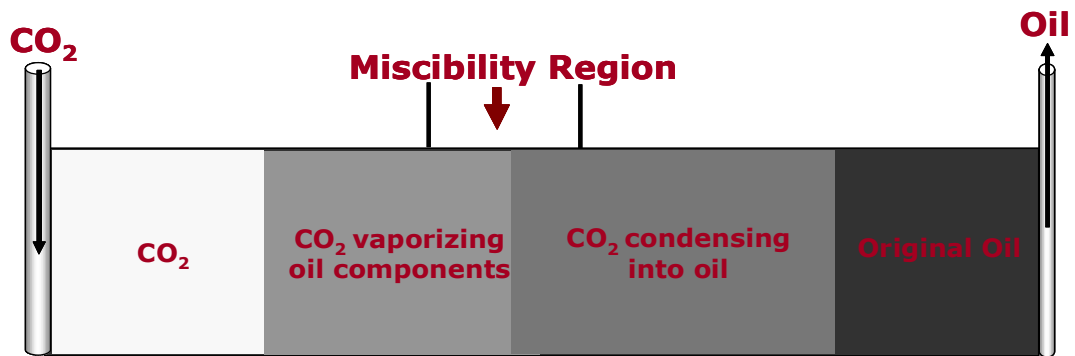


Figure 2.1- One-dimensional schematic showing how CO<sub>2</sub> becomes miscible with crude oil <sup>7</sup>.

## 2.2 Water-Alternating-Gas (WAG) Process

The WAG process was initially proposed as a method to increase sweep efficiency during gas injection. In practice the WAG process consists of the injection of water and gas as alternate slugs by cycles or simultaneously (SWAG), with the objective of improving the sweep efficiency of waterflooding and miscible or immiscible gas-flood projects by reducing the impact of viscous fingering.<sup>8</sup> The WAG process is schematically shown in Figure 2.2.

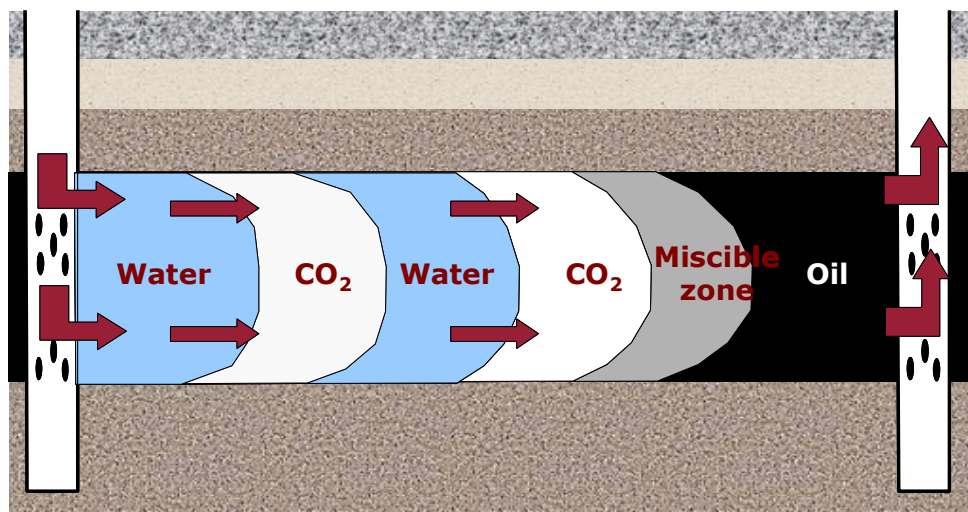


Figure 2.2- Schematic of the WAG process (Kinder Morgan Co.).

During a WAG process, the combination of higher microscopic displacement efficiency of gas with better macroscopic sweep efficiency of water helps significantly increase the incremental production over a plain waterflood.

WAG process has had a wide acceptance in field operations in the United States. A wide variety of gases have been employed for a wide range of reservoir characteristics in the miscible mode; however, CO<sub>2</sub> and hydrocarbon gases represent approximately 90% of the injectant gases used.<sup>7</sup>

The mobility ratio between injected gas and the displaced oil bank by CO<sub>2</sub> and other miscible gas displacement processes is typically very unfavorable because of the relatively low viscosity of the injected phase. A very unfavorable mobility ratio results in viscous fingering and reduced sweep efficiency. The WAG process is an injection technique developed to overcome this problem by injecting specified volumes, or slugs, of water and gas alternatively. As results of this process, the mobility of the injected gas alternating with water is less than that of the injected gas alone, and thus the mobility ratio of the process is improved.

In WAG injection, water/gas injection ratios have ranged from 0.5 to 4.0 volumes of water per volume of gas at reservoir conditions. The sizes of the alternate slugs range from 0.1% to 2% of the pore volume (PV).<sup>9</sup> Total or cumulative slug sizes of CO<sub>2</sub> in reported field projects typically have been 15% to 30% of the hydrocarbon pore volume (HCPV), although smaller and larger slugs have been reported.<sup>10</sup>

The main factors affecting the WAG injection process are the reservoir heterogeneity (stratification and anisotropy), rock wettability, fluid properties, miscibility conditions, gas trapped, injection technique and WAG parameters such as slug size, WAG ratio and injection rate.<sup>11</sup>

### **2.3 WAG Process Classification**

Although Claudle and Dyes<sup>8</sup> suggested simultaneous injection of oil and gas to improve mobility control, the field reviews show that they are usually injected separately.<sup>12</sup> The main reason for this injection pattern is the better injectivity when only one fluid is injected.

WAG processes have been classified into four types: miscible, immiscible, hybrid and others on the basis of injection pressures and method of injection. Many reservoirs specific processes have been patented and are generally grouped under the “other” WAG classification.<sup>12</sup>

A number of different WAG schemes are used to optimize recovery. Unocal patented a process called “Hybrid-WAG” in which a large fraction of the pore volume of CO<sub>2</sub> is injected continuously, followed by the remaining fraction divided into 1:1 WAG ratios.<sup>13</sup> Shell developed a similar process called DUWAG<sup>14</sup> (Denver Unit WAG) by comparing continuous injection and WAG processes

### **2.4 Design Parameters for a WAG Process**

Miscible gas injection has been implemented successfully in a number of fields around the world.<sup>12</sup> In principal the WAG process combines the benefits of miscible gas injection and waterflooding by injecting the two fluids simultaneously or alternatively. Miscible gas injection has excellent microscopic sweep efficiency but poor macroscopic sweep efficiency due to viscous fingering and gravity override. Furthermore it is expensive to implement in contrast to waterflooding, which is relatively cheap and is less subject to gravity segregation.

For this reason, it is very important to develop various CO<sub>2</sub> flood designs to determine the optimum near-term cash flow, overall project economics, and oil recoveries. The major design issues for a WAG injection process are reservoir characteristic and

heterogeneity, rock and fluids characteristics, injection pattern, WAG ratio, injection rate, ultimate CO<sub>2</sub> slug size.

#### 2.4.1 Reservoir Heterogeneity and Stratification

Reservoir and heterogeneity stratification have a strong influence on the water/gas displacement process.<sup>11</sup> The degree of vertical reservoir heterogeneity can affect the CO<sub>2</sub> performance. Reservoirs with higher vertical permeability are influenced by cross-flow perpendicular to the bulk flow direction.<sup>15</sup> Cross-flow may increase the vertical sweep, but generally the gravity segregation and decreased flood velocity in the reservoir reduce the oil recovery (Figure 2.3). As CO<sub>2</sub> flows preferentially toward the top portion of thick, high permeability zone, injected water may flow preferentially toward the lower portion of the zone.

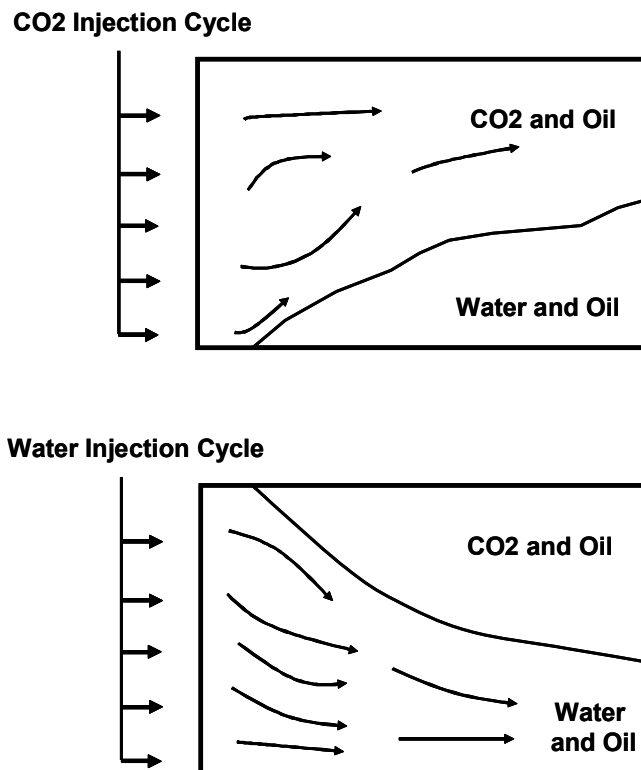
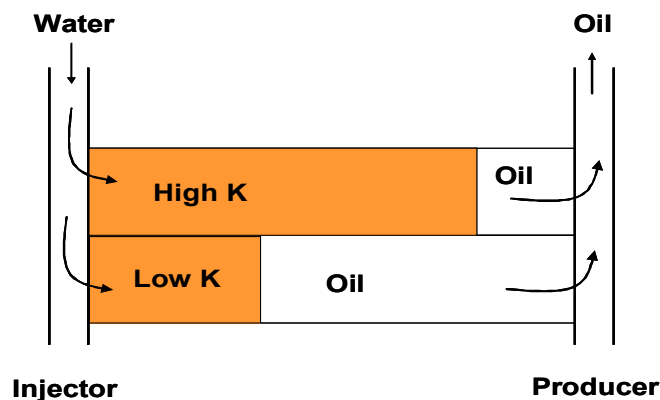


Figure 2.3- Effect of gravity during WAG injection <sup>7</sup>.

Reservoir heterogeneity controls the injection and sweep patterns in the flood. Reservoir simulation studies<sup>16</sup> for various vertical to horizontal permeability ( $k_v/k_h$ ) ratios suggest that higher ratios adversely affect oil recovery in WAG process.

Other studies<sup>17</sup> have reported that the vertical conformance of WAG displacements is strongly influenced by conformance between zones. In a non communicating layered system, vertical distribution of CO<sub>2</sub> is dominated by permeability contrasts. Flow into each layer is essentially proportional to the fractional permeability of the overall system [(average permeability x layer thickness ( $kh$ ))] and is independent of WAG ratio, although the tendency for CO<sub>2</sub> to enter the high permeability zone with increasing WAG ratio cannot be avoided. Due to the cyclic nature of the WAG, the most permeable layer has the highest fluid contribution, but as water is injected it quickly displaces the highly mobile CO<sub>2</sub> and all the layers attain an effective mobility nearly equal to the initial value.

In highly stratified reservoirs, the higher permeability layer(s) always respond first, resulting in an early breakthrough and poor sweep efficiency. See Figure 2.4. For these heterogeneous reservoirs, a WAG process would reduce the mobility in the high permeability layer, resulting in a larger amount of the CO<sub>2</sub> contacting the crude oil in that particular layer.



**Figure 2.4- Displacement of oil by water in a stratified reservoir.**

Alternate CO<sub>2</sub>/water injection is more sensitive to changes in reservoir properties, such as different permeabilities, than is waterflooding. Continuous CO<sub>2</sub> injection is even more sensitive to reservoir properties because there is no injected water to help control volume sweep by slowing down the movement of CO<sub>2</sub>.

High-permeability layers, directional permeability trends, and natural fractures all cause sweep problems. If a reservoir is naturally fractured to the extent that fractures have adversely affected waterflood sweep, a CO<sub>2</sub> flood using the same pattern is very likely to be unsuccessful.

#### **2.4.2 Relative Permeabilities**

Relative permeability is an important petrophysical parameter, as well as a critical input parameter, in predictive simulation of miscible floods. However, relative permeability is a lumping parameter that includes the effects of wetting characteristics, heterogeneity of reservoir fluids and rock and fluid saturations.<sup>18</sup>

During a typical CO<sub>2</sub> flood that includes injecting water alternately with CO<sub>2</sub> to remedy areal and vertical sweep problems, saturation changes during each injection period.<sup>7</sup> These changes in saturation also result in changes in the water relative permeability.

Among one of the most common problems associated with relative-permeability changes during alternate water/CO<sub>2</sub> floods are injectivity losses.<sup>18</sup> Water injectivity undergoes significant changes after the first cycle of injected CO<sub>2</sub>. These changes are related to the effect that CO<sub>2</sub> has on the relative permeability of the water. A quantitative understanding of the relative permeability curves is important because is an input to reservoir simulators to forecast the CO<sub>2</sub> flood performance.<sup>7</sup>

Simulation sensitivities<sup>19</sup> have shown that a sharp injectivity reduction at the start of the water cycle can be associated with relative permeability reduction near the well that can gradually experience an increasing injectivity trend throughout the rest of the cycle.

This behavior is suggested to be caused by two-phase flow of gas and water initially near the well; as the cycle proceeds, the saturations and the relative permeabilities change.<sup>18</sup>

Laboratory floods attempting to emulate CO<sub>2</sub> flood<sup>20</sup> experienced appreciable water relative permeability reductions after CO<sub>2</sub> injection. In addition, data have shown significant hysteresis effects in the water relative permeability between the drainage and imbibition curves. Irreducible water saturations after drainage cycles were 15 to 20% higher than the initial connate water saturation.<sup>18</sup>

Hysteresis refers to the directional saturation phenomena exhibited by many relative permeability and capillary-pressure curves when a given fluid phase saturation is increased or decreased.<sup>21</sup> This phenomenon is illustrated in Figure 2.5.

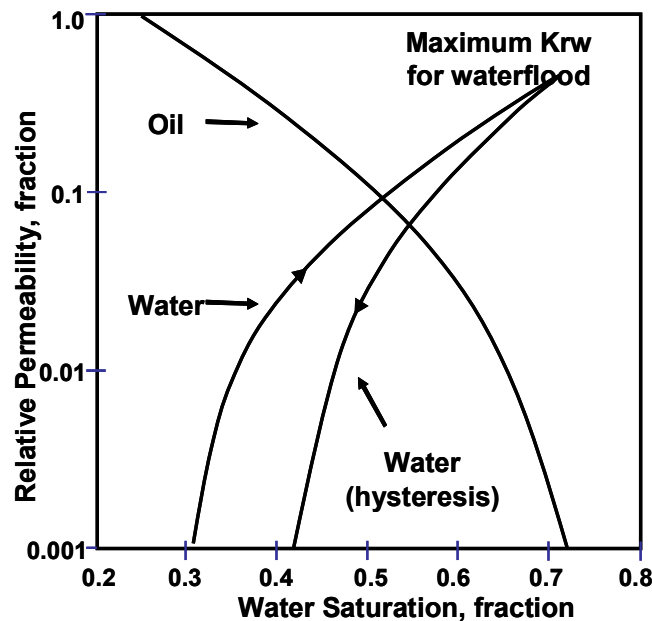


Figure 2.5- Two-phase relative permeability diagram<sup>7</sup>.

The figure represents a test of bidirectional water/oil relative permeability that depicts the water relative permeability and water injectivity. The relative permeability of the oil is 1.0 at connate water saturation and declines as a waterflood is performed until residual



oil saturation is reached. Simultaneously, the relative permeability of water increases until a maximum value is reached.

Then, oil is injected until water ceases to flow. For an oil-wet reservoir, oil can flow back through the same pores that it previously vacated, and the oil relative permeability can increase along the same path. The water relative permeability, however, shows hysteresis because the drainage (decreasing oil and increasing water saturation) and imbibition (increasing oil and decreasing water saturation) curves do not follow the same path. As a result, the new minimum value of irreducible water saturation does not go back to the original connate-water saturation.

The result of water-permeability hysteresis in an oil-wet reservoir is that water injectivity can be severely reduced. In addition, oil relative permeability can not return to 1.0 because the increased residual water saturation reduces the maximum oil saturation possible, consequently reducing the tertiary oil rate.<sup>7</sup>

### **2.4.3 Injection Patterns**

Well injection patterns and well spacing have a great impact on the sweep efficiency in a CO<sub>2</sub> flood. Additionally, well spacing is a strong indicator of the average reservoir pressure (as the ratio of injector to producers increases, so does the average reservoir pressure).<sup>7</sup>

The most popular pattern injections in the field are the five-spot pattern and the inverted nine-spot patterns. The 5-spot pattern gained high popularity in field operations during CO<sub>2</sub> floods because its well spacing makes it attain better flood-front control and helps to maintain higher average reservoir pressure.<sup>7</sup> The inverted nine-spot pattern was also very common in the early years of many CO<sub>2</sub> floods in west Texas.<sup>4,22</sup>

Regardless of the type of pattern used for a CO<sub>2</sub> flood, it is very important and critical to prevent major volumetric sweep problems under the operation. Problems with low

reservoir pressure and poor sweep efficiency during a waterflooding will definitely get worse during a CO<sub>2</sub> flooding.<sup>7</sup>

In general, fields with high well spacing (greater than 80 acres) are likely to have a poor CO<sub>2</sub> flooding incremental recovery due to low sweep efficiency. Those fields would likely require a significant additional capital investment in infill wells to improve the production and the economic attractiveness of CO<sub>2</sub> flooding development.<sup>4,23</sup>

#### **2.4.4 WAG Ratios**

WAG ratio is the ratio of injected water to CO<sub>2</sub>. WAG ratios may be expressed in terms of reservoir injection (i.e., barrels of water injected at reservoir conditions) or in terms of duration (i.e., the time over which injection takes place).<sup>7</sup> The WAG ratio is controlled by the gas availability as well as the wetting state of the reservoir rock.<sup>16</sup>

Injecting water with miscible gas reduces the instability of the gas/oil displacement process that results from relative permeability effects, thus improving the overall sweep efficiency. It also improves the economics by reducing the volume of gas that needs to be injected into the reservoir.

An optimum WAG ratio is a major parameter design that has a significant effect on both operation and economics of a CO<sub>2</sub> flood. An approach to maximize the net present value of a CO<sub>2</sub> flood<sup>24</sup> suggests that WAG ratio should be increased gradually after the optimum gas production is reached through the life of the flood. The gradual increase of injected water (a decrease in the WAG ratio) results in increased mobility control and a constant produced gas profile.

Laboratory studies<sup>16</sup> on WAG ratios showed that tertiary CO<sub>2</sub> floods have maximum recoveries at a WAG ratio of about 1:1 in floods dominated by viscous fingering whereas 0:1 WAG ratio (continuous gas injection) showed optimum recovery in floods dominated by gravity tonguing. Hence, continuous gas injection is recommended for

secondary as well as tertiary floods in water-wet rocks, whereas 1:1 WAG is recommended for partially oil-wet rocks.

In practice all patterns may start at the same WAG ratio. Later, as the CO<sub>2</sub> production increases due to poor volumetric sweep efficiency, the WAG ratio is usually increased on a pattern-by-pattern basis starting with the highest GOR patterns.<sup>7</sup>

#### **2.4.5 Slug Size**

Slug size refers to the cumulative of CO<sub>2</sub> injected during a CO<sub>2</sub> flood. The slug volume is usually expressed as a percentage of the hydrocarbon pore volume (%HCPV).<sup>7</sup>

Selecting an optimum CO<sub>2</sub> slug size is critical in a proper design of a hydrocarbon miscible flood.<sup>25</sup> Generally, the more CO<sub>2</sub> injected, the greater the incremental oil recovery. However, a large CO<sub>2</sub> slug size diminishes the return of the project. The larger the CO<sub>2</sub> bank size, the greater the ultimate recovery, but the increment gets smaller and smaller.<sup>26</sup>

Economic sensitivities must be performed to determine the optimum CO<sub>2</sub> slug size. The optimum CO<sub>2</sub> slug size for a particular project will depend upon economic factors such as crude price, CO<sub>2</sub> cost, and the amount and timing of the incremental recovery. The economic optimization process is carried out by systematically repeating simulation runs until optimum design parameters are achieved.<sup>27</sup> Total slugs of CO<sub>2</sub> equal to about 20 to 50% HCPV have been used in different projects in U.S.A.<sup>28</sup>

The ultimate CO<sub>2</sub> slug size can be determined after the start of project, when more information is known about future price of oil and production response of the reservoir. The optimum CO<sub>2</sub> bank size should be determined on an individual pattern basis rather than on a total project evaluation.<sup>26</sup>

## 2.5 Conformance Control

Conformance is a measure of where injected fluids (water or CO<sub>2</sub>) are entering the pay zone. Ideally, injected fluids enter the formations only at pay zones and spread out evenly across these zones to avoid early breakthrough.<sup>7</sup>

When a WAG has failed to control sweep, other techniques such as surfactant foams, gel polymers and conventional plugging methods can be used to improve the sweep efficiency of the injection process.<sup>7</sup>

The objective of gel treatments and similar blocking-agent treatments is to reduce channeling through fractures or high-permeability zones without significantly damaging hydrocarbon productivity. The idea is to achieve a permeability reduction in high permeability layers, while minimizing gel penetration and permeability reduction in less-permeable, hydrocarbon-productive zones. This objective can be met by mechanically isolating zones during the gel-placement process, so that gel injection occurs only in the high-permeability zones.<sup>28</sup> See figure 2.6.

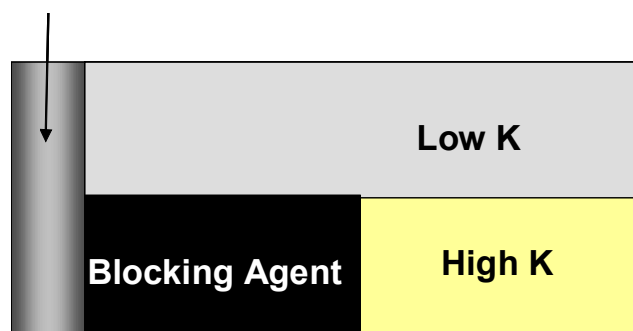


**Figure 2.6- Placement of a blocking agent in a high permeability layer.**

If analogous flood suggests that premature water/CO<sub>2</sub> breakthrough will be a problem, or representative core data indicate that the reservoir will not flood uniformly, polymers or blocking agent treatments should be carried out to avoid sweep efficiency problems. Expected results are more oil produced faster and at lower gas/oil ratios.

The initial step in treatment design is selecting a process appropriate for the reservoir problem. Choices to be made include near-wellbore versus deep gel treatments, type of polymer, crosslinking agent, and crosslinking process. On-site and laboratory testing by service companies with actual treating/reservoir fluids assists in chemical selection and treatment design.<sup>29</sup>

A critical step is the calculation of the treatment volume and the prediction of variation in polymer composition. Diverse tools, such as production/injection histories, well logs, surveys, workover history and personal knowledge of the formation and geographical area are critical for prediction of treatment volume. It is impossible to calculate treatment volume exactly, but estimation within reasonable limits is possible. That is why it is essential that injection rate and pressure be continuously monitored during treatment and appropriate changes made to optimize treatment. The polymer solution should be injected until parting pressure is approached while injecting, the injected slug is produced at a peripheral producer, or the maximum design size is achieved. In most cases, parting pressure is the limiting factor for treatment size.<sup>30</sup>

## CHAPTER III

### GEOLOGY REVIEW

#### 3.1 Introduction

Wasson Field is situated near the central part of the Staked plain in Yoakum and Gaines Counties on the southeastern margin of the northwest shelf of the North Basin Platform of the Permian Basin, west Texas (Figures 1.1 and 3.1). It occupies a triangular area 15 miles long and 14 miles wide, containing approximately 55,000 acres or 86 square miles, and includes only a few dry holes.<sup>31</sup>

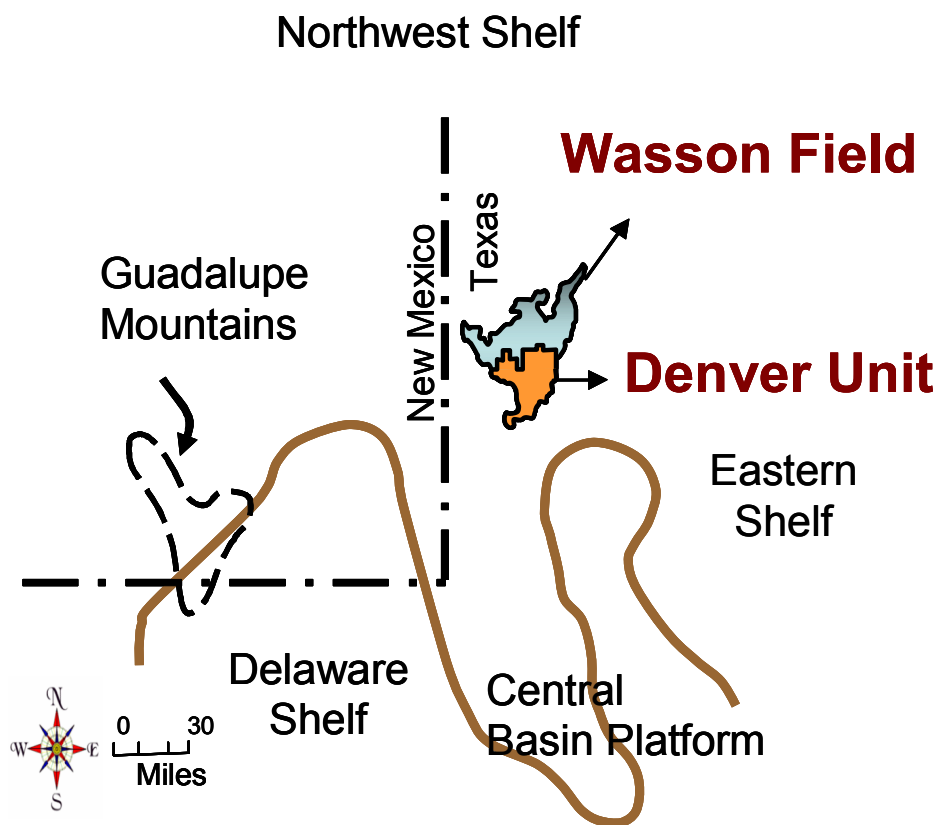


Figure 3.1- Location of Wasson Field in the Permian Basin<sup>32</sup>.

Geologically, the field lies on the extended axis of the Central Basin platform, but appears to be separated from it by a trough in northern Gaines County. The combined effect of the structural elements gives the appearance of a terraced platform tilted northeastward by post-Permian movement.<sup>32</sup>

Wasson Field produces oil from the Permian San Andres dolomite. The stratigraphy of San Andres Formation is typical of west Texas. Massive and porous dolomites with few clastics grade basinward into sections of interbedded dolomite, anhydrite and minor limestones. The San Andres Formation is overlain by the Grayburg formation which is not productive in the Wasson field.<sup>32, 33, 34</sup> Figure 3.2 is a generalized stratigraphic column showing Permian formations present at Wasson Field. Within this section, production is predominately from dolomites of the Guadalupian-aged Andres Formations.

PERIOD	EPOCH	FORMATION
Permian	Ochoan	Dewey Lake
		Rustler
		Salado
	Guadalupian	Tansill
		Yates
		Seven Rivers
		Queen
		Grayburg
		San Andres
		Glorieta
		Leonardian
	Blinebry	
	Tubb	
	Yeso	
	Drinkard	
		Abo
Wolf-campian	Wolfcamp	

**Figure 3.2- Generalized stratigraphic column showing Permian Section at the Wasson Field. Productive interval San Andres Formation is shaded.**<sup>34</sup>

Wasson field is a combination of structural/stratigraphic trap controlled by a combination of an extensive dolomitization and anhydrite plugging.<sup>34</sup> The structure is an anticline capped by dense dolomite and underlain by an essentially inactive aquifer.

Structure and stratigraphy in San Andres Formation appear to have controlled the permeability, porosity, and the accumulation of fluids.<sup>32</sup> San Andres Formation at Wasson Field presents vertical and lateral variations with respect to petrophysical properties that make the formation highly heterogeneous. The stratigraphic component of vertical heterogeneity is apparent in the cyclic character of the San Andres Formation caused by high-frequency changes in relative sea level during San Andres deposition. Vertical heterogeneity within the San Andres is also strongly affected by post-depositional and diagenetic processes.<sup>34, 35</sup>

Lateral variability in porosity and permeability patterns is a function of both depositional and post-depositional processes. Depositional causes such as lateral carbonate texture variation and variations in water depth produced by paleotopography and by relative facies positions on the ramp contribute to lateral heterogeneity within the San Andres Formation.<sup>36, 37</sup> Post depositional controls on lateral heterogeneity include spatially varying degrees of dolomitization, anhydritic replacement of dolomite crystals, anhydritic filling of void space and moldic porosity development. In addition to these post-depositional effects, faults, fractures and associated diagenesis quite likely contribute to lateral heterogeneity within the Permian carbonate section.<sup>33, 37</sup>

Analyses of core and log data indicate the presence of extensive dolomitization, moldic and vuggy porosity development, and anhydrite emplacement.<sup>37</sup> Six pore types have been identified in San Andres Formation related to both depositional and diagenetic changes. The pores types include intercrystal, vug, moldic, intracrystal, fracture, and intraparticle.<sup>33</sup> These processes act at a variety of scales and impose a substantial contribution to vertical heterogeneity within the reservoir.



### 3.2 Structure

Wasson Field resulted from structural drape over the buried Abo trend on the southeast and the stratigraphic facies changes to the northwest.<sup>35</sup>

San Andres Formation combines stratigraphic trapping of hydrocarbons from porosity pinch-outs and anhydrite plugging with subtle structural nosing and changes in dip. These structural elements on both local and regional scale have an important influence in the location of hydrocarbons in the San Andres Formation.<sup>34</sup>

The present structural attitude of the beds is the result of the cumulative, gentle pre-Tertiary folding plus the eastward tilting of the region during the Tertiary. The present structure is best shown by contouring the “solid lime” or top of the San Andres Formation. It is compound, consisting of two dominant lines of folding: one trending N 30° E, along the east edge of the field; the other N 65° W, along the southwest edge.<sup>32</sup>

San Andres Formation has a triangular shape on an areal perspective (Figure 3.3). The structure is bordered by relatively steep flanks on the southeast and southwest which dip approximately 3°. The dip in the north flank of the formation is less than 100 ft/mile. The southeastern limit of the field closely parallels the edge of the North Basin Platform, which is the shelf margin of the underlying Lower Clearfork and Wichita Formations.<sup>31, 32</sup>

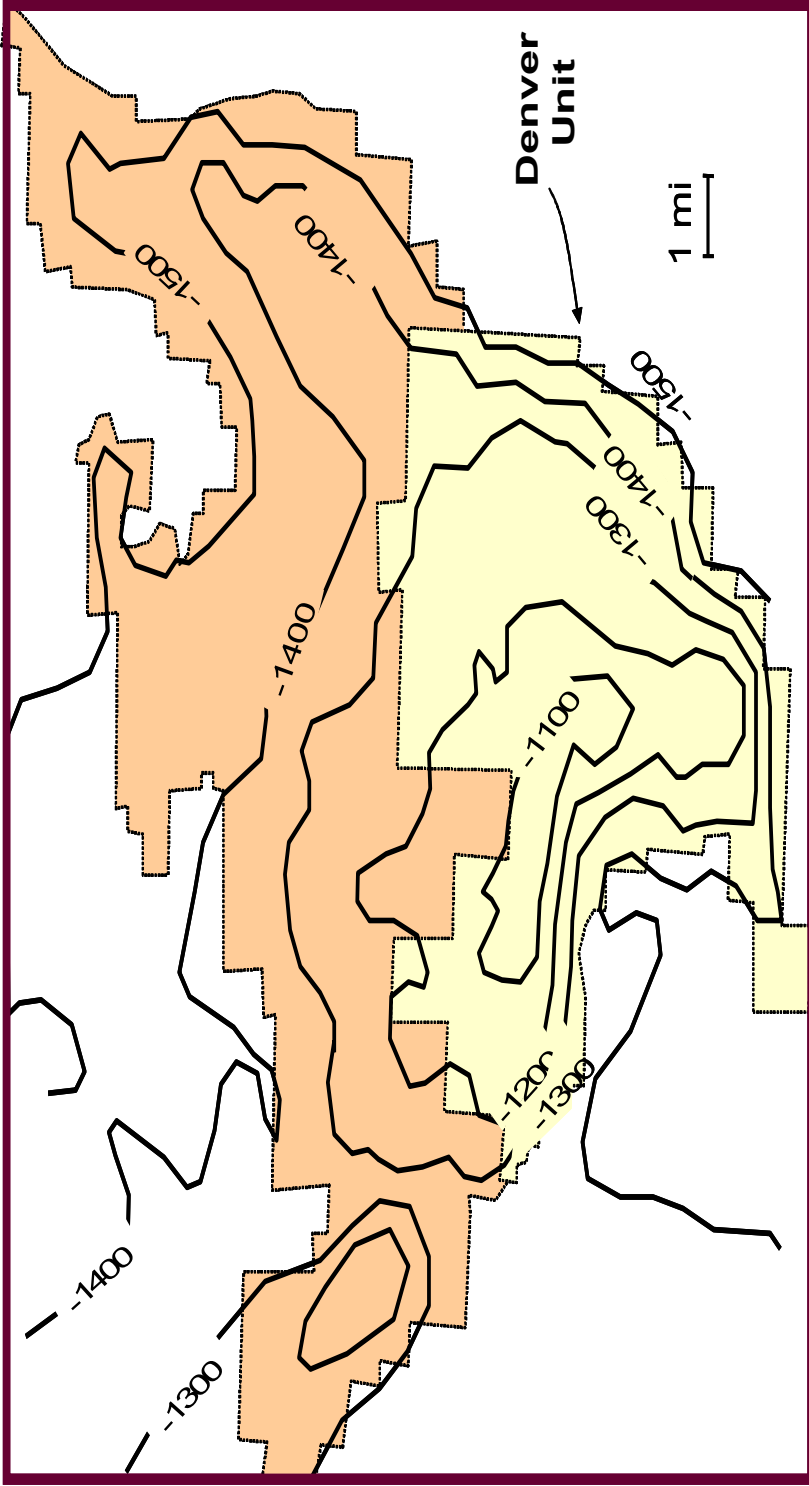


Figure 3.3- Structural map of top of San Andres Formation in the Wasson Field<sup>2</sup>.

### 3.3 Stratigraphy

San Andres Formation is Middle Permian (Guadalupian) in age and in the Wasson Field consists in 1,300 feet of dolomite.<sup>31</sup> It is located between the evaporitic dolomites of Grayburg Formation, which is not productive in the Wasson area, and the sandy anhydritic dolomites of Glorieta Formation. The reservoirs are located in the lower part of the San Andres and are capped by nearly 400 ft of a dense nonporous dolomite.<sup>31,35</sup>

The Wasson San Andres field is a classic example of a carbonate reservoir located on a regressive carbonate shelf platform. Core examination reveals a classic example of a shoaling-upward sequence where the original sedimentary environments clearly influenced the development and distribution of porosity.<sup>31</sup>

The San Andres Formation in the Northwest Shelf represents a regressive series of cyclic deposits that prograded southward across a broad, low relief, shallow-water shelf. San Andres Formation consists of interbedded dolomites, anhydrites, and minor limestones. The lower part of San Andres is up to 800 ft thick and is a large-scale shoaling depositional cycle composed, from bottom to top, of open marine shelf deposits; restricted-marine, subtidal dolostones that form the reservoir facies; intertidal and supratidal dolostones, and salina and sabkha anhydrites.<sup>34</sup>

The San Andres Formation is characterized by a basinward progradational shift in facies; this overall shift is interrupted by several transgressions, which result in the cyclical nature of the carbonate section. Gradual return to the regressive conditions resulted in the deposition of intertidal to supratidal nonporous dolomite interbedded with anhydrite that caps the lower San Andres productive interval.<sup>35</sup>

The principal reservoir rocks are a mixture of two end-member rock types: pelletal packstones and moldic (skeletal) wackestones. The pelletal packstones are usually well burrowed, contain varying amounts of skeletal debris, and are usually less than 10 ft thick. The moldic wackestones are slightly burrowed and occur as patchy accumulations.

Fluid-flow properties reflect the relative proportions of pelletal packstone and moldic wackestone. The pelletal packstones have abundant interparticle porosity with varying amounts of moldic pores; their porosity commonly ranges between 15 and 20%, but locally is as high as 25%. Permeability is usually between 10 and 50 md, but very locally exceeds 100 md. The most abundant pore type in the wackestones is moldic. This rock type has a permeability of less than 1 md, although moldic porosity may range as high as 10%.<sup>33</sup>

The San Andres Formation has been stratigraphically divided into two major intervals known as “First Porosity” and “Main Pay.” The Main Pay, which is the lower interval, consists of dolomitized open marine packstones and wackstones and exhibits better quality rock than the First Porosity interval. The First Porosity interval possesses poor-quality reservoir rock and was deposited in shallower-water, restricted marine and intertidal environment. The First Porosity has finer crystalline matrix and is less continuous than the “Main Pay” (Figure 3.4).<sup>31</sup>

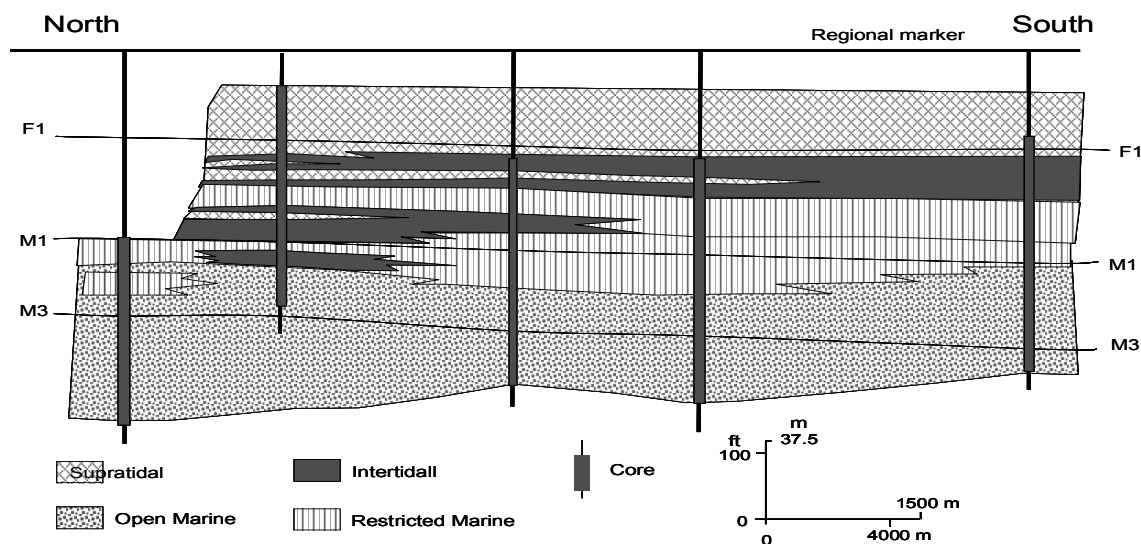


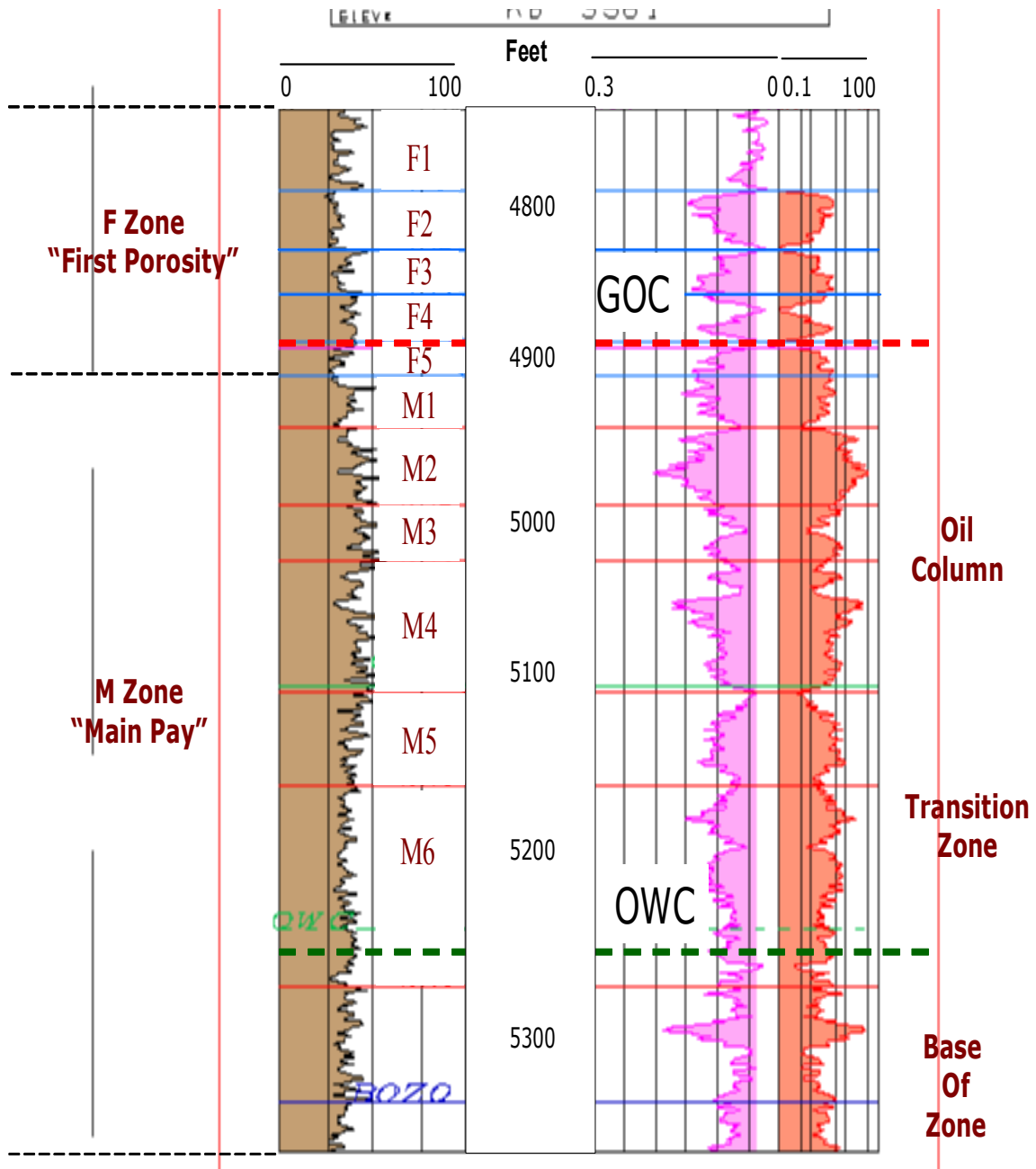
**Figure 3.4- North-south cross section showing the distribution of the depositional facies across Denver Unit in Wasson Field.**<sup>31</sup>

Main Pay subtidal pelletal packstones in the Denver Unit have porosity of 15 to 20% and permeability from 10 to 50 md, whereas the Main Pay moldic wackestones have porosity as high as 10 percent but permeability less than 1 md.<sup>31</sup>

On the basis of the gamma ray and sonic logs, the first porosity was divided into five intervals (F1 through F5), and the main pay was divided into six zones (M1 through M6). These zones can be recognized throughout the Denver Unit. Figure 3.5 is a type log showing the present divisions of the San Andres Formation in the Denver Unit.<sup>2</sup>

Simulation layers were built on the basis of the actual stratigraphical division of the San Andres Formation. This representation of the flow units would honor the heterogeneity and zonation of the formation.

In the simulation model, additional divisions of the existing geologic zones were necessary to represent large variations in porosities and permeabilities within the geologic zones. For example, the “M1” interval was subdivided into four layers because has high permeability contrast. Similarly, the “M3” interval has also divided into three layers since the upper part of interval presents a high permeability value in comparison with the rest of the zone. See Figure 3.5.



Courtesy of Occidental Oil and Gas

Figure 3.5- Denver Unit type log.

### 3.4 Environment of Deposition

Deposition occurred in a shallow marine shelf environment. Moldic wackestones represent the original sediment. Pelletal packstones are probably the remains of fecal pellets produced by organisms which burrowed through the muddy sediment. When this burrowing was very intense, a sediment consisting entirely of pellets was produced as organisms reworked sediment. When burrowing was less prevalent, pellets were restricted to well-defined burrows cutting through wackestone sediment. Both dolomitizing and anhydrite precipitating fluids were probably derived from overlying, supratidal sediments deposited after the open marine reservoir rocks. The original sediment was composed entirely of calcite and aragonite with no associated dolomite or gypsum.<sup>33</sup>

### 3.5 Reservoir Geology of the Area

Cores analyses have revealed that the Main Pay interval presents three rock types: a pelletal dolomite packstone with interparticle and intercrystal porosity (pelletal packstone); a fossiliferous dolomite wackestone with moldic porosity (moldic wackestone); and a fossiliferous dolomite packstone with moldic and interparticle porosity (moldic packstone).<sup>33</sup>

The pelletal packstone rocks occur both as homogeneous units and in burrows and irregular patches in the wackestones. They have excellent reservoir rock properties; permeability can be as high as 152 md and interparticle porosity is up to 24.3%.<sup>33</sup>

In the wackestone rocks, molds and vugs are the dominant pore types, ranging in size up to 6 mm. Within the rock, molds are not in contact with other; core observation has revealed that the molds are isolated in the rock by a relatively tight matrix. This isolated moldic porosity negatively affects the reservoir properties of the rock. Permeability is less than 1 md, even though moldic porosity may range as high as 10%.<sup>33</sup>

The moldic packstone rock is medium crystalline, with more moldic than intercrystal porosity and light brown. Due to the connection of the moldic pores through interparticle pores, these rocks exhibit higher permeabilities and lower residual oil saturations than any other rock types in the area.<sup>33</sup>

Average reservoir porosity and permeability are 12% and 5 md, respectively. Lateral reservoir continuity at the pattern scale (injector to producer distance averages approximately 1,000 ft) is generally considered good.



## CHAPTER IV

### RESERVOIR PERFORMANCE

#### 4.1 Reservoir Basic Data

The Denver Unit is the largest unit in Wasson Field. The unit produces oil from the San Andres Formation, a Middle Permian dolomite located at subsea depths ranging from approximately -1,250 to -2,050 ft.

The Denver Unit initially contained more than 2 billion bbl of oil in the oil column, which is the interval of the San Andres hydrocarbon accumulation above the producing oil/water contact (OWC). In addition, the San Andres Formation contains more than 650 million bbl of oil in a transition zone (sometimes referred to as a paleo residual oil zone).

The gross oil pay thickness of the San Andres Formation varies from 200 to 500 ft. The formation contains a primary gas cap. The subsea depth of the initial gas/oil contact (GOC) was estimated to be -1,325 feet. Because the San Andres Formation in the Denver Unit is stratigraphically highest among all units operating the Wasson Field, more than 90% of the gas cap resides within the western portion of the Denver Unit. The presence of the gas cap has had a great impact on the CO<sub>2</sub> flood performance. The formation is underlain by an essentially inactive aquifer. Solution drive has been the primary producing mechanism.<sup>2,3</sup>

Table 4.1 summarizes basic reservoir and fluid data.

**Table 4.1- Summary of reservoir data**

<b>Reservoir Characteristics</b>	<b>Values</b>
Producing area	25,505 acres
Formation	Permian San Andres Dolomite
Average Depth	5,200 ft
Gas-oil Contact	-1,325 ft
Average Permeability	5 md
Average Porosity	12%
Average net oil pay thickness	137 ft
Oil Gravity	33° API
Reservoir Temperature	105°F
Primary production mechanism	Solution-gas drive
Secondary production mechanism	Waterflood
Tertiary production mechanism	CO <sub>2</sub> miscible
Original reservoir pressure	1,805 psi
Bubble point pressure	1,805 psi
Average pressure at start of secondary recovery	±800 / ±1100 psi
Target reservoir pressure for CO <sub>2</sub>	2,200 psi
Initial FVF (Formation Volume Factor)	1.312 res bbl/bbl
Solution GOR at original pressure	420 res bbl/bbl
Solution GOR at start of secondary recovery original pressure	1,060 scf/bbl
Oil viscosity at 60° F and 1100 psi	1.18 cp
Minimum miscibility pressure	1,300 psi

#### **4.2 Reservoir Development (Denver Unit Overview)**

Wasson Field was discovered in 1936. Primary depletion drive production began in 1936 with single-well production rates in excess of 1,500 barrels of oil being common.<sup>1</sup> By the mid 1940s, the field was largely developed on a 40-acre well spacing. The 27,848 acre Denver Unit, covering the southern portion of Wasson Field, was formed in 1964 for the purpose of implementing a secondary flood. In 1966, supplemental recovery

operations were initiated and waterflood operations began. Peak secondary oil production of 37,100 BOPD occurred in 1975.<sup>3</sup>

In 1984 as the waterflood was maturing, a tertiary enhanced oil recovery project using carbon dioxide was implemented. The Denver Unit CO<sub>2</sub> flood, ranks among the largest EOR projects currently operating in the United States. Historical waterflood and tertiary performance of Denver Unit are shown in Figure 4.1.

CO<sub>2</sub> was initially injected only in the eastern half of the unit. Floods were regularized with infill drilling to become inverted nine-spot patterns. From 1989 to 1991, CO<sub>2</sub> injection was expanded aerially to include most of the western half of the field. In 1994, the area of the field with the highest transition zone oil in place, commonly known as the TZ sweet spot, also began CO<sub>2</sub> injection. Infill drilling and pattern reconfiguration development were initiated in 1995 and continued to the present time.<sup>4</sup>

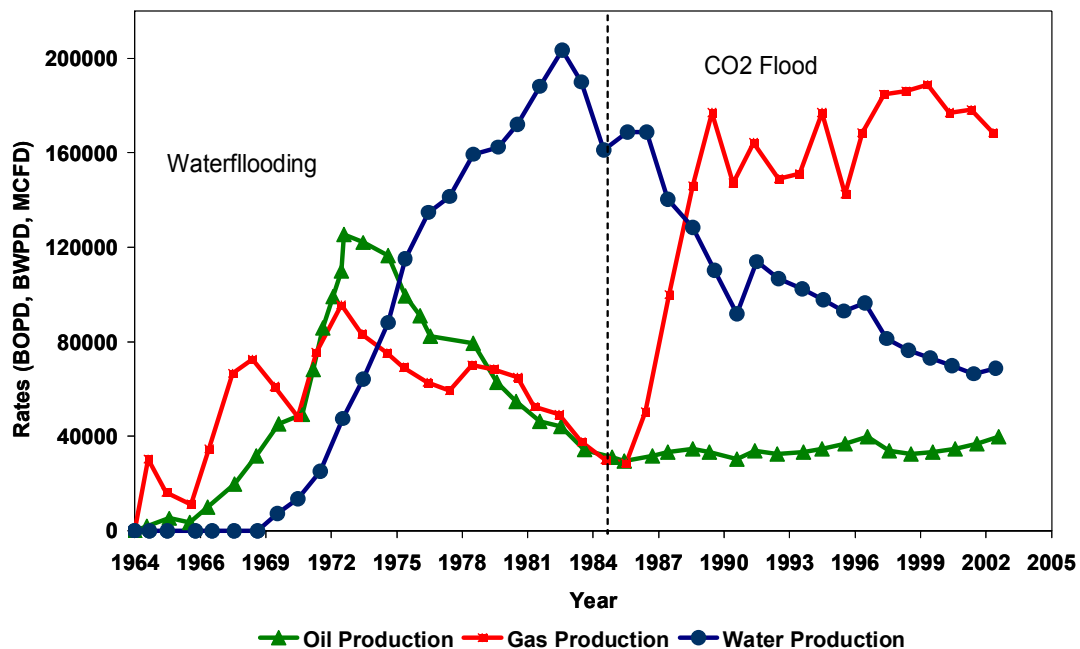


Figure 4.1- Denver Unit production performance.

### 4.3 CO<sub>2</sub> Flood Development

Following the success of the Denver Unit waterflood and the high waterflood residual oil saturations (approximately 40%), EOR process studies and laboratory experiments indicated that miscible CO<sub>2</sub> injection could result in significant EOR potential in this reservoir.

A CO<sub>2</sub> pilot was initiated in 1978, and analysis of this pilot confirmed that adequate CO<sub>2</sub> injection followed by water injection could be attained. The pilot also quantified the reduction in oil saturation resulting from CO<sub>2</sub> injection at waterflood residual oil saturation.

Following extensive coring and a brine pre-flood to establish the baseline oil saturations and a uniform reservoir pressure, CO<sub>2</sub> was injected at miscible conditions. The cored interval extended 50 ft below the estimated original oil/water contact, allowing the evaluation of CO<sub>2</sub> floodable oil saturation in the transition zone.<sup>38</sup>

Throughout the CO<sub>2</sub> and brine post-flood phases of the pilot, logging observation wells continuously monitored changes in oil saturation attributable to the CO<sub>2</sub> contacting and swelling, and displacement of the remaining oil. Post-flood cores confirmed the desaturation of oil interpreted from logging runs.<sup>18, 39, 40</sup>

In preparation for the CO<sub>2</sub> flood, the random waterflood pattern was converted into a nine-spot pattern (Figure 4.2). In addition, reservoir pressure was reduced from 3,200 psi to 2,200 psi in order to improve the volumetric efficiency of the CO<sub>2</sub> (and yet maintain reservoir pressures above the MMP of 1300 psi).<sup>39</sup>

Miscible carbon dioxide injection began in 1984 when nine-spot patterns were placed on CO<sub>2</sub> injection. Production response to CO<sub>2</sub> has been impressive, with over half of the current daily oil production attributable to CO<sub>2</sub> injection. In fact, oil production has substantially exceeded original project performance predictions.<sup>38</sup> Historical waterflood and tertiary performance of Denver Unit are shown in Figure 4.1.

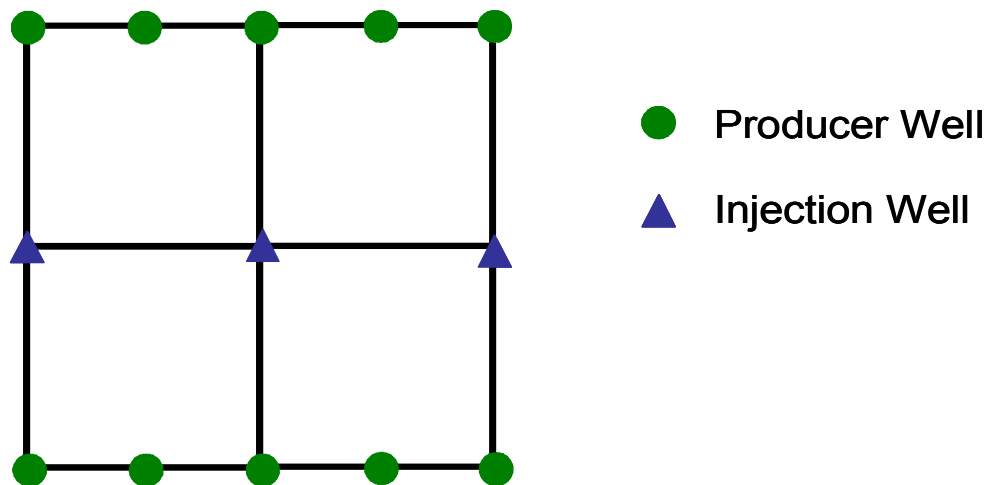


**Figure 4.2- Denver Unit typical well pattern configuration.**

To determine the best injection strategy for the Denver Unit, two simultaneous CO<sub>2</sub> floods were carried out in different areas of the reservoir. One area was operated under a continuous CO<sub>2</sub> injection flood, whereas in the other area, a Water-Alternating-Gas (WAG) CO<sub>2</sub> injection was implemented.

In both cases, an injection of a 40% hydrocarbon pore volume (HCPV) CO<sub>2</sub> slug was planned, followed by water injection until the economic limit was reached. The WAG operating scheme was used for mobility control to maximize flood profitability through improved sweep efficiency and to minimize the volume of the more expensive CO<sub>2</sub> required.

The early production performance of the continuous CO<sub>2</sub> injection flood area was very encouraging. Oil production response was observed soon after injection began (Figure 4.3) and the oil cut rose from a low of 14% to 31%. CO<sub>2</sub> response can be clearly seen on a plot of oil cut vs. cumulative production (Figure 4.4).

Following a short period of CO<sub>2</sub> injection, the oil cut deviated markedly upward from what would have been expected under continued waterflood conditions. Another indicator of EOR response in the early years of the CO<sub>2</sub> flood was the rising GOR as the

flood progressed. This increase in the GOR was a consequence of the stripping of the lighter hydrocarbon components out of the remaining oil as CO<sub>2</sub> contacts oil in the reservoir.

Wells located east to west of pattern injection experienced an earlier EOR response, whereas wells located north to south of CO<sub>2</sub> injectors, or diagonally to pattern injectors, responded more slowly to CO<sub>2</sub> injection. This oil response characteristic of the continuous area producers relative to their relative location in the nine-spot pattern suggests a permeability anisotropy favoring displacement oriented east to west

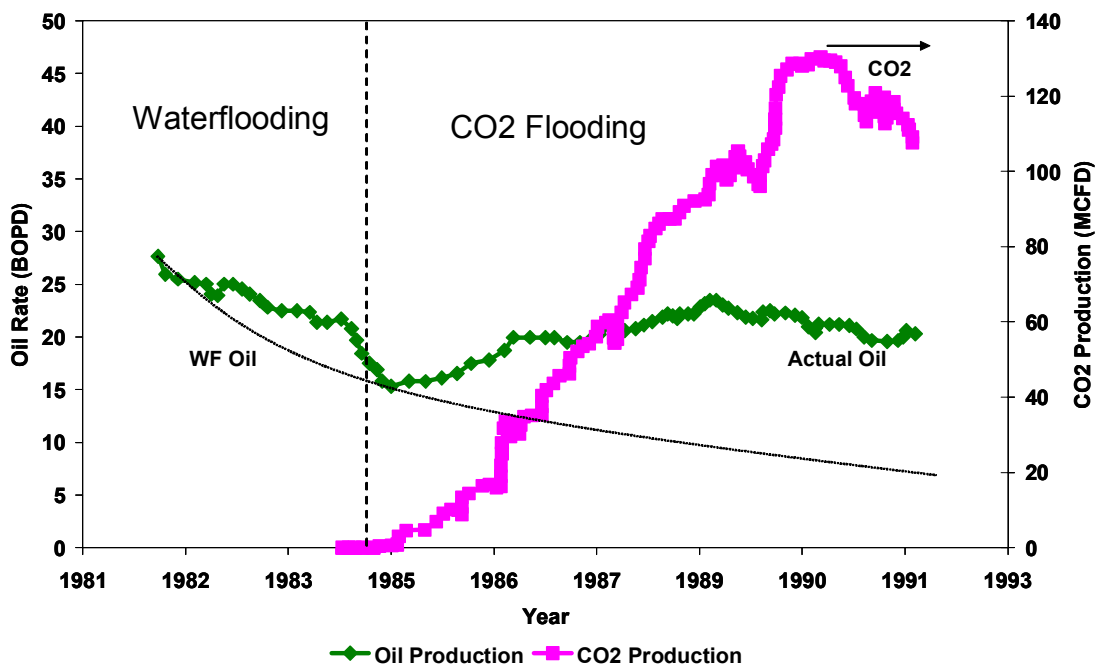


**Figure 4.3- Continuous CO<sub>2</sub> flood area production performance**<sup>14</sup>.

The WAG flood in the WAG area was started with a constant 1:1 gas/water ratio (1% HCPV CO<sub>2</sub> and 1% HCPV water). The original injection schedule involved injecting alternating 6-month slugs of CO<sub>2</sub> and water until a 40% HCPV slug of CO<sub>2</sub> had been injected. Injectivity problems in the WAG area prevented maintenance of the injection

rates at comparable levels with the continuous area, especially during the water-injection cycle. Low WAG injectivity, out-of-zone injection losses, and waterflood-induced fractures contributed to the poor EOR performance in the WAG area.<sup>39</sup> Oil production continued to decline with only a marginal improvement over the waterflooding for a number of years after CO<sub>2</sub> began (Figure 4.5)

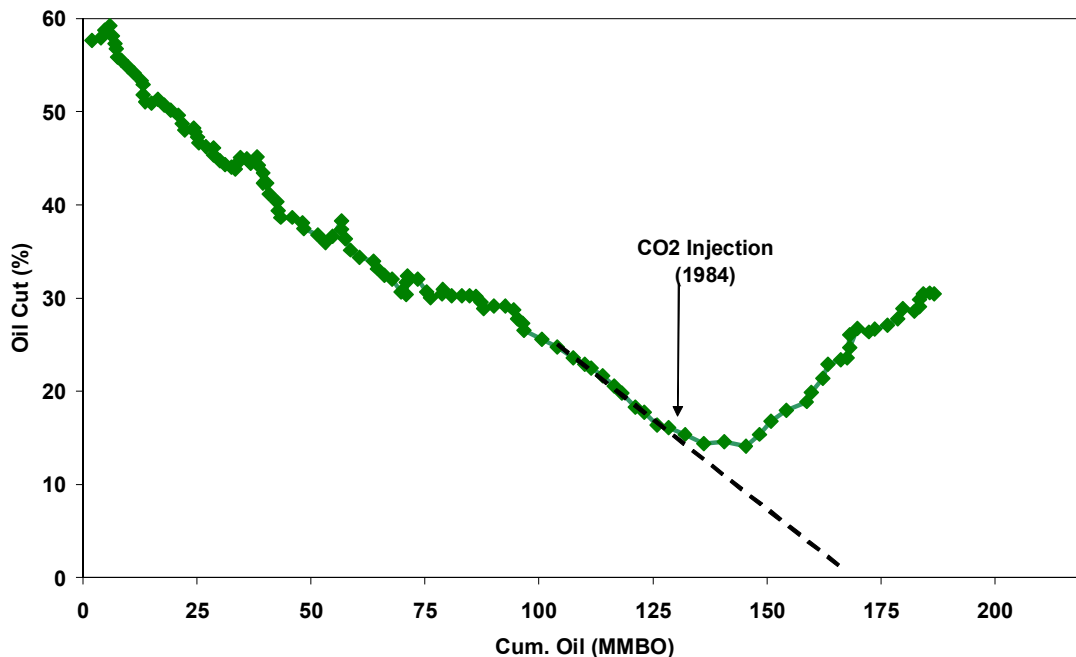


**Figure 4.4- Continuous CO<sub>2</sub> flood area oil cut vs. cumulative oil<sup>14</sup>.**

Reviews of the performance of the two EOR processes confirm the positive response of the continuous process while suggesting the long-term manageability advantages of WAG injection. Simulation models were used to analyze the long term performance of various flood options. The flood options included continuous CO<sub>2</sub> injection, 1:1 WAG ratio injection and Denver Unit WAG (DUWAG), which combines continuous injection and WAG processes. DUWAG flood suggested injecting four to six years of continuous CO<sub>2</sub> injection followed by 1:1 WAG.

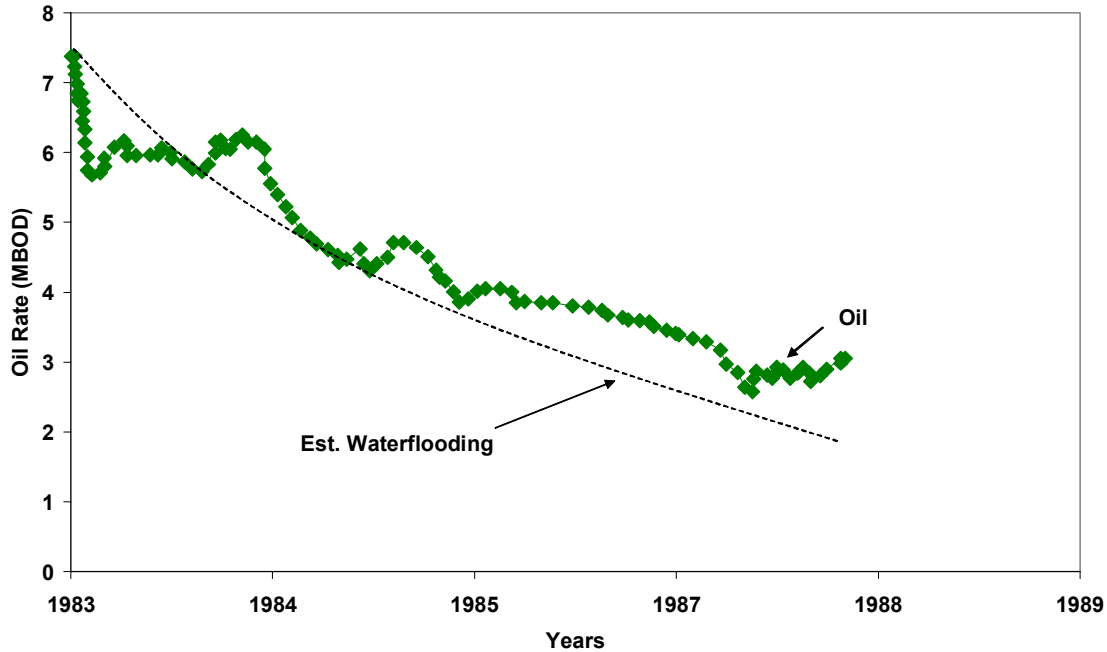


**Figure 4.5- WAG area oil production**<sup>14</sup>.

Simulation results showed that the DUWAG process offered most benefits for the field in terms of oil recovery since it combined the early EOR response of the continuous CO<sub>2</sub> injection and the higher ultimate recovery of the WAG injection (Figure 4.6). The DUWAG process was successfully implemented in the field and was rapidly extended to the continuous area which was converted to this new injection process.<sup>39</sup>

The heterogeneity of the field causes the CO<sub>2</sub> response to vary widely across the field, and so do the injectivity related problems such as injection losses in the WAG area, low water injectivity, and problems associated with flowing wells. For this reason, pattern tailored flood designs should be developed to address particular problems and conditions for a particular injection pattern.<sup>39</sup>

The ultimate goal of this strategy would be determining the best time to switch from continuous to WAG injection, the optimum WAG cycle length, the best WAG ratio and CO<sub>2</sub> optimum slug size.



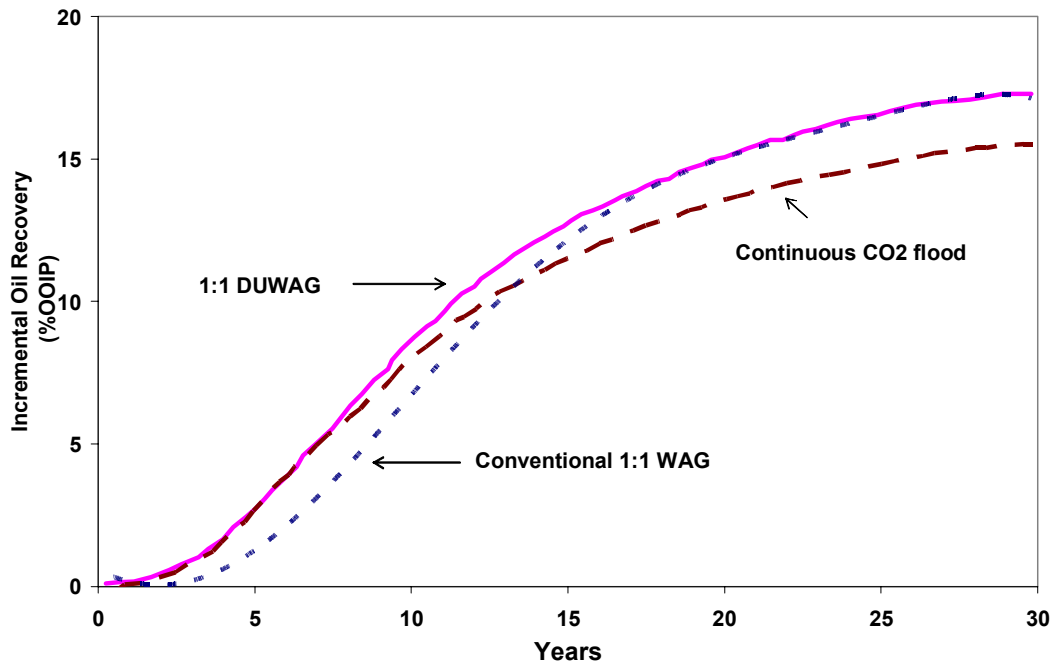


Figure 4.6- Cumulative incremental EOR recovery vs. time<sup>14</sup>.

## CHAPTER V

### SIMULATION PARAMETERS AND MODEL

In this chapter, the simulation parameters used in this simulation study are presented. Reservoir engineering techniques are applied to improve the understanding of the reservoir performance and fluid properties. The process includes the calibration of an EOS to describe the phase behavior of the reservoir fluid; input data tables for PVT fluid properties and rock-saturation dependent properties such as relative permeability; the initialization of the simulation model to assess the volume of the original hydrocarbon in place; and the history match to test the validity of the simulation model and prepare the model to predict future reservoir performance.

#### 5.1 Numerical Simulator

The simulator used was ECLIPSE 300<sup>41</sup> which is finite-difference compositional simulator with a cubic EOS, pressure-dependant K-value, and black oil fluid treatments. The simulator reproduces the major mass-transport and phase-equilibria phenomena associated with the miscible CO<sub>2</sub> flooding process. The ECLIPSE compositional simulator has several EOSs. These include the Redlich-Kwong, Soave-Redlich-Kwong, Soave-Redlich-Kwong 3-parameter, Peng-Robinson and Peng-Robinson 3-parameter. The simulator allows the complex description of CO<sub>2</sub>/oil phase behavior and CO<sub>2</sub> solution in aqueous phase.

#### 5.2 Fluid Properties

The reservoir oil is a saturated black oil with a stock tank gravity of 33°API and an initial GOR of 660 scf/stb. Initial reservoir pressure and bubble point pressure are 1,805 psi at a reference depth of 5,000 ft and 105°F (See Table 4.1). The CO<sub>2</sub> minimum miscibility pressure was determined experimentally to be 1,300 psi. Table 5.1 shows the fluid composition.

**Table 5.1- Reservoir fluid composition in mole fractions**

CO <sub>2</sub>	N <sub>2</sub>	C <sub>1</sub>	C <sub>2</sub>	C <sub>3</sub>	i-C <sub>4</sub>	n-C <sub>4</sub>	i-C <sub>5</sub>	n-C <sub>5</sub>	C <sub>6</sub>	C <sub>7+</sub>
0.0297	0.0040	0.0861	0.0739	0.0764	0.0095	0.0627	0.0159	0.0384	0.0406	0.5628
Temperature, °F:				105						
C7+ Molecular weight:				229						
C7+ Density @ 60 °F, gr/cm3:				0.88						

### 5.3 Equation-of-State Characterization

An essential part of a compositional reservoir simulation of a miscible EOR method is the prediction of the complex phase equilibria during EOR processes. The objective of the fluid study was to tune an EOS that would reproduce the observed fluid behavior and production characteristics seen in field operations and to predict the CO<sub>2</sub> /oil phase behavior in the compositional simulation.

Cubic EOSes have found widespread acceptance as tools that permit the convenient and flexible calculation of the phase behavior of reservoir fluids. They facilitate calculations of the complex behavior associated with rich condensates, volatile oils and gas injection processes.<sup>42</sup>

The tuning of the EOS in this work followed the methodology suggested by Kkan<sup>43</sup> to characterize CO<sub>2</sub> oil mixtures. The Peng Robinson<sup>44</sup> EOS was chosen to generate the EOS model because it has been found adequate for low-temperature CO<sub>2</sub>/oil mixtures<sup>43</sup>. The viscosity model considered to match the oil viscosity of the reservoir fluid was the Lohrenz-Bray-Clark (LBC) model,<sup>45</sup> which is a predictive model for gas or liquid viscosity.

PVT laboratory sample data of the San Andres Formation were used in the tuning of the EOS. PVT laboratory data included differential liberation (DL) experiments, constant-composition-expansion (CCE), and swelling and separator tests. These data were used

to tune an EOS capable of characterizing the CO<sub>2</sub>/reservoir-oil system above the minimum miscibility pressure (MMP).

Table 5.2 lists the experiments and the measured parameters loaded into the PVT software.

**Table 5.2- P.V.T experimental data**

<b>Reservoir Fluid Composition</b>	Mole fractions, C <sub>7+</sub> density and molecular weight
<b>Constant Composition Expansion</b>	Relative volumes, saturation pressure, oil density
<b>Separator Test</b>	Gas/oil ratio, $B_g$ , FVF
<b>Differential Liberation</b>	GOR, relative oil volume, gas $Z$ factor, oil density, FVF
<b>Injection Test</b>	Swelling test

Each laboratory experiment was first simulated with the cubic Peng Robinson EOS without performing any regression and compared to the laboratory observations (PVT). The preliminary results after the simulation were fairly good, demonstrating that the behavior of the fluid was being reproduced with a basic (not yet tuned) EOS; however, some experiments were not fully matched. This was a clear indication that the parameters of the EOS needed some adjusting in order to reproduce the behavior of the reservoir fluid.

Figures 5.1 through 5.6 show the preliminary match of the experiments by the basic EOS.

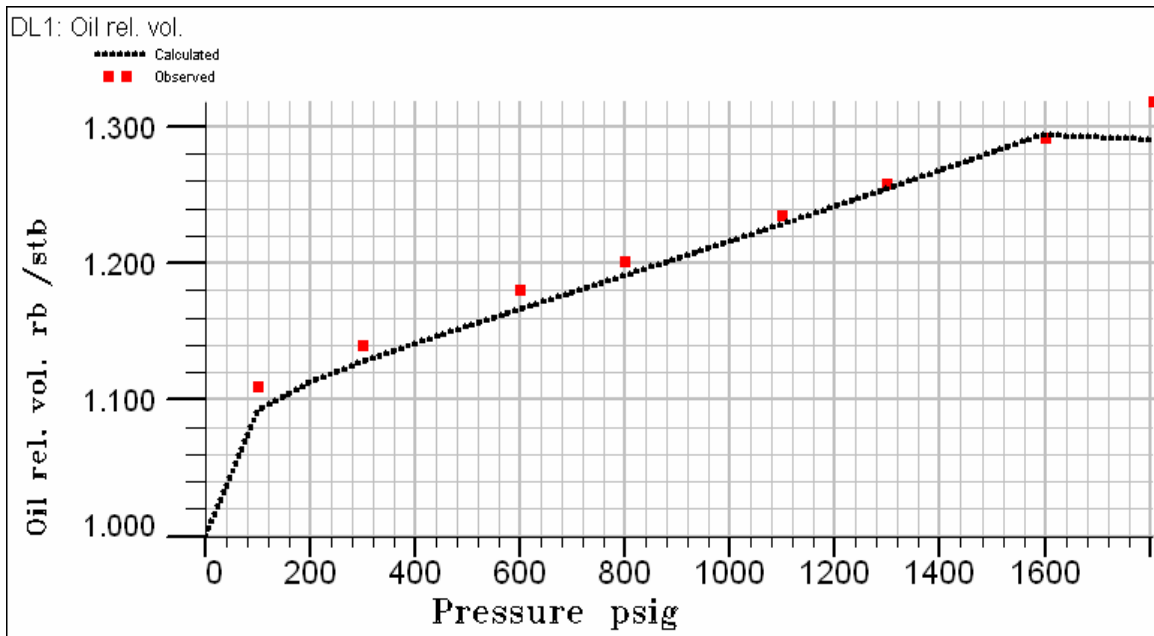


Figure 5.1- Preliminary match for the oil FVF.

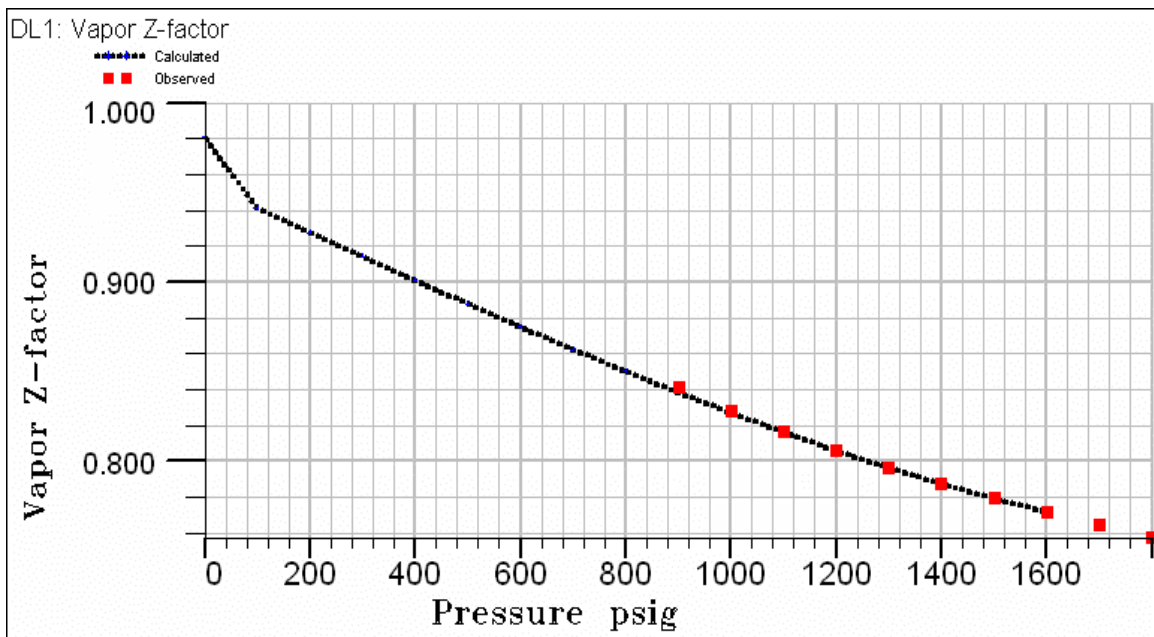


Figure 5.2- Preliminary match for the deviation factor (Z).

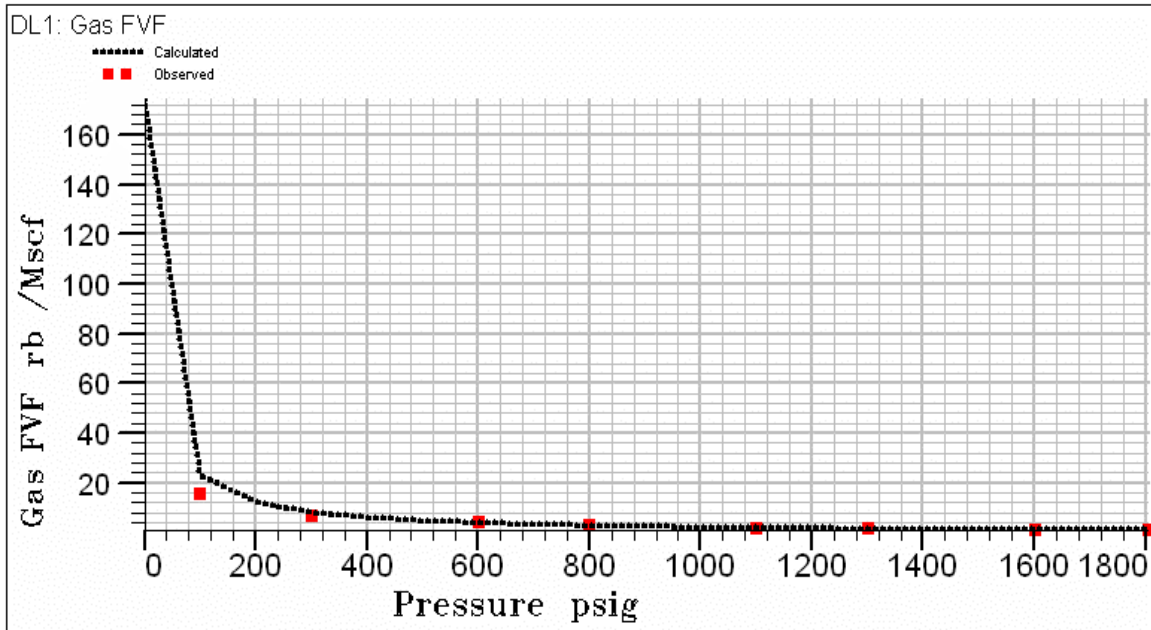


Figure 5.3- Preliminary match for the gas FVF.

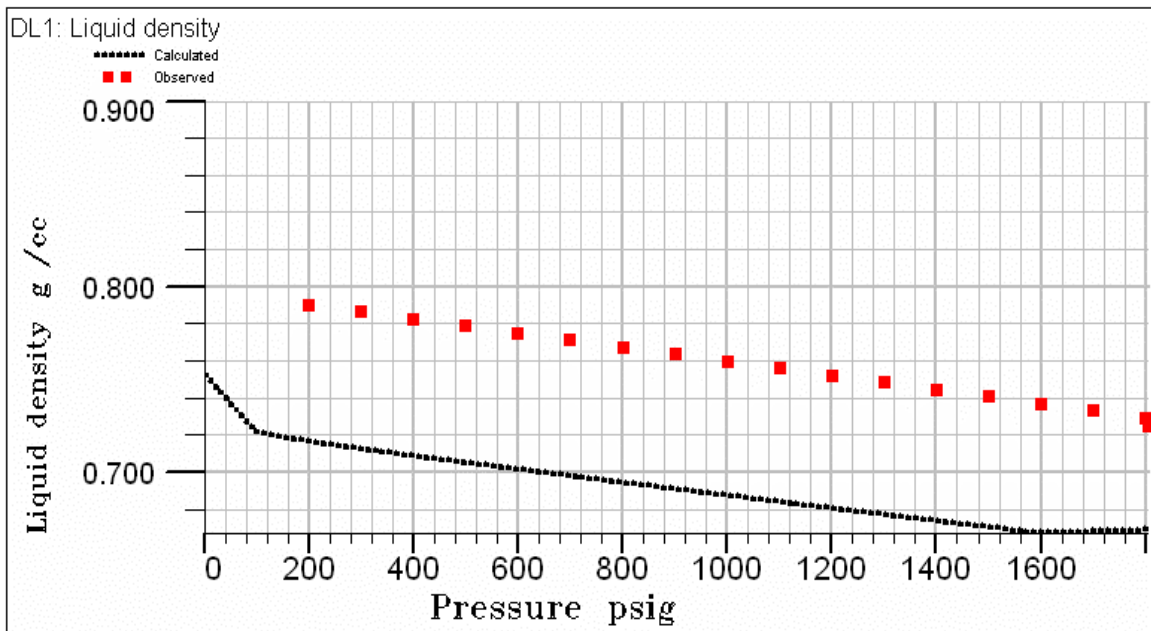


Figure 5.4- Preliminary match for the oil density ( $\rho_o$ ).

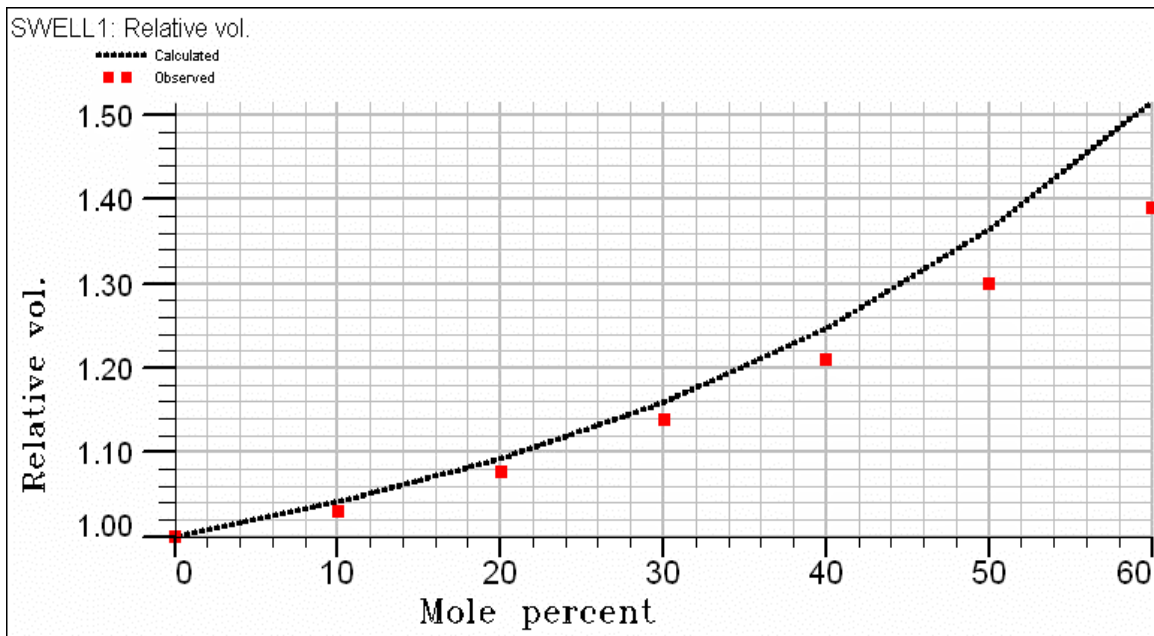


Figure 5.5- Preliminary match for the CO<sub>2</sub> swelling factor.

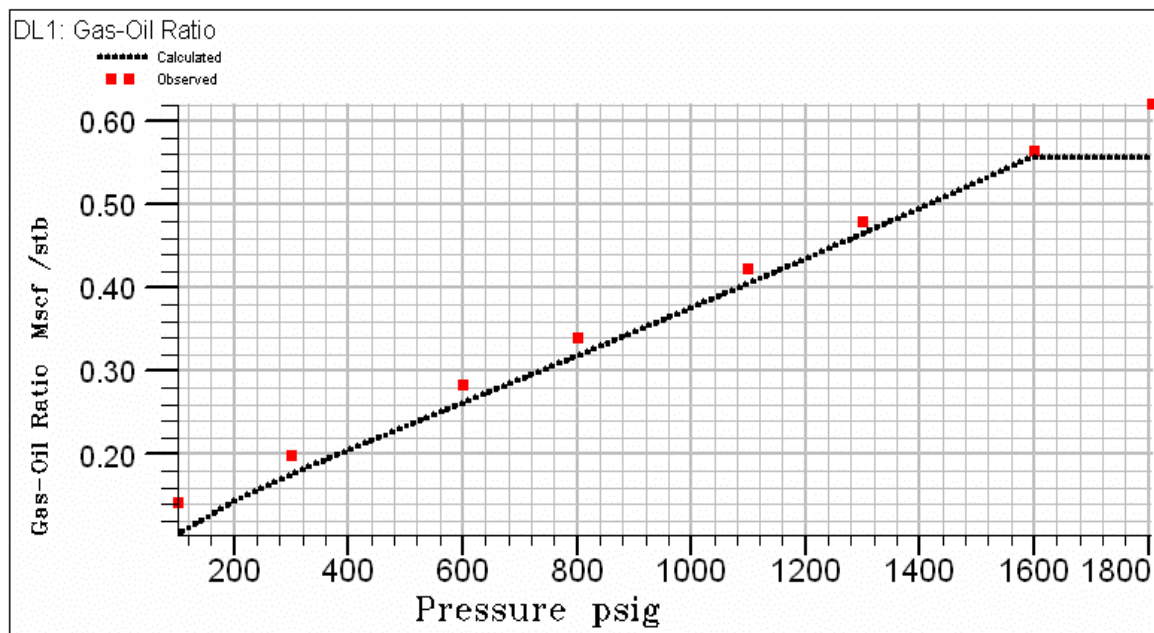


Figure 5.6- Preliminary match for the GOR.

Next step was to tune or characterize the EOS so that it is able to reproduce the PVT experiments. This was a multistep process that started by the splitting the heavy component as proposed by Whitson.<sup>46</sup> Whitson's method uses a three-parameter gamma probability function to characterize the molar distribution (mole fraction/molecular weight relation) and physical properties of petroleum fractions such as heptanes-plus ( $C_7+$ ). This method is used to enhance the EOS predictions.

The heavy component ( $C_7+$ ) was split into three pseudocomponents based on its relative mole fraction as suggested by Khan.<sup>43</sup> The pseudocomponents were identified as  $C_7+(1)$ ,  $C_7+(2)$  and  $C_7+(3)$ . By splitting the heavy component ( $C_7+$ ), the total number of components of the reservoir fluid was then increased from 11 to 13 components. This 13-component mixture was used to tune the EOS by regressions to match the observations.

Since a single heptanes-plus ( $C_7+$ ) fraction lumps thousands of compounds with a carbon number higher than seven, the properties of the heavy component  $C_7+$  are usually not known precisely, and thus represent the main source of error in the EOS and reduce its predictive accuracy. For this reason, regressions were performed against the pseudocomponents to improve the EOS predictions.

Several regressions were carried out during the process of tuning the EOS. The first regression was performed on all the experiments against the critical pressure of the pseudocomponents,  $C_7+(1-3)$ . The results provided very good predictions with little error when compared against PVT data.

In general, the regression parameters were basically the  $C_7+(1$  to 3) pseudocomponents critical pressure ( $P_c$ ), critical temperature ( $T_c$ ), acentric factor ( $\omega$ ) and binary interaction coefficients ( $\delta$ ). The shift parameters of the  $C_7+(1$  to 3) pseudocomponents were also regressed together, so that changes within the  $C_7+$  fraction were consistent.



For the simulation of CO<sub>2</sub> miscible EOR processes, the EOS must be capable of predicting phase equilibria over a wide range of CO<sub>2</sub> compositions. For this reason, CO<sub>2</sub>/hydrocarbon binary interaction parameters (BIC) were numerically regressed to achieve the match of the swelling-test experimental data.

After a satisfactory match of all the experimental data, the next step was to group the 13-component EOS into a reduced pseudocomponent EOS acceptable for a compositional simulation. Doing this reduction, minimized the computational time constraint and the numerical complexity of the simulation.

The methodology for a stepwise regression presented by Fevang<sup>47</sup> was used for the lumping process from 13 to 10 components. The Fevang lumping process consisted of forming new pseudocomponents from existing components. Then regressions were performed to fine-tune the newly-formed pseudocomponent EOS properties. This process was repeated a number of times to select the best grouping at each stage in the pseudoization process.

Since various combinations of grouped components are possible, the criteria for grouping were selecting components with similar properties and molecular weight and having as few components as necessary to match the PVT experiments.

A series of grouping exercises were performed. First, a 10-component EOS model was obtained after grouping C<sub>1</sub>+N<sub>2</sub>, i-C<sub>4</sub>+n-C<sub>4</sub>, and i-C<sub>5</sub>+n-C<sub>5</sub>, leaving the remaining components ungrouped.

The regression parameters to tune the EOS were the critical properties of the newly formed pseudocomponents. After performing these regressions, the PVT properties of the 10-component EOS model matched the 13-component EOS model almost exactly.

From the 10-component EOS model, another grouping was conducted. The C<sub>7+</sub> pseudo components, C<sub>7+</sub>(1 to 3), were grouped into a single fraction (C<sub>7+</sub>). Additionally, C<sub>2</sub> + C<sub>3</sub> and i-C<sub>4</sub> + n-C<sub>4</sub> + i-C<sub>5</sub> + n-C<sub>5</sub> + C<sub>6</sub> were also lumped together. With this grouping a

6-component EOS model was obtained. The 6-component EOS model contained the following components: ( $\text{CO}_2$ ); ( $\text{N}_2$ ,  $\text{C}_1$ ); ( $\text{C}_2$ ,  $\text{C}_3$ ); ( $\text{C}_4$ ); ( $\text{C}_5$ - $\text{C}_6$ ), and ( $\text{C}_7+$ ). Regression was performed again, and the 6-component EOS model predicted PVT properties very similar to the 10-component EOS model. This EOS was accepted for use in simulation.

As a final step, regression was performed against both gas and oil viscosity to ensure correct estimation of reservoir fluid viscosity. Regressions against the critical-volume ( $Z_c$ ) variable were carried out to predict realistic values of viscosity.

Figures 5.7 through 5.12 show the comparison of results of selected experiments. As can be seen, the results provided very good predictions when compared against the observations.

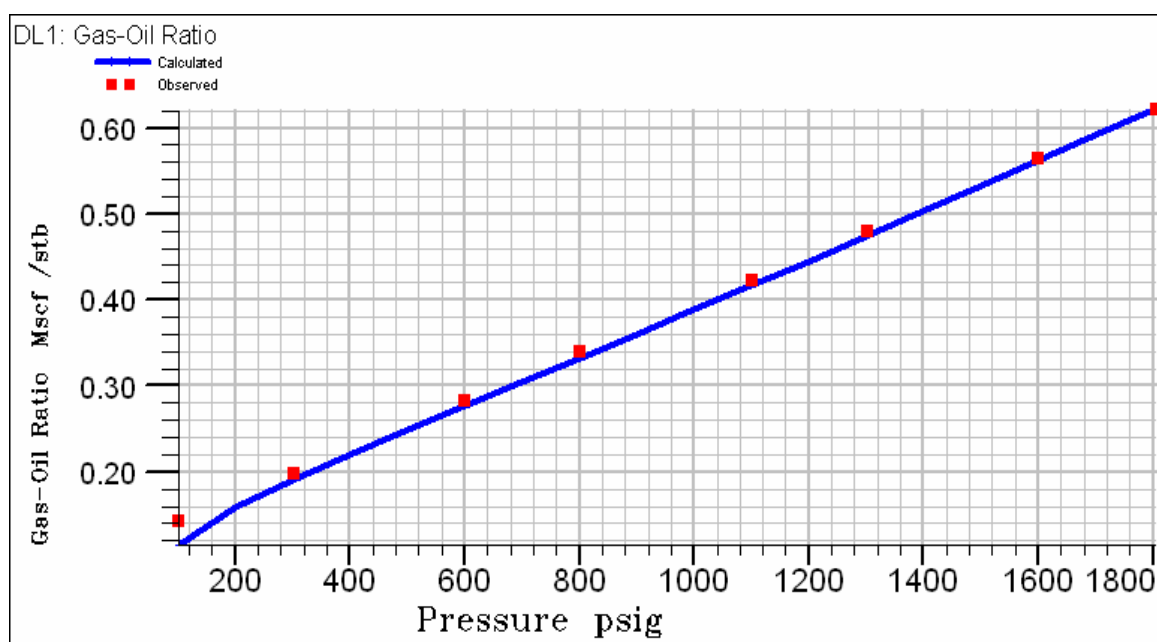


**Figure 5.7- Comparison of the predicted and observed values for the GOR.**

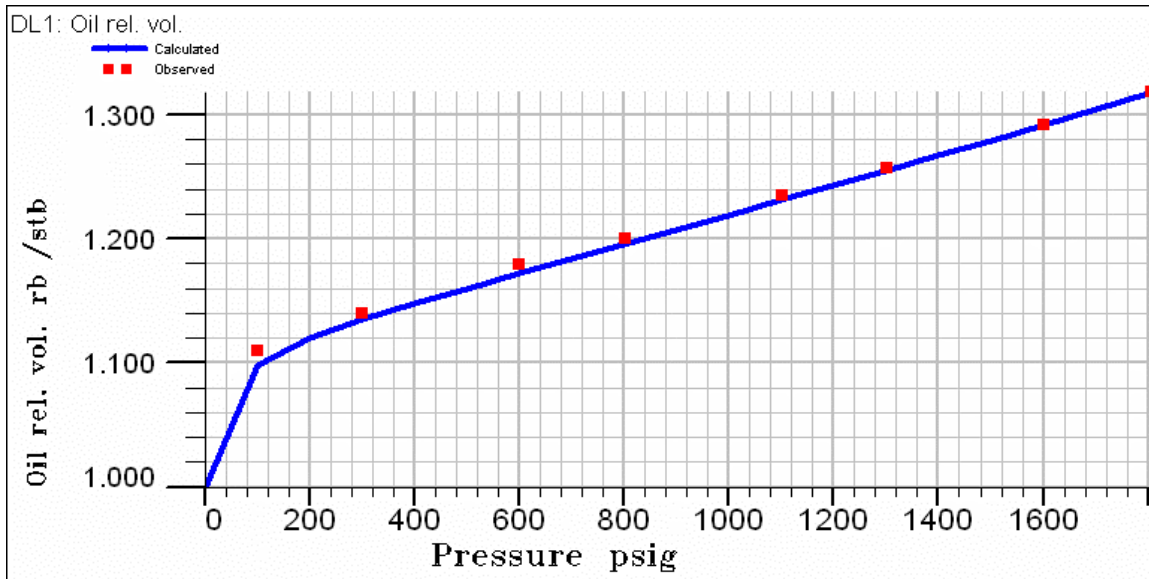


**Figure 5.8- Comparison of the predicted and observed values for the oil FVF.**

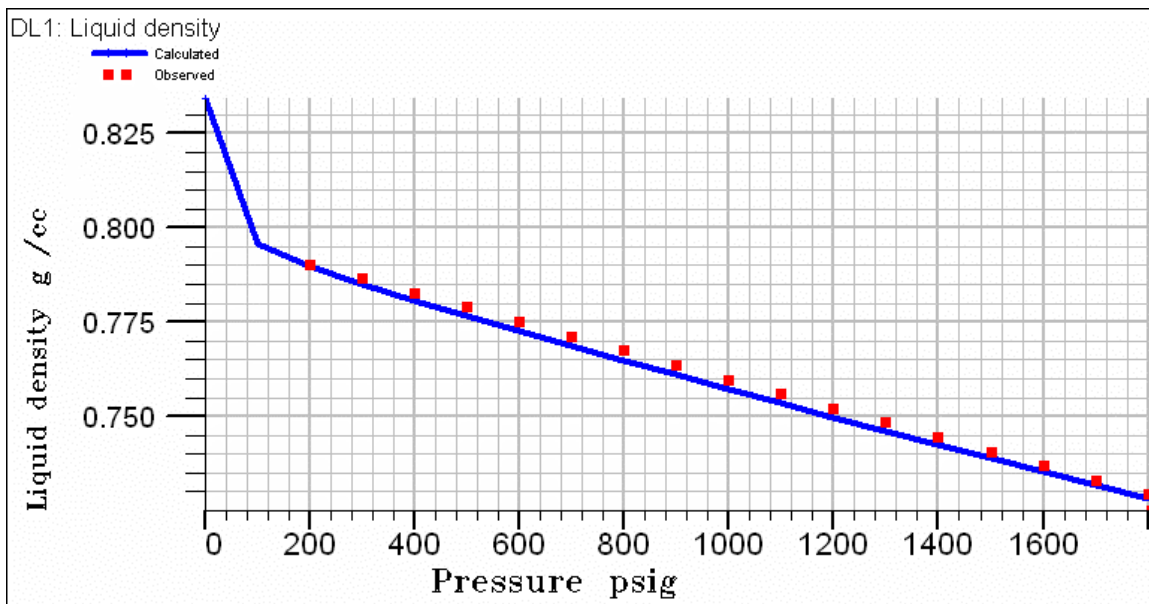


**Figure 5.9- Comparison of the predicted and observed values for oil density ( $\rho_o$ ).**

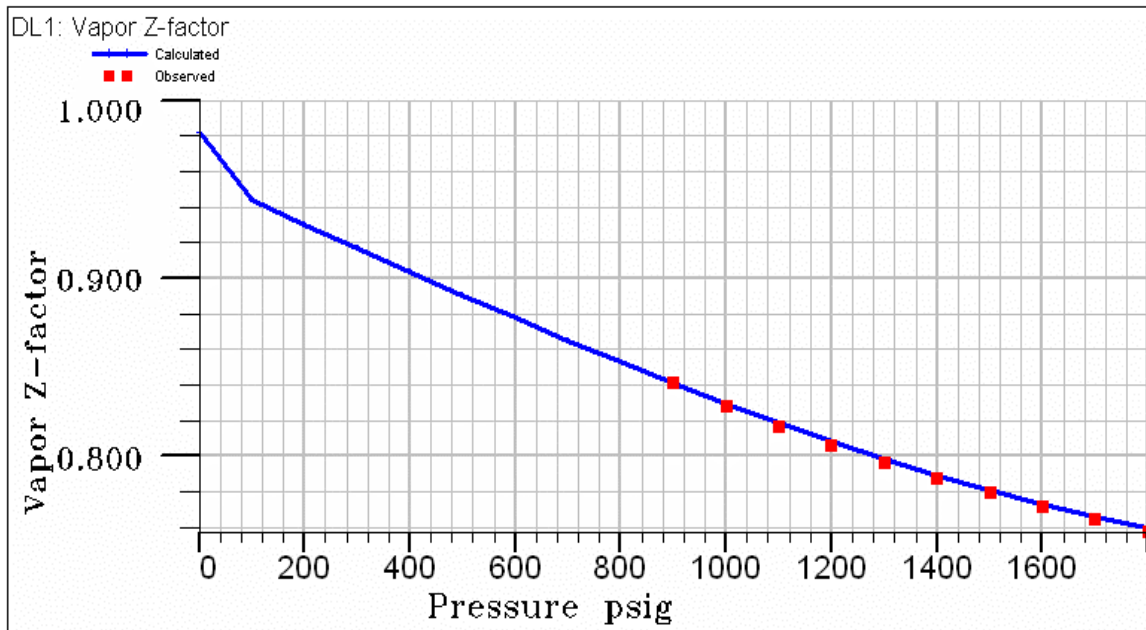


**Figure 5.10- Comparison of the predicted and observed values for the gas deviation factor (Z).**

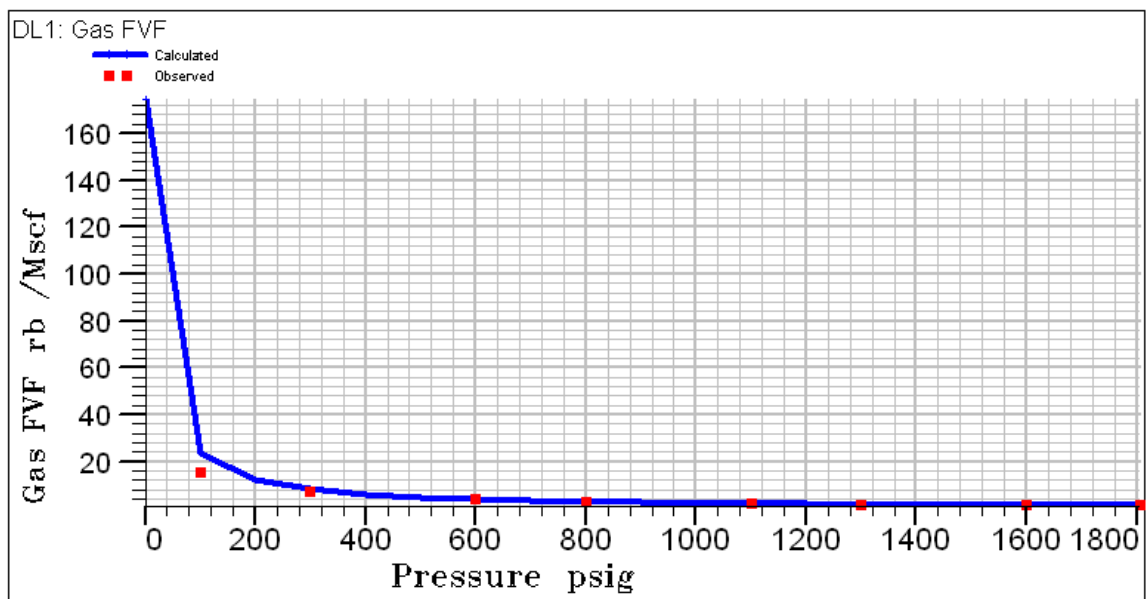


**Figure 5.11- Comparison of the predicted and observed values for the gas FVF.**

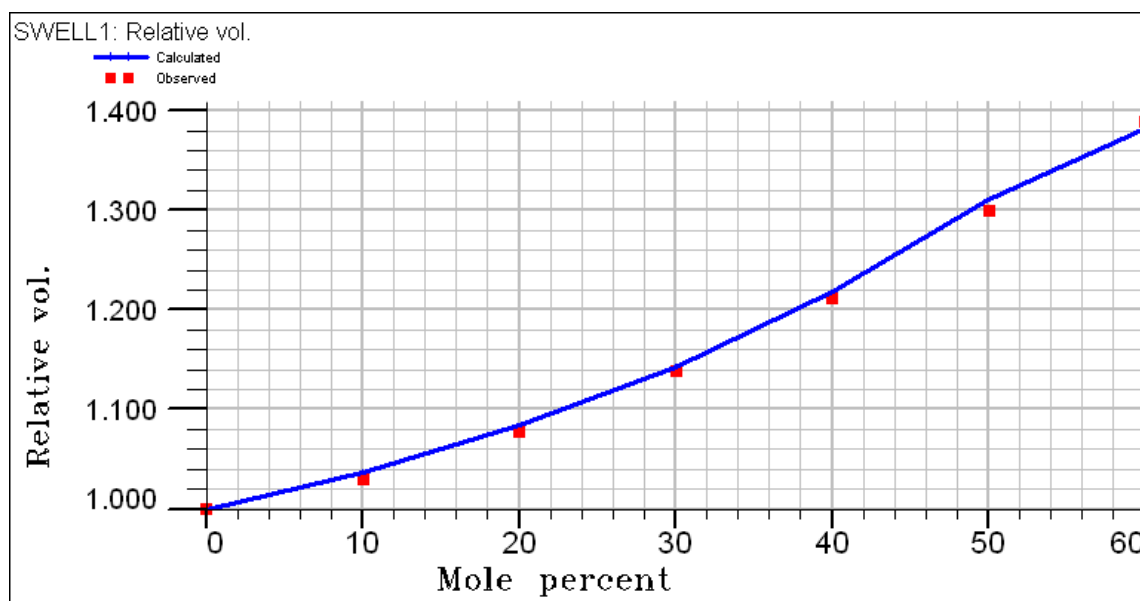


**Figure 5.12- Comparison of the predicted and observed values for the CO<sub>2</sub> swelling factor.**

Table 5.3 summarizes the best fit parameters of Peng-Robinson EOS for Denver Unit reservoir fluid.

**Table 5.3- Fluid description for San Andres reservoir fluid**

Component	Mw	Pc (psig)	Tc (R)	Omega A	Omega B	Acentric Factor	V Crit (ft <sup>3</sup> /lb-mole)	Z Crit
CO2	44.01	1056.6	548.46	0.4572	0.0778	0.2250	1.5057	0.2741
N2C1	16.14	651.63	342.12	0.4572	0.0778	0.0132	1.5688	0.2847
C2C3	37.42	646.69	610.46	0.4572	0.0778	0.1268	2.8070	0.2834
INC4	58.12	527.79	753.72	0.4572	0.0778	0.1949	4.1332	0.2772
C5C6	80.50	387.02	822.01	0.4572	0.0778	0.1584	6.1030	0.2779
C7+	220.00	262.79	1283.4	0.4572	0.0778	0.7040	11.5740	0.2332

#### 5.4 Relative Permeability

The two-phase oil/water at  $S_g = 0$  and gas/oil relative permeability curves used for the waterflood simulation are shown in Figures 5.13 and 5.14. The relative permeability data are based on laboratory analyses. To avoid complication and make the model

simulation simple, this set of curves was used to describe both the oil column and the transition zone.

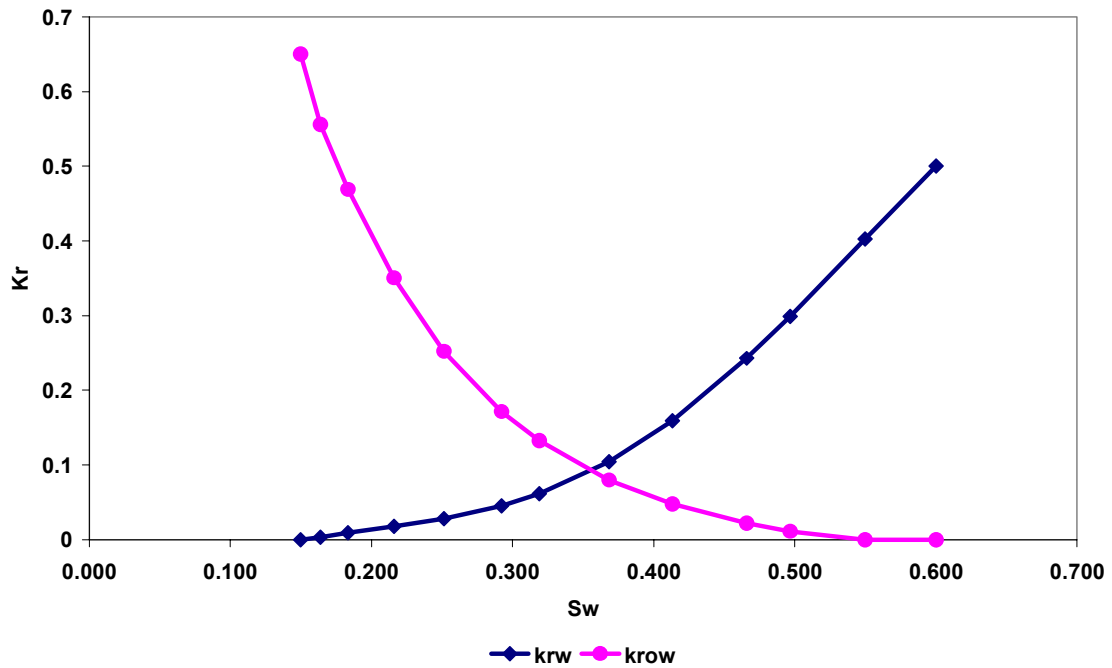


**Figure 5.13- Water and oil relative permeability curves as a function of water saturation.**

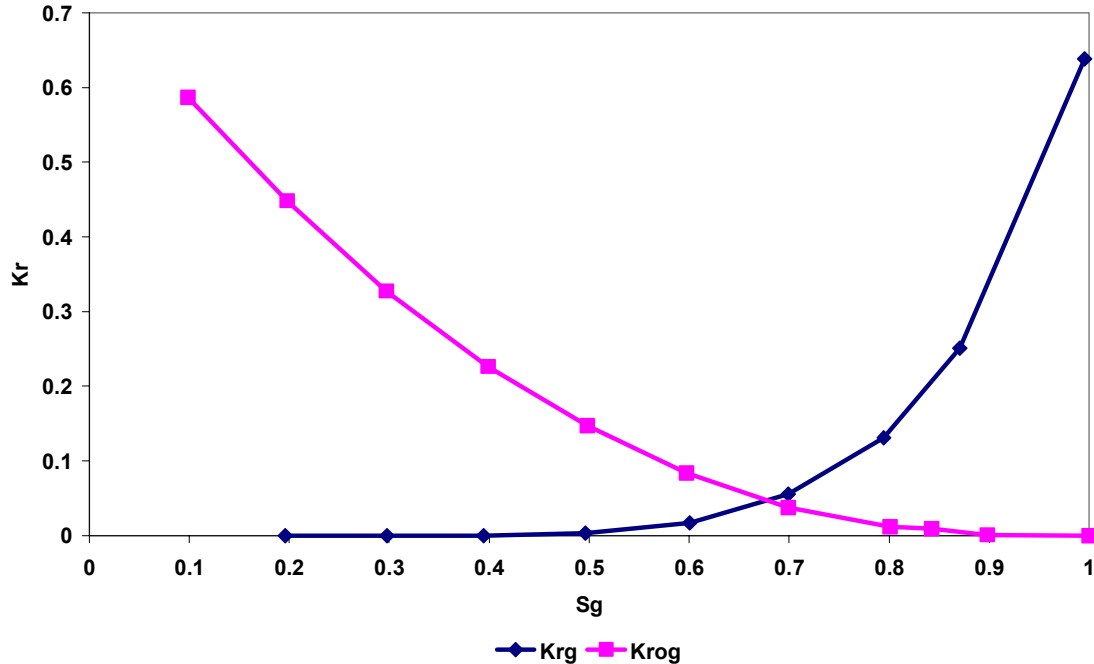


**Figure 5.14- Gas and oil relative permeability curves as a function of gas saturation.**

Figure 5.13 shows that the oil relative permeability declines as the water saturation increases in the pore volume and restricts the flow of oil. As oil relative permeability decreases, so does velocity, and eventually the oil ceases to flow. The maximum oil relative permeability is 0.65 at connate water saturation,  $S_{wc} = 15\%$ . At 60% water (40% residual oil saturation to water,  $S_{or}$ ), the oil relative permeability is zero. As water is injected, the water relative permeability increases, reaching a maximum value of 0.5 at 60% water saturation.

During a WAG injection, each cycle of water injection is of an imbibition type, whereas as soon as gas injection begins the process will switch to the drainage flow. Therefore, the hysteresis effects have to be considered. Hysteretic effects on the relative

permeability curves were included in the simulation model to consider the impact of saturation cycles as water and gas slugs move through the reservoir.

Hysteresis refers to the directional saturation phenomena exhibited by many relative permeability and capillary pressure curves. In many porous media, relative permeability values can have different values when a given phase saturation is being increased than when it is being reduced.<sup>48</sup>

The hysteresis effects in this work were represented by a model based on two-phase flow. The two-phase model considers the trapping of the non wetting phase and permeability reduction when the saturation change direction is reversed.

Figure 5.15 shows the relative permeability curves used in the simulation model for the WAG process. Imbibition and secondary drainage curves are shown. The water relative permeability curves show the expected behavior by consolidated media, where the imbibition curve lies below the drainage curve.

The major characteristic of the hysteresis curve is the increase in the connate water saturation from 15% on imbibition to 25% on secondary drainage. This increase occurs because the water is trapped by the wetting oleic phase during the secondary drainage. This trapped water reduces the water relative permeability on secondary drainage and also reduces the oil end-point relative permeability.

Since the San Andres Formation is an oil-wet reservoir, the oil relative permeability curve does not exhibit any hysteresis, and oil can flow back through the same pores along the same drainage relative permeability path.

Water permeability hysteresis may have a negative influence in an oil-wet reservoir performance. One of the adverse effects is a severe reduction of the water injectivity, additionally, oil relative permeability can not return to its maximum value (at  $S_{wc}$ ) because the increased residual water saturation reduces the maximum oil saturation possible, causing low tertiary production oil rates.<sup>7</sup>



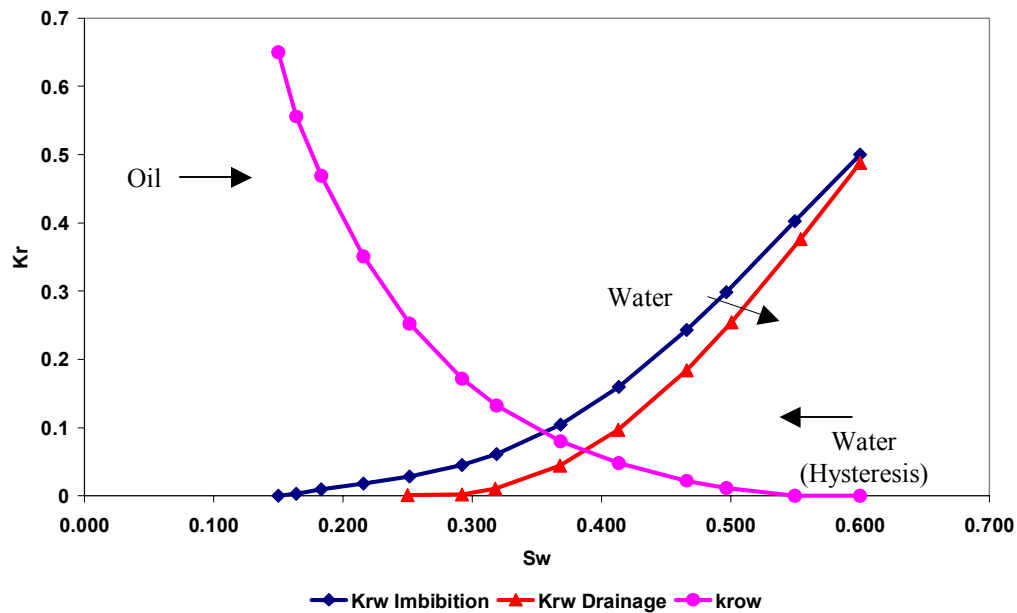


**Figure 5.15 Imbibition and secondary drainage water relative permeability (hysteresis).**

### 5.5 Reservoir Model

The reservoir model for the simulation study is a quarter of an 80-acre inverted nine spot pattern. The model covers 20 acres and contains 3 production wells (NS-Prod, EW-Prod and Diag-Prod) and one injection well (Inj). Both production and injection wells are vertical and completed in all the layers of the simulation model. There are 4,800 cells in the model with 49.12 ft on the sides. Areal gridding sensitivities provided the grid size needed for the model. The 20 x 20 grid design provided satisfactory results when compared to more finely gridded models. Figure 5.16 shows an areal view of the 20 x 20 x 12 simulation grid for the Denver Unit Pattern 48.

The geologic description provides the defining layers of the simulation model. Twelve different layers described in the geologic model represent the actual geology. Simulation layers were constructed to represent the actual reservoir zonation and resemble actual flow units.

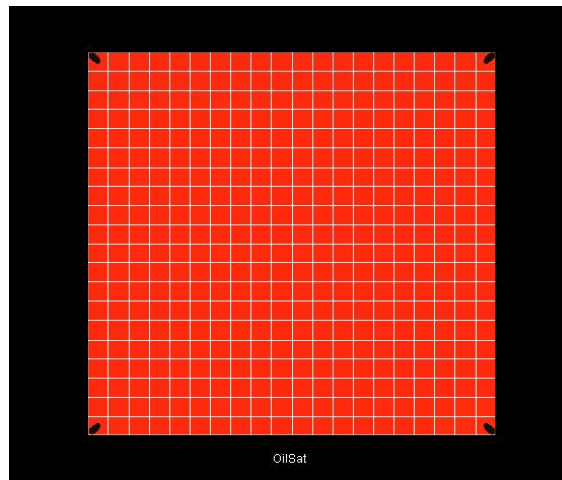


**Figure 5.16 Simulation grid for Denver Unit section 48.**

Layer thicknesses were determined from marker tops in well logs. Average porosity for each layer was calculated from sonic logs between markers. Permeabilities were calculated from  $\phi/k$  correlations derived from core measurements.<sup>38</sup> There are no areal variations of thickness, porosity and permeability across each single simulation layer. Table 5.4 lists the values of permeability, porosity and net pay of each of the layers in the simulation model.

**Table 5.4- Net pay, porosity and permeability in the simulation model**

<b>Layer</b>	<b>Net Pay (Ft)</b>	<b>Porosity</b>	<b>Kx (md)</b>
F4	10.50	0.102	0.767
F4/F5	37.50	0.114	1.212
M1	19.00	0.125	6.002
M1	9.50	0.177	23.00
M1	6.00	0.151	12.43
M2	20.50	0.106	3.352
M2/M3	37.50	0.090	1.765
M3	12.50	0.142	10.82
M3	46.00	0.099	2.562
M4	15.00	0.067	0.630
M4	28.50	0.105	2.707
M4/M5	50.00	0.107	2.880

## 5.6 Initial Conditions

The reservoir model was initiated at a uniform pressure of 1,805 psia and constant temperature of 105°F. The initial water saturation from the relative permeability curve was 0.15. Initial oil saturation within the gridblocks was 0.85.

The geologic model provided an estimate of OOIP of 2.29 million bbls at initialization.

## 5.7 History Match

Usually the only way to test the validity of a model is to simulate past performance of the reservoir and compare the simulation results with historical performance.

The pattern was history matched for both waterflood (from 1970 to mid 1986) and CO<sub>2</sub> flood (from mid 1986 to 2004). The oil production and injection rates were specified in each well and the model reproduced the reservoir pressure and the gas and water production. The quality of the history match was judged from how well the simulated water and gas production and reservoir pressure fitted historical data.

An important factor of the numerical modeling of the CO<sub>2</sub> and water advance through each of the layers was the understanding of the reservoir heterogeneities and the identification of the main flow channels. This allowed for the identification of the distribution of the remaining oil and gas in place.

For the history match, the relative permeability curves were slightly adjusted to obtain a better producing water/oil ratio (WOR). The relative permeability curves were normalized so that the end-point of the oil and water relative permeability at the connate water saturation and the residual oil saturation was equal to 1.

Additionally, well connection factors to the simulation grid were because most of the wells have been fractured and the wells's permeability-thickness product,  $kh$ , and the skin factor,  $S$ , were unknown. Since the connection factor is calculated from the cell properties, cell geometry and completion information, modification of the connection

factor was accomplished by enlarging the completion interval of the production wells to account for the effect of hydraulic stimulation.

During the WAG process, equal volumes of water and gas (at reservoir conditions) were injected during each slug resulting in a WAG ratio of approximately 1. This WAG ratio was kept constant for the CO<sub>2</sub> flood history match.

During the waterflood period, water cut match is fairly good at early times. However, the overall water production matches very well. A reasonable match of the gas production was also obtained. Figure 5.17 through 5.19 contrast historical and simulated gas and water production during the history match period.

Unfortunately, there is a lack of pressure data throughout the producing life of the reservoir. The reservoir pressure in the pattern increases up to 3,150 psi during the waterflood period, then decreases to 1,850 psi right before the CO<sub>2</sub> injection starts. According to previous studies on the production performance of the Denver Unit CO<sub>2</sub> flood,<sup>39</sup> the reservoir pressure was reduced from 3,200 psi to 2,200 psi in preparation for the CO<sub>2</sub> flood to improve the volumetric efficiency of the CO<sub>2</sub>. Figure 5.20 shows the predicted average reservoir pressure performance for the model area.

Oil and water production from individual wells was also very good. The predicted simulation production compared to actual production for the wells completed in the pattern are shown in Figures 5.21 through 5.26. This indicates that the simulation model was calibrated and can be used for making future predictions of reservoir performance.

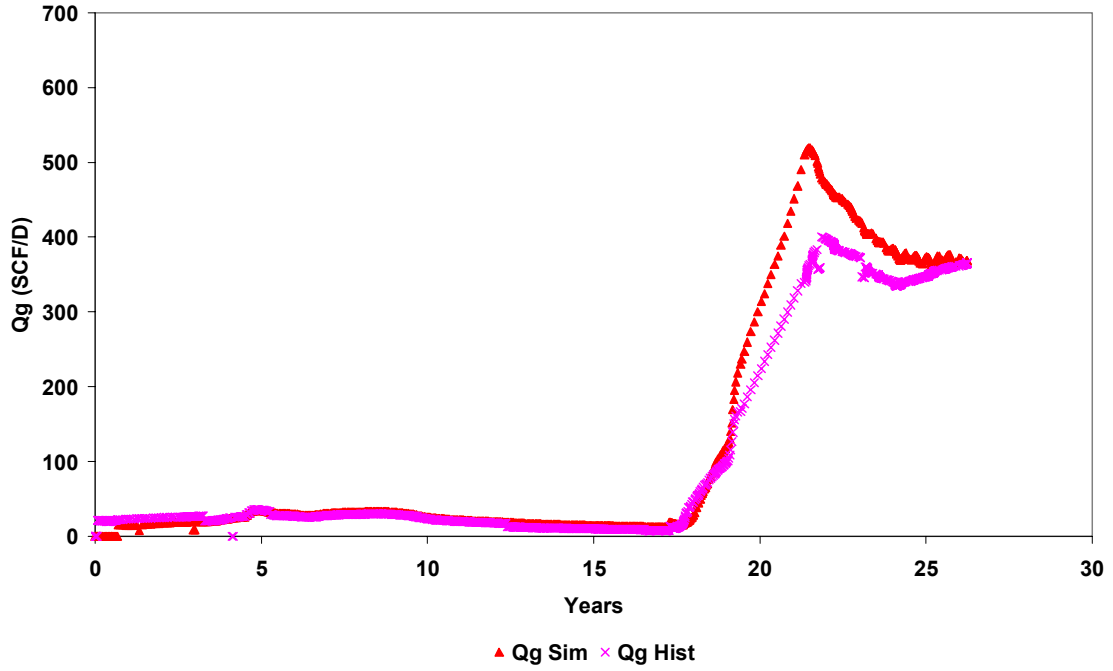


Figure 5.17- Gas production history match.

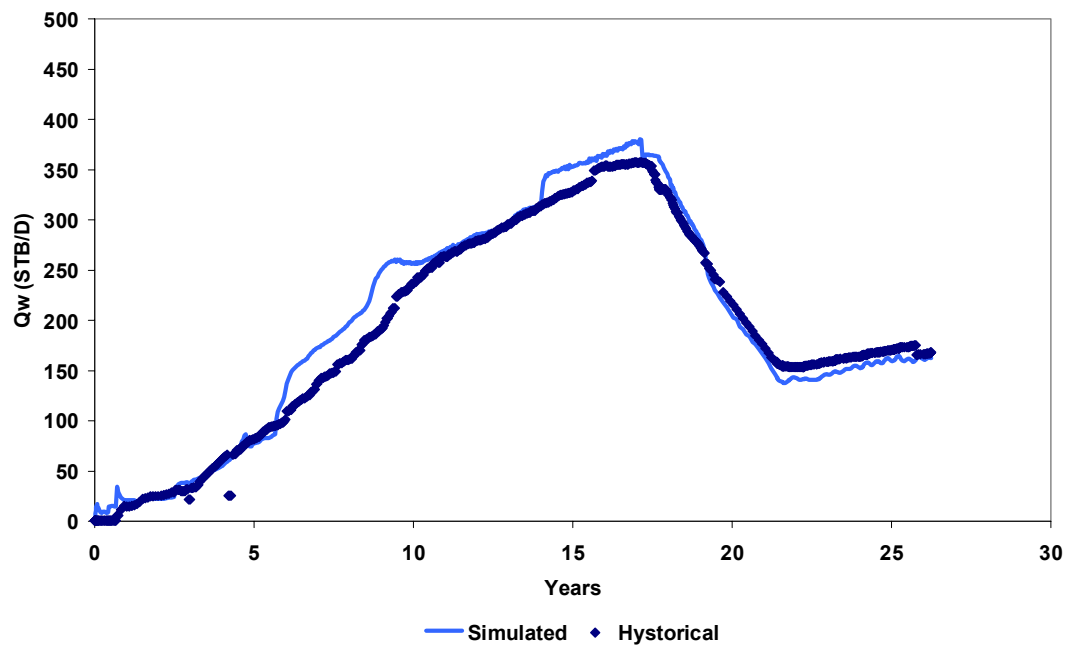


Figure 5.18- Water production history match.

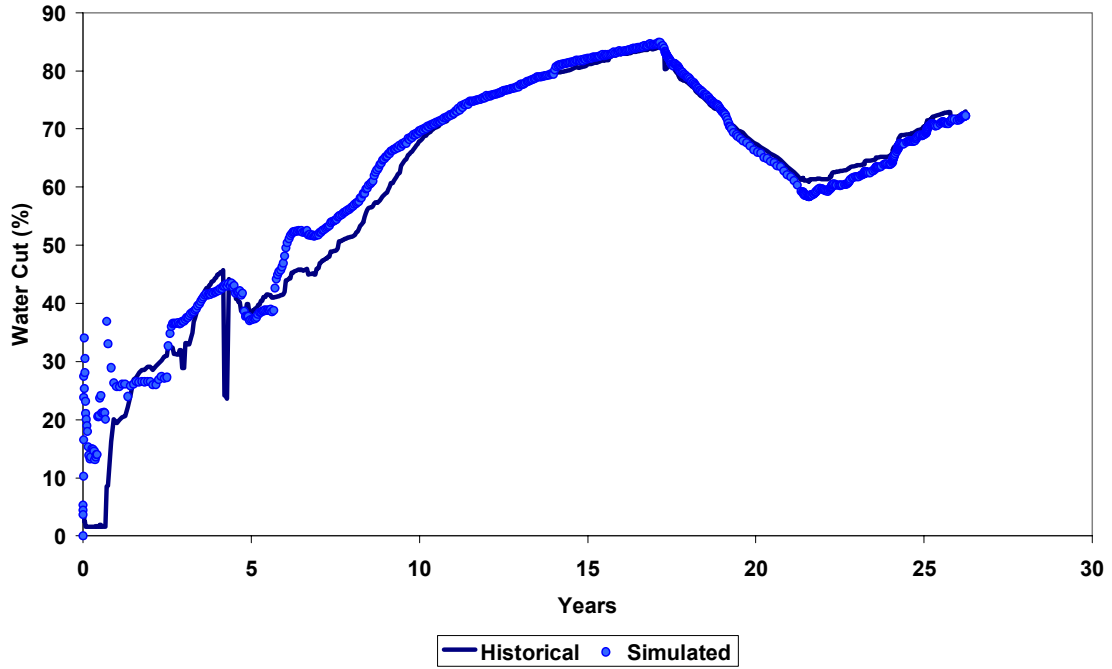


Figure 5.19- Water cut history match.

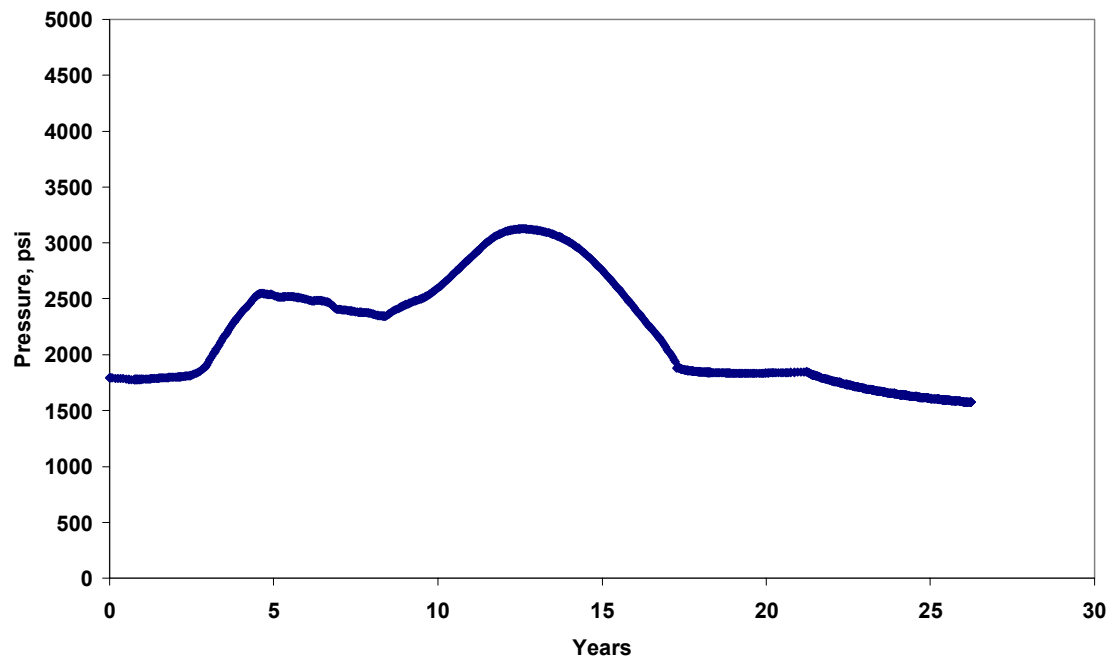


Figure 5.20- Simulated reservoir pressure.

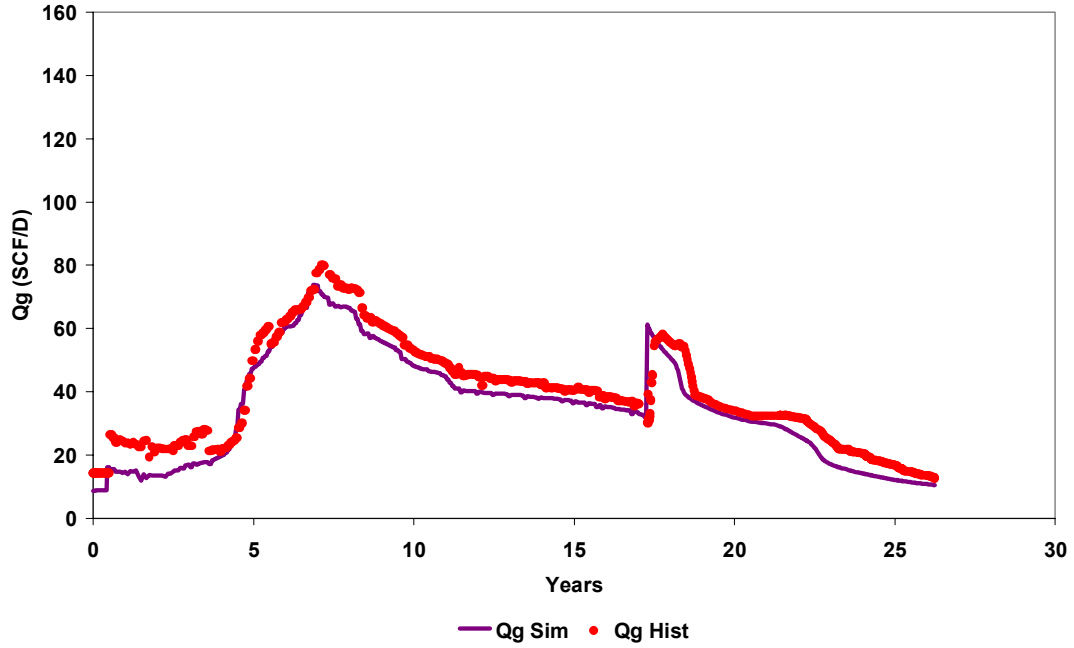


Figure 5.21- Diag-Prod well: Gas production rate history match.

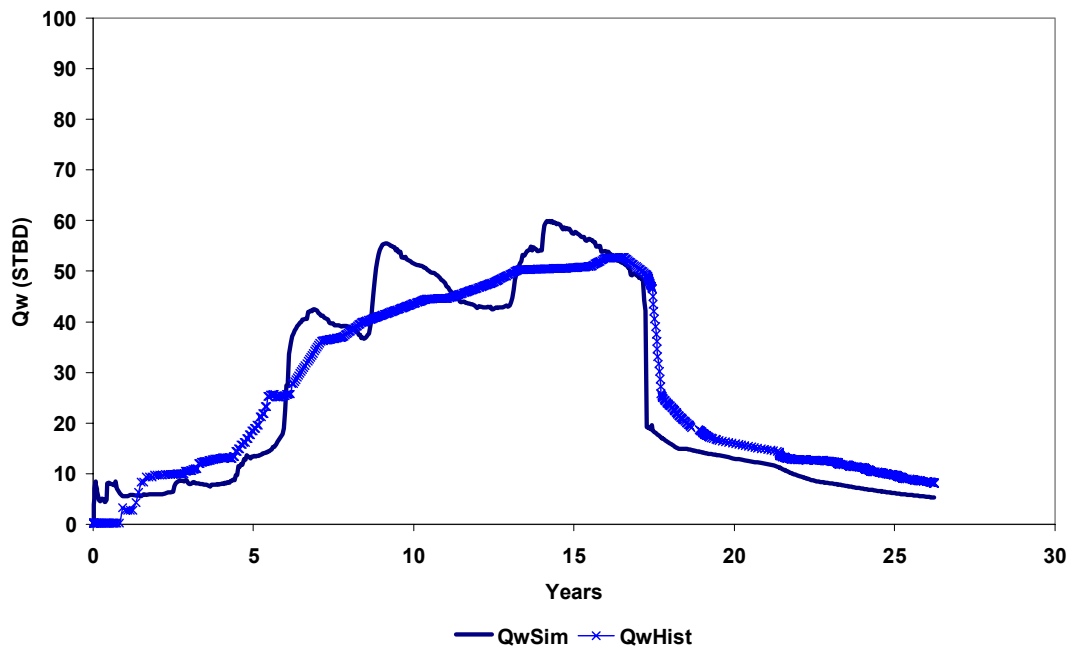


Figure 5.22- Diag-Prod well: Water production rate history match.

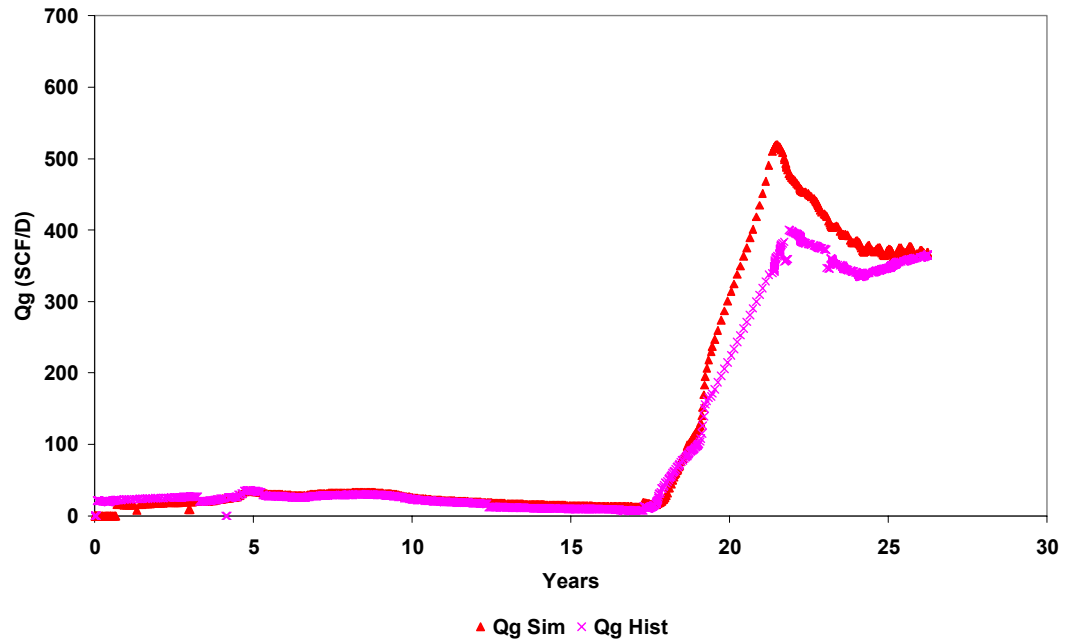


Figure 5.23- NS-Prod well: Gas production rate history match.

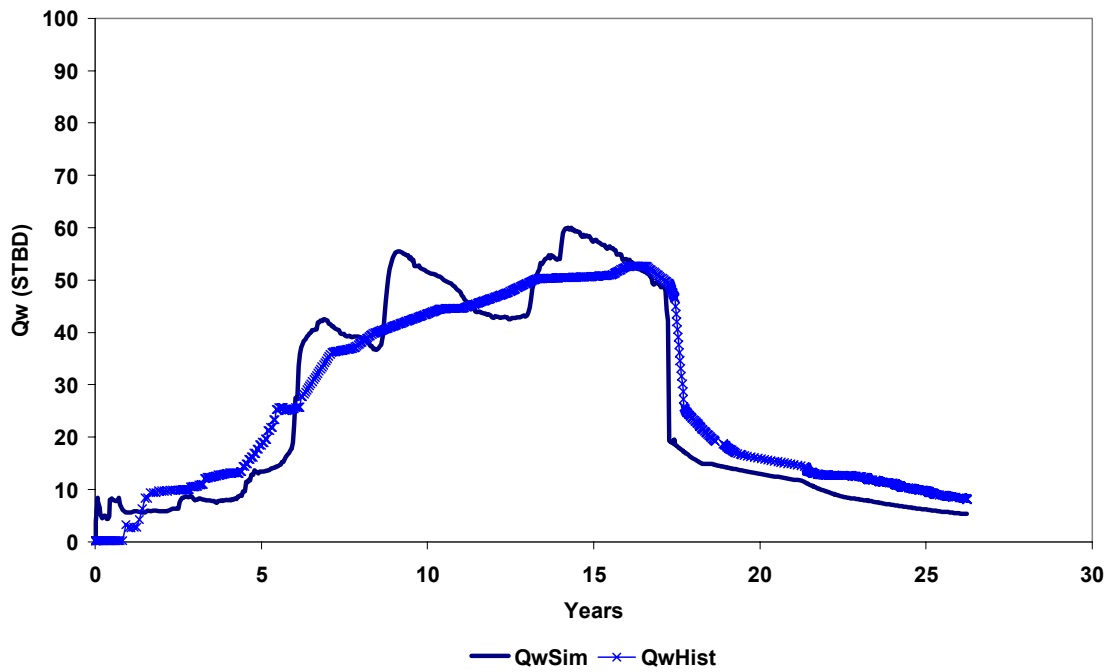


Figure 5.24- NS-Prod well: Water production rate history match.



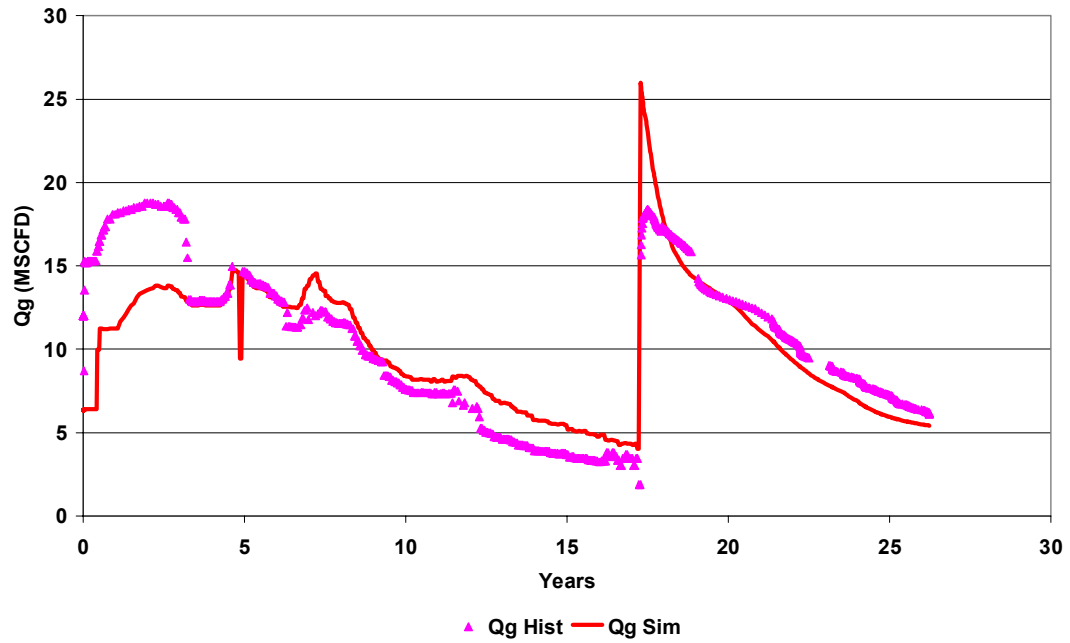


Figure 5.25- EW-Prod well: Gas production rate history match.

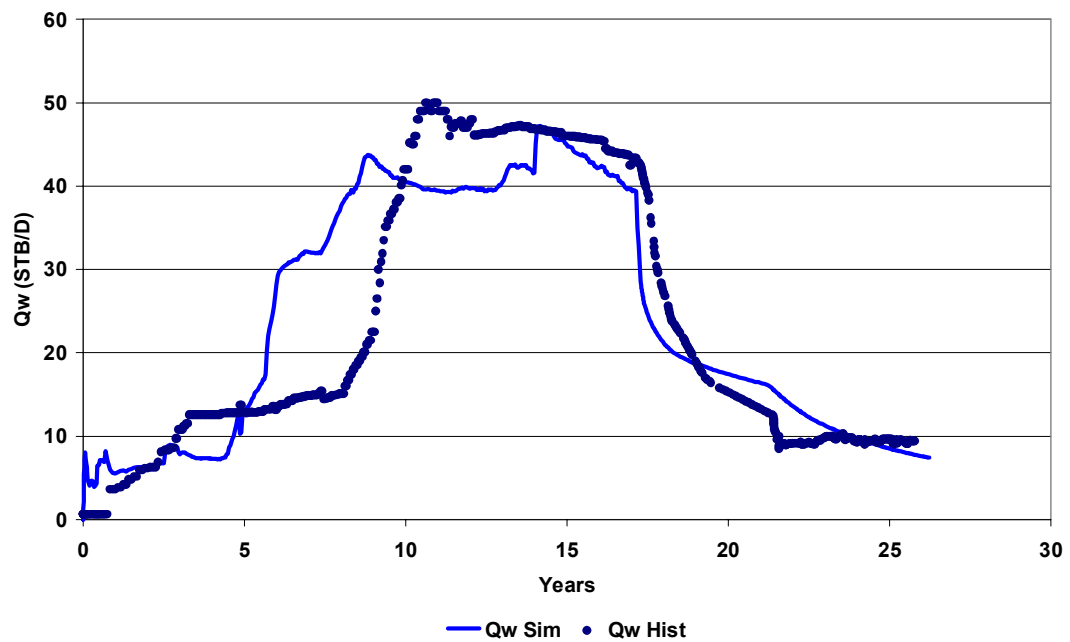


Figure 5.26- EW-Prod well: Water production rate history match.

At the end of the history match period, layers F4 through M5, which initially contained 2.29 million STBO, had produced 893,862 STB or 39% of the OOIP, thus leaving a remaining volume in place of 1.39 million STBO. The average remaining oil saturation at the end of the history match was 45%. Figures 5.27 through 5.39 show the transition of the distribution of the oil saturation during the history match period. Similarly, Figures 5.40 through 5.52 show a cross-section view of oil saturation distribution in the model throughout the history match.

The channeling of the injected fluids within the reservoir is clearly seen in the cross sections. This causes a non-uniform movement of the front and therefore poor sweep efficiency. High-permeability layers break through earlier than the low-permeability layers, leaving some untapped reserves behind.

The pattern experienced a severe breakthrough that reduced the overall sweep efficiency of the pattern. Additionally, little oil displacement was observed in the upper layers of the San Andres Formation in the simulation model. The sweep efficiency of the patterns was merely impacted by the contrast in permeability between the upper and lower layers of the San Andres Formation. As a result, the injection well injected most of the fluids into the lower layers even though the upper San Andres layers have commercial permeability.

Results of the simulation not only highlighted reservoir areas with high oil saturation for the future CO<sub>2</sub> flooding but also reveal that mobility ratio needs to be improved and the breakthrough has to be controlled to improve the injection profile and increase the incremental oil recovery of the pattern.

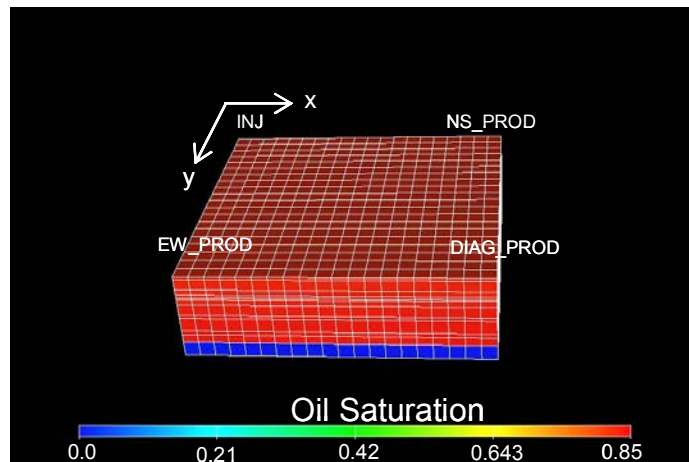


Figure 5.27- Areal view of the oil saturation distribution. Year 0.

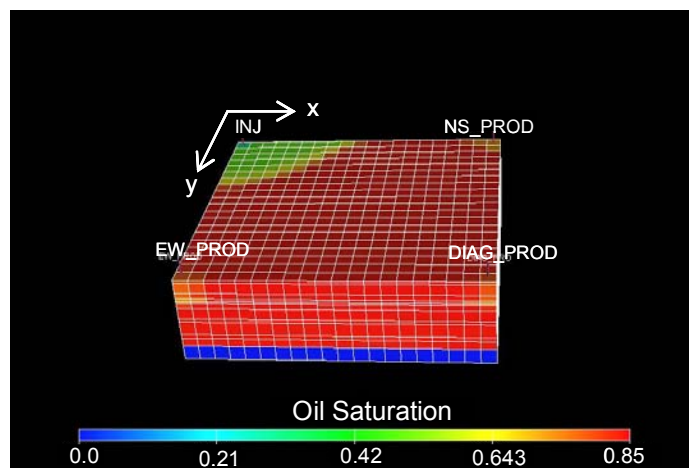
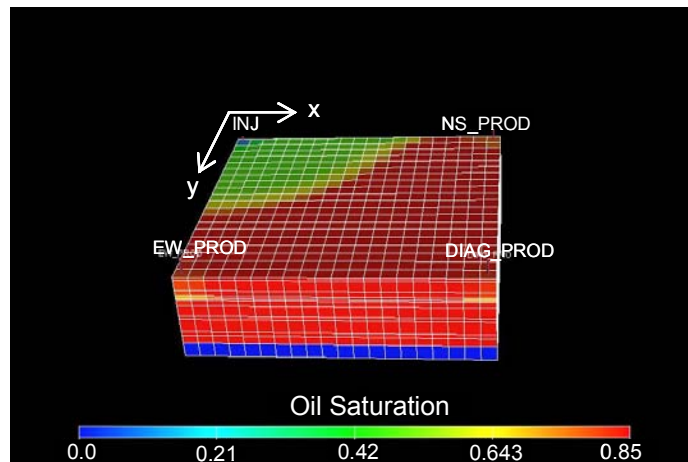
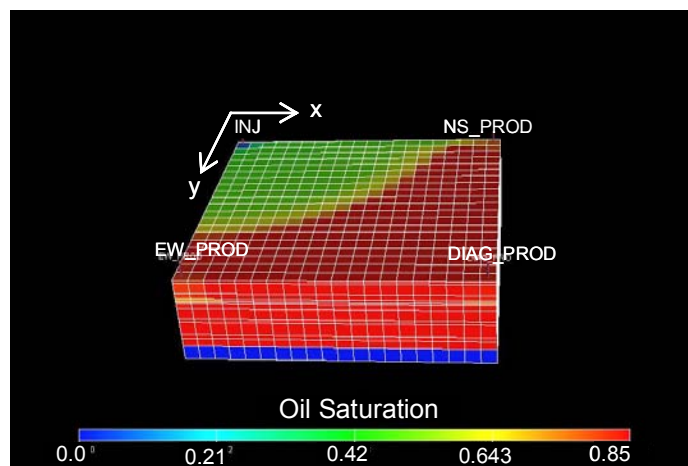


Figure 5.28- Areal view of the oil saturation distribution. Year 2.



**Figure 5.29-** Areal view of the oil saturation distribution. Year 4.



**Figure 5.30-** Areal view of the oil saturation distribution. Year 6.

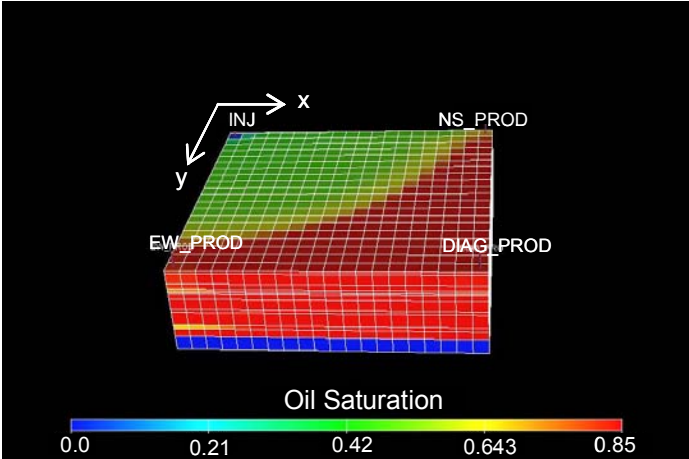


Figure 5.31- Areal view of the oil saturation distribution. Year 8.

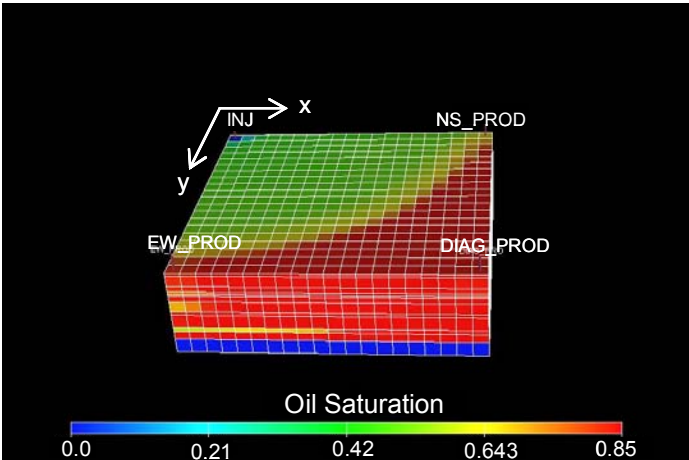
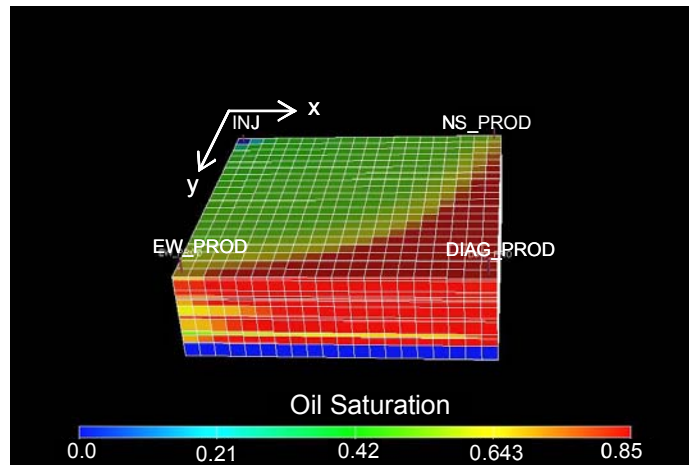
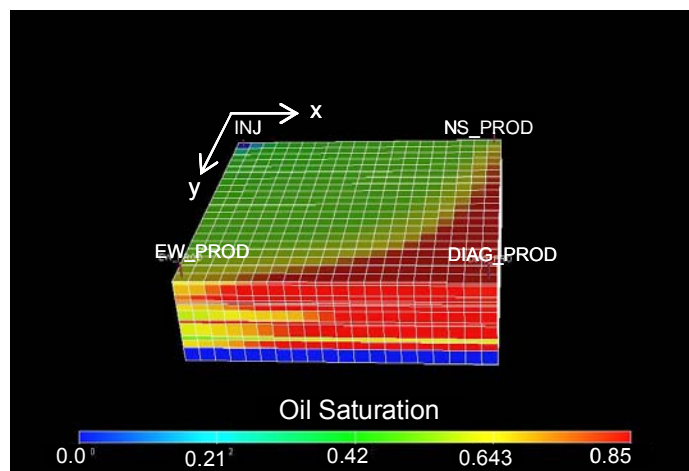


Figure 5.32- Areal view of the oil saturation distribution. Year 10.



**Figure 5.33- Areal view of the oil saturation distribution. Year 12.**



**Figure 5.34- Areal view of the oil saturation distribution. Year 14.**

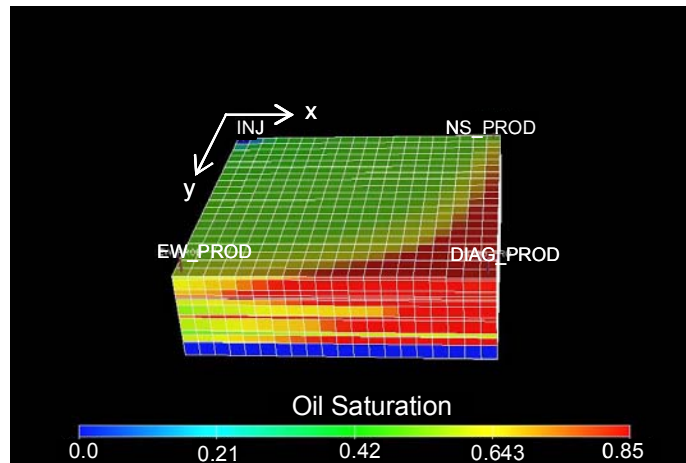


**Figure 5.35- Areal view of the oil saturation distribution. Year 16.**

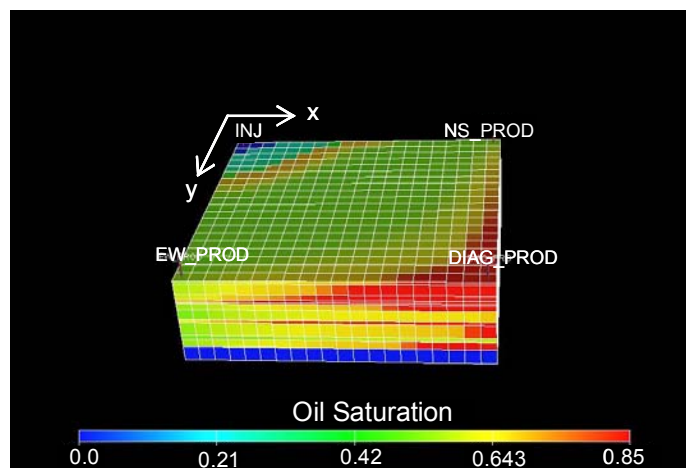


**Figure 5.36- Areal view of the oil saturation distribution. Year 18.**

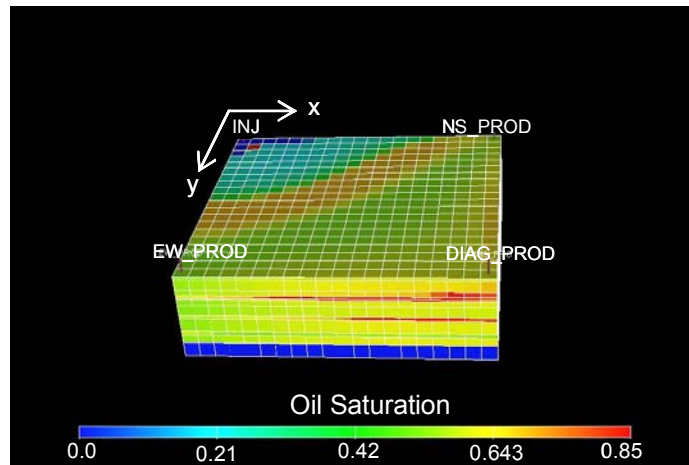


**Figure 5.37-** Areal view of the oil saturation distribution. Year 20.

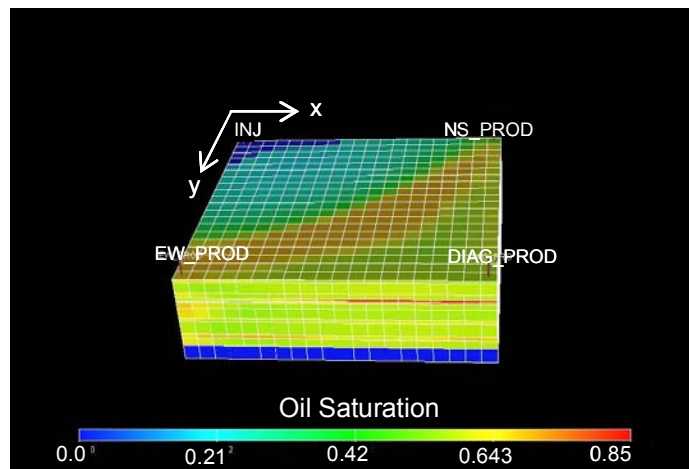


**Figure 5.38-** Areal view of the oil saturation distribution. Year 22.



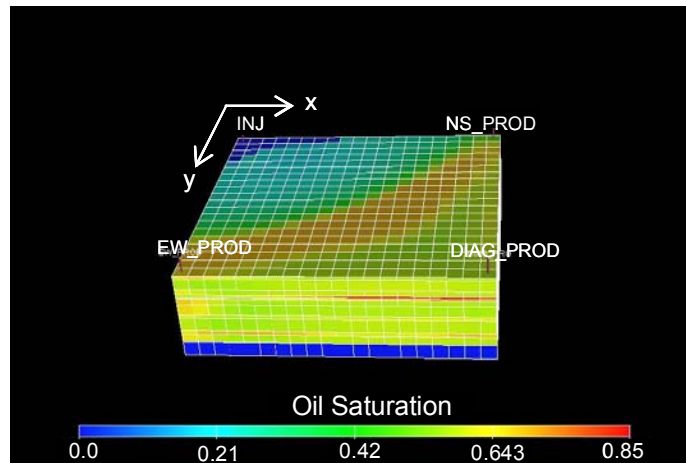


**Figure 5.39- Areal view of the oil saturation distribution. Year 24.**

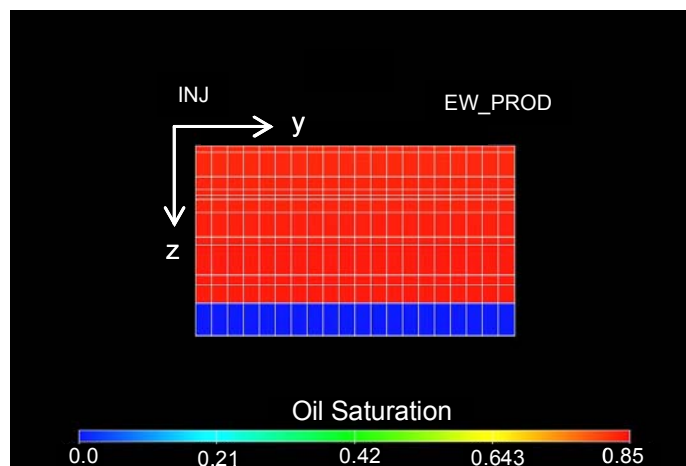


**Figure 5.40- E-W cross section view of the oil saturation distribution.  
Year 0.**

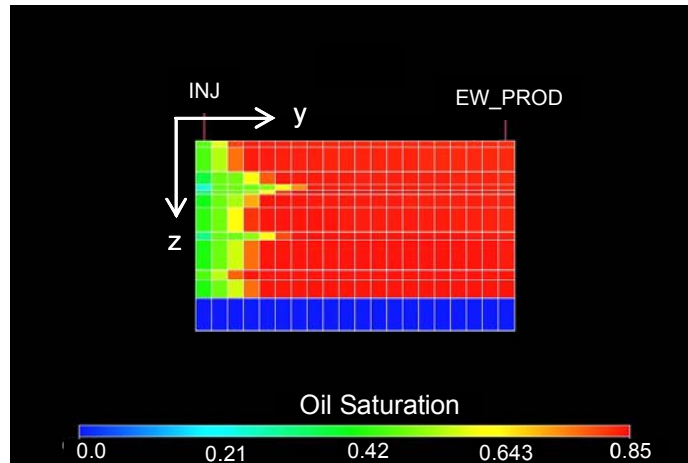


**Figure 5.41- E-W cross section showing oil saturation. Year 2.**

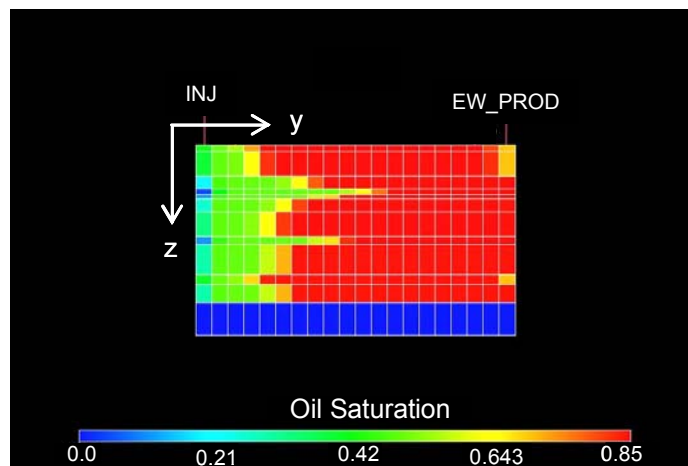


**Figure 5.42- E-W cross section showing oil saturation. Year 4.**

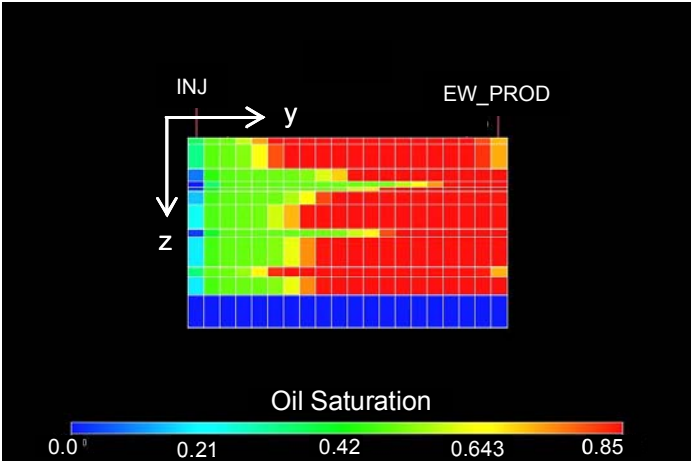


Figure 5.43- E-W cross section showing oil saturation. Year 6.

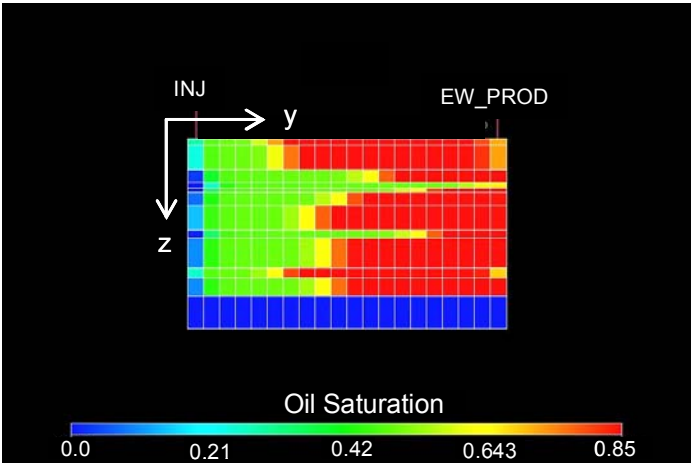
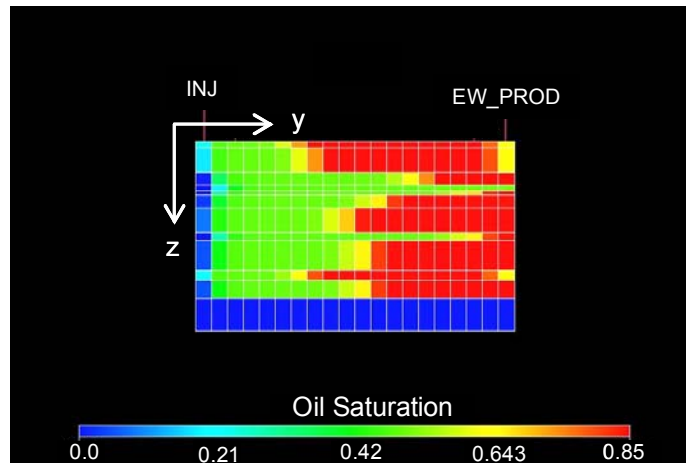
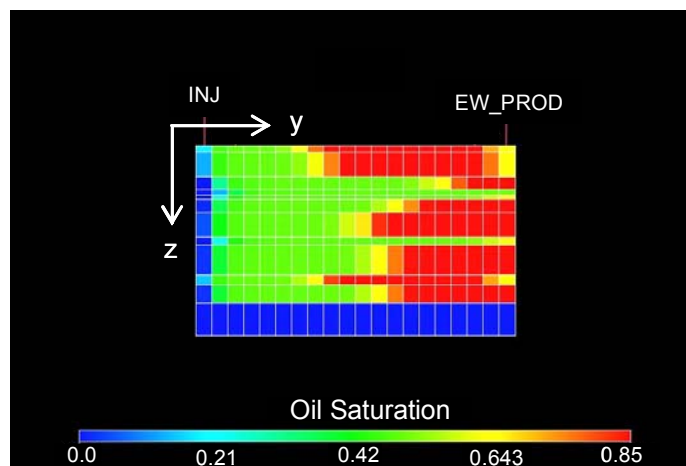


Figure 5.44- E-W cross section showing oil saturation. Year 8.



**Figure 5.45- E-W cross section showing oil saturation. Year 10.**



**Figure 5.46- E-W cross section showing oil saturation. Year 12.**

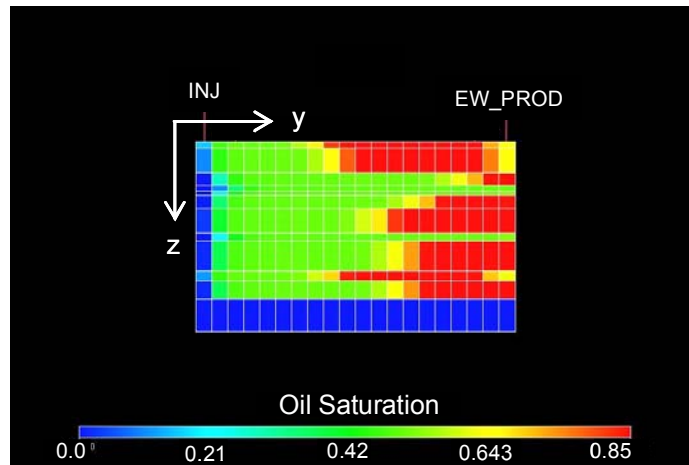


**Figure 5.47- E-W cross section showing oil saturation. Year 14.**

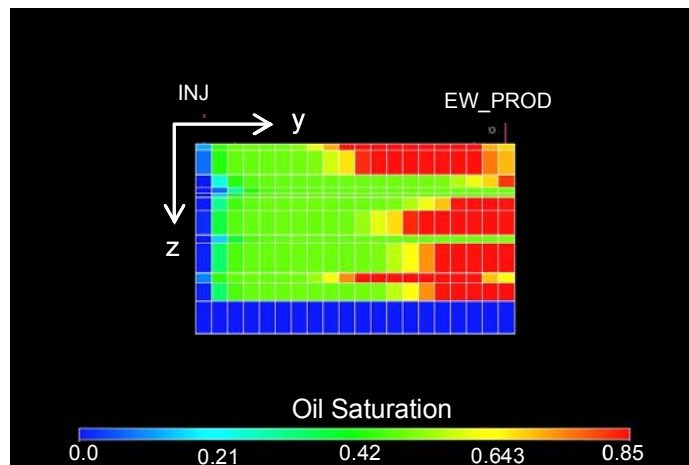


**Figure 5.48- E-W cross section showing oil saturation. Year 16.**

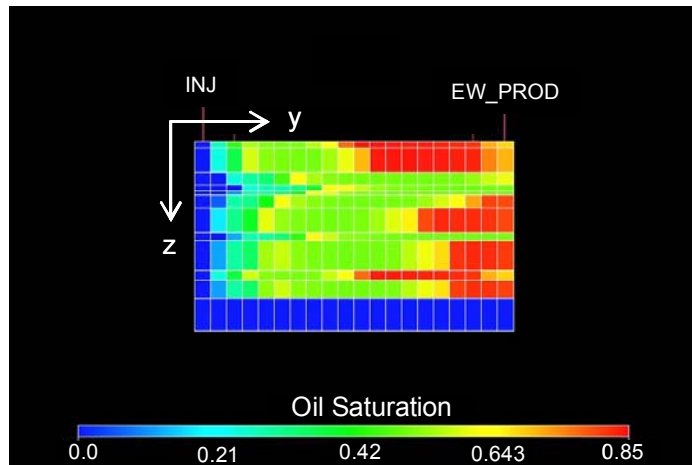


**Figure 5.49- E-W cross section showing oil saturation. Year 18.**

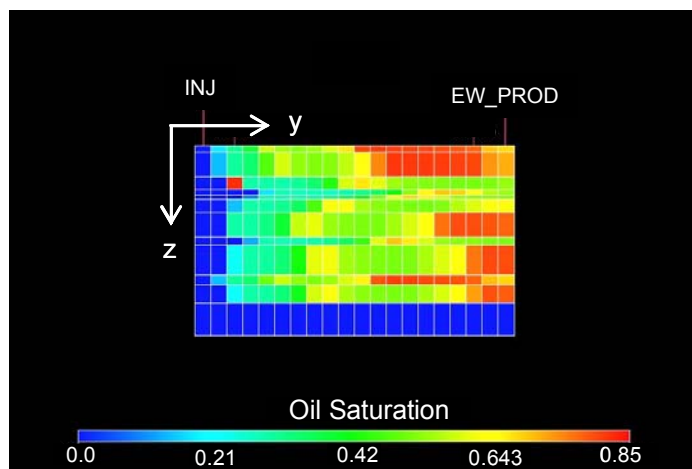


**Figure 5.50- E-W cross section showing oil saturation. Year 20.**

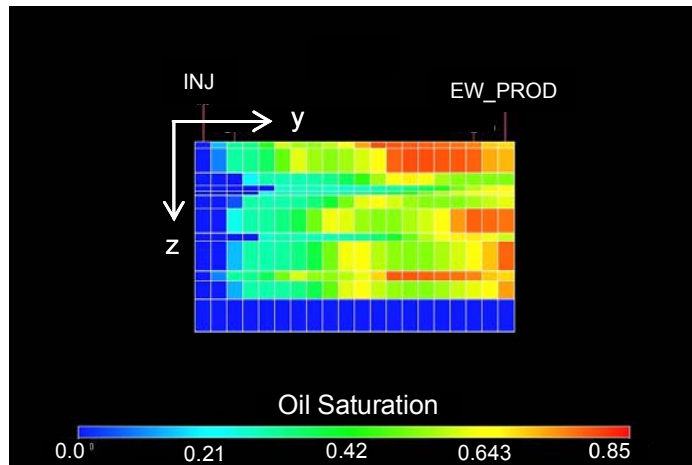


**Figure 5.51- E-W cross section showing oil saturation. Year 22.**

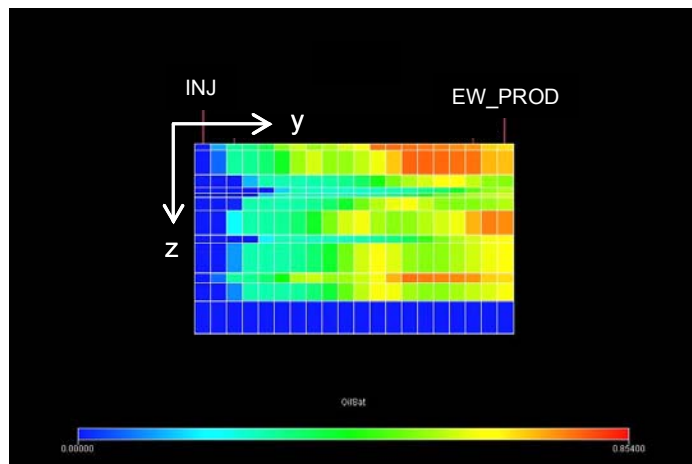


**Figure 5.52- E-W cross section showing oil saturation. Year 24.**

## CHAPTER VI

### OPTIMIZATION OF MISCIBLE WAG PROCESS

In this chapter, the optimization of water-alternating-gas (WAG) processes is discussed. The effect of WAG ratios, CO<sub>2</sub> slug sizes, CO<sub>2</sub> injection rate, conformance control and well geometry on the ultimate recovery are analyzed to make operational recommendations.

#### 6.1 CO<sub>2</sub> Injection Rate Optimization

To investigate the effect of the injection rate on the WAG process four sensitivities were performed at a WAG ratio of 1:1 using constant rates of 100, 200, 300 and 500 res bbl/D (233.5, 467, 762 and 1167 Mscf/D respectively) of CO<sub>2</sub>. Half cycle of 3% HCPV CO<sub>2</sub> and 3% HCPV of water were injected until a fixed total CO<sub>2</sub> slug of 30% HCPV was reached. The recovery from WAG changes as a function of the injection rate. Figure 6.1 indicates that the optimum injection rate for a 1:1 WAG ratio is approximately 300 res bbl/D (762 Mscf/D).

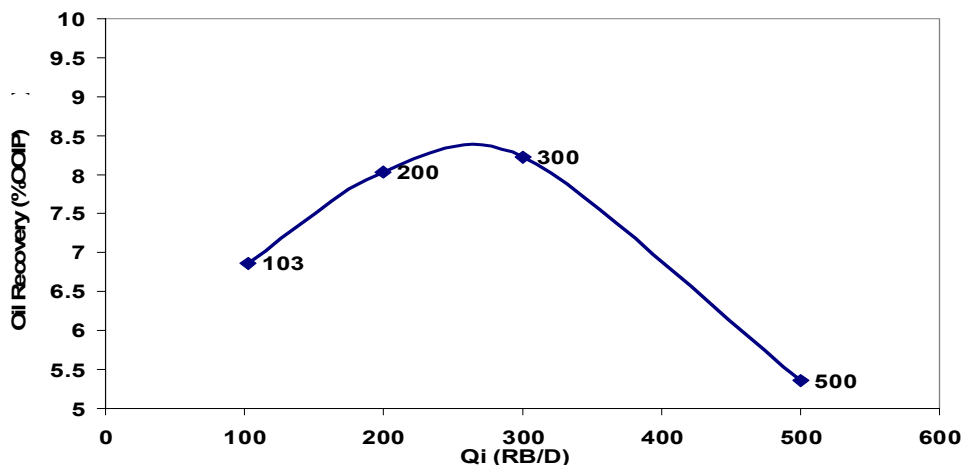


Figure 6.1- Oil recovery at a WAG ratio of 1:1 as a function of injection rates.



## 6.2 Optimum Water-Alternating-Gas (WAG) Ratio

Two of the most important design issues for WAG process optimization are the WAG ratio and the amount of gas injection or slug size. Various compositional simulations were conducted to determine the optimum WAG ratio and the optimum slug size.

A series of WAG ratio sensitivities were compared. Water alternating with CO<sub>2</sub> injections at four different WAG ratios (1:1, 1:2, 2:1, and 4:1) were performed. The runs evaluated CO<sub>2</sub> slug sizes up to 100% HCPV. The gas and water injections were carried out in cycles, injecting both fluids in the same well.

Model results showed sensitivity to the WAG ratio used. Results indicate that injecting a 100% hydrocarbon pore volume (HCPV) slug of CO<sub>2</sub> with a 1:1 WAG ratio would yield the maximum incremental oil recovery. The design included injection of alternating volumes (3.0% HCPV) of CO<sub>2</sub> and water into each pattern until the target 100% slug size was reached.

Figure 6.2 shows the CO<sub>2</sub> flood performance for the different WAG ratios as a function of total CO<sub>2</sub> injection. The recovery profiles indicate that the best incremental oil recovery is obtained at a WAG ratio of 1:1. As shown in figure 6.2, the highest recovery is obtained at the smallest WAG ratio during the optimization process. Much of the oil obtained with high WAG ratios is recovered at a very high and uneconomical water cut (>95%), even though the planned CO<sub>2</sub> slug size had not been injected.

A continuous CO<sub>2</sub> flood and waterflooding recovery profiles are also shown in Figure 6.2 for comparison. The incremental oil recovery obtained with the continuous CO<sub>2</sub> flood was low. CO<sub>2</sub> injected this way broke through the high permeability layers of the pattern.

Figure 6.3 shows the residual oil saturation in the reservoir for all the cases after 100% HCPV have been injected. As expected, the 1:1 WAG ratio exhibits the lowest remaining oil saturation.

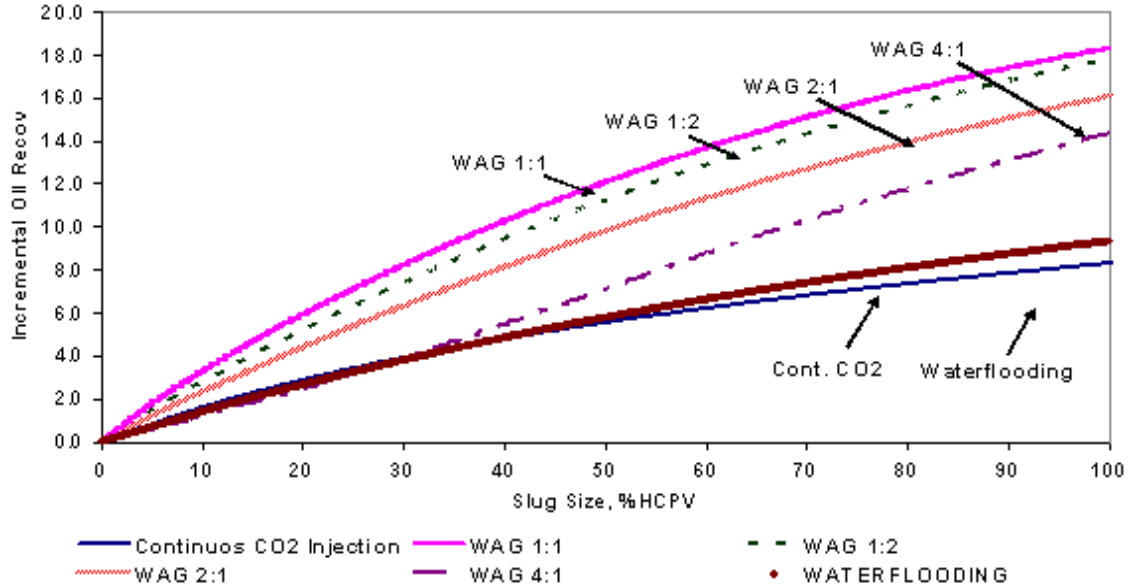


**Figure 6.2- Comparison of different WAG ratios in terms of the incremental oil recovery as a function of the CO<sub>2</sub> slug size.**

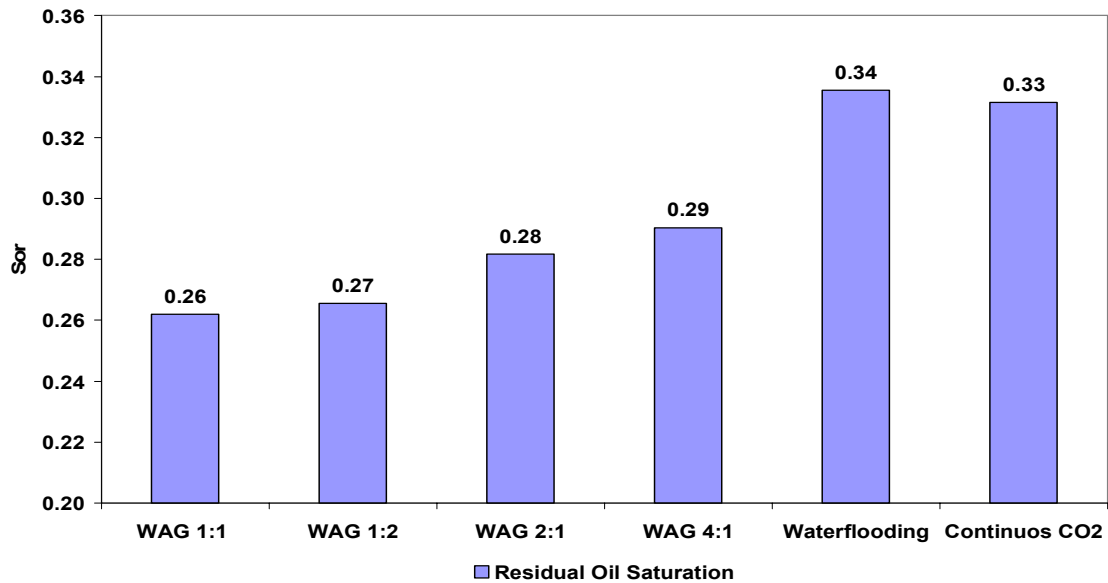


**Figure 6.3- Comparison of the residual oil saturation for various WAG ratios after injection of 100% HCPV of CO<sub>2</sub>.**

### 6.3 Conformance Control

Channeling of the injected CO<sub>2</sub> during a WAG process has been a major area of concern in the oil industry.<sup>30</sup> During the course of CO<sub>2</sub> injection multiple profile control treatments have been conducted to improve the sweep efficiency.

To reduce the CO<sub>2</sub> mobility and delay the breakthrough of the CO<sub>2</sub>, simulations of polymer injection and a blocking agent treatments were performed with a WAG ratio of 1:1. Polymer injection reduces CO<sub>2</sub> cycling through a high-permeability layer between the injection well and offset producing wells. This simulation allowed for the investigation of the effect of these treatments on the sweep efficiency and conformance control.

To simulate the effect of placing the surfactant in the “thief” zone, a high-permeability layer was identified (layer 4, M1 formation) in the simulation model and the gridblock next to the injector well was plugged by assigning it a zero permeability value. See Figure 6.4.

Polymers have been used at CO<sub>2</sub> WAG injection wells to form an in-situ gel. The gel must be selectively injected so that it flows to the most permeable zones. After a certain amount of time, the gel stiffens and blocks fluid through those zones.

For the polymer injection treatment, the injected water viscosity was increased from 1 to 20 cps. For this run, care was taken not to increase the injection pressure above the formation parting pressure where it might subsequently create an injection-induced fracture. As can be noted from Figure 6.5, the injection pressure is between 3,100 and 3,900 psi during the process.

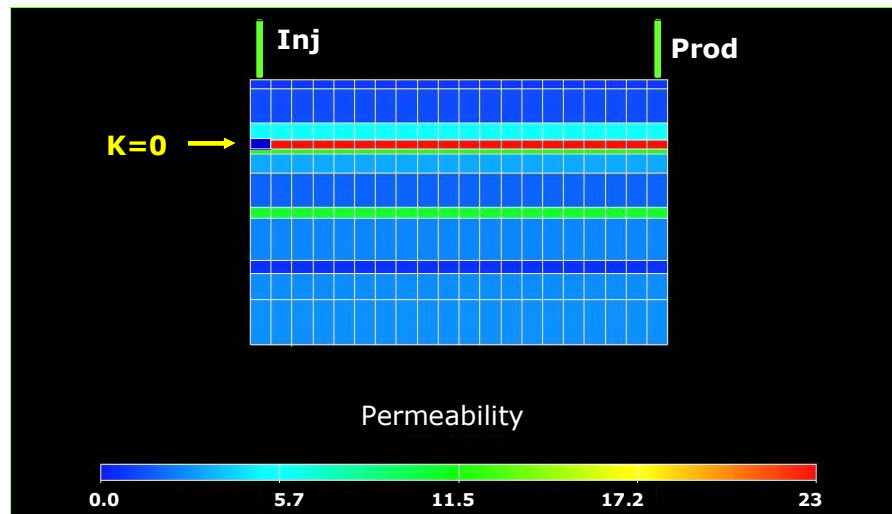


**Figure 6.4- East –West cross section view of the simulation model showing the permeability block by the polymer.**

Production rates before and after the treatments were compared (Figure 6.6). The oil production rate of the pattern exhibits a significant response to the profile control treatments performed on the injection well. However, the effectiveness of the treatments does not last long (in time) and the production rate declines quickly after the treatments, which indicate that the positive effects of the treatments are not permanent.

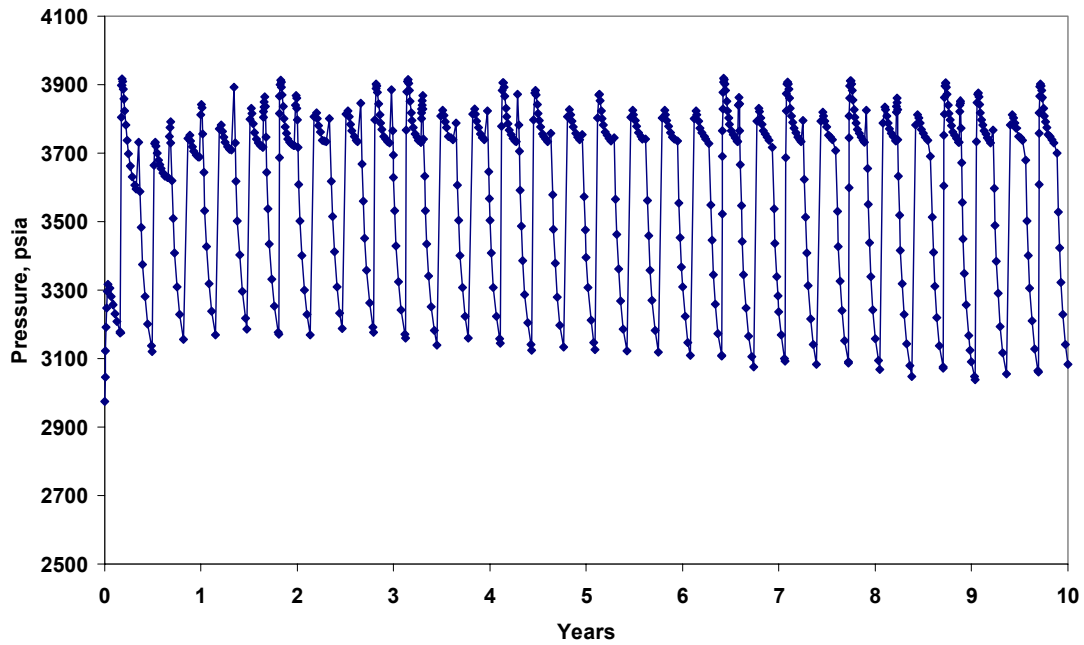


Figure 6.5- Injection pressure profile during the viscous water treatment.

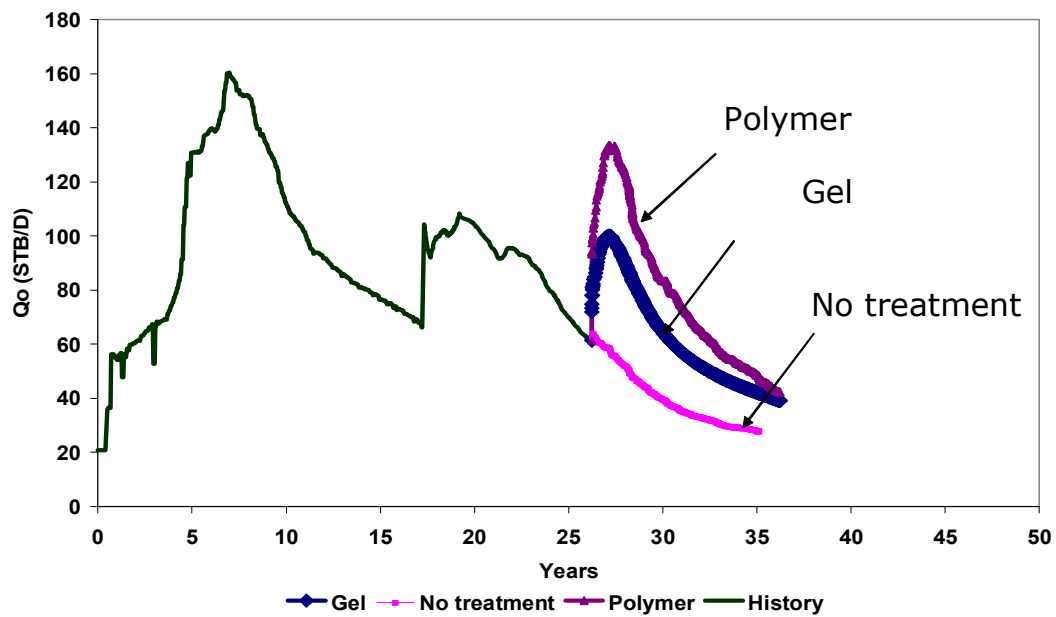
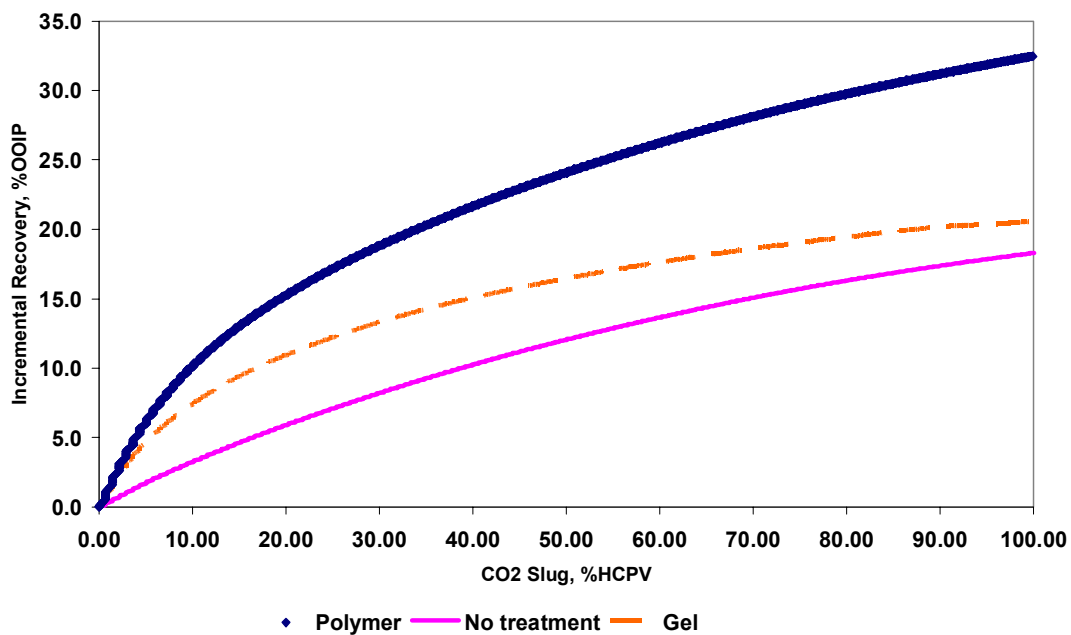


Figure 6.6- Comparison of conformance control treatments as a function of oil production rate.

Figure 6.7 shows the effect of the conformance control on the incremental recovery as a function of the volume of CO<sub>2</sub> injected. The incremental recovery obtained from the polymer injection and the viscous water treatments is compared to the recovery obtained from a WAG 1:1 ratio injection process without any treatment.

Even though results indicate that the application of these treatments can significantly increase the oil production, the success of this technique in the field will depend on the correct placement of the polymer without damaging other adjacent layers. Additionally, it depends on the periodic repetition of the treatment to positively affect areal sweep efficiency.



**Figure 6.7- Comparison of conformance control treatments in terms of the incremental oil recovery as a function of the CO<sub>2</sub> slug size.**

## 6.4 Optimum Well Pattern

This section analyzes the effect of pattern reconfiguration on the CO<sub>2</sub> displacement. Pattern conversion is a viable option to achieve an incremental recovery in a mature field with high remaining oil saturations.

A pattern reconfiguration can improve the performance by improving the geometry, decreasing the spacing of the patterns, reducing the producer/injector ratio, and hence improving areal and vertical efficiency.

This sensitivity includes infill drilling and well conversion from producer to injector to achieve a better CO<sub>2</sub> displacement throughout the reservoir and ultimately obtain a substantial increase in production from the existing CO<sub>2</sub> flood.

Different well configurations were simulated and analyzed. The typical Denver Unit inverted nine-spot pattern was converted to a staggered line-drive pattern, a line-drive pattern and a nine-spot pattern in the simulation model.

The new patterns were forecast using the saturations and pressures at the end of the history match. Figure 6.8 shows the geometric patterns considered in this work. The gridded zone represents the simulated area of the full pattern

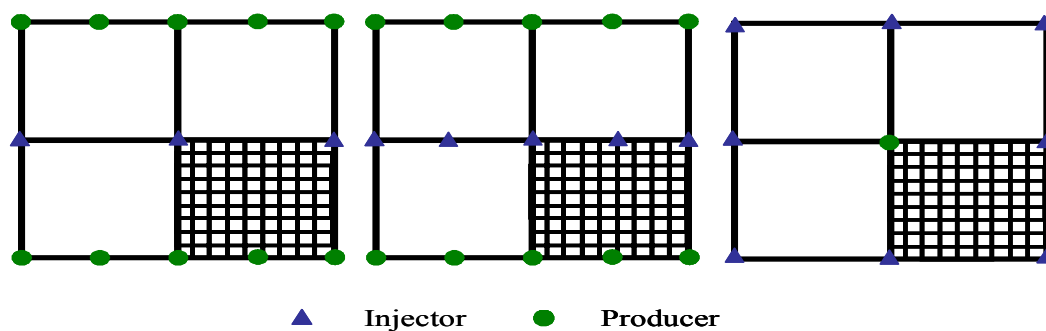


**Figure 6.8- (a) Staggered line drive, (b) line drive and (c) nine-spot well patterns.**

For the staggered-line-drive pattern, the EW-Prod production well was converted into an injection well and a new production (infill) well was incorporated. With this well configuration, the well spacing was modified from 20 acres to 10 acres. The new injector well was set up to inject water alternating CO<sub>2</sub> at a WAG ratio of 1:1.

To create a line-drive pattern, a new injector well was incorporated in the model and aligned with the other injectors in the staggered-line-drive pattern as shown in Figure 6.8. For the nine-spot pattern, a single producer well and three injectors were kept in the model.

Figure 6.9 compares the production performance obtained from each pattern investigated. The figure also shows a plot of the actual production rate of the pattern. The sharp rise in the production rate is very evident after redefining the well pattern geometry to staggered-line-drive and line-drive patterns. Simulation results showed both the staggered-line-drive pattern and the line-drive pattern create an immediate peak above 100 STB/D in the production rate, which represents approximately a 66% of increase in production as a result of the pattern reconfiguration.

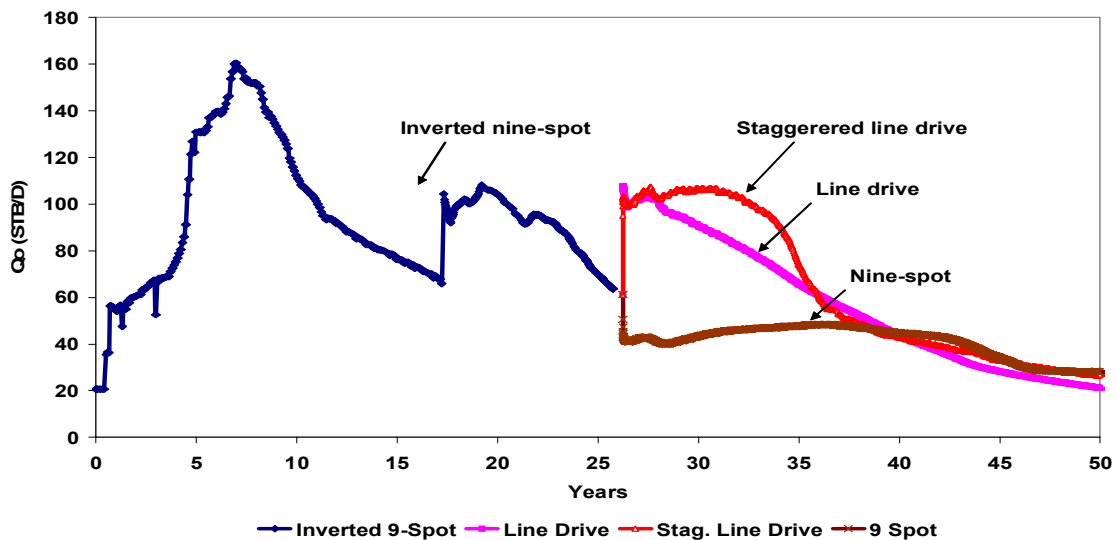


**Figure 6.9-Comparison of staggered-line-drive, line-drive and nine-spot well patterns.**



The production rates obtained from the inverted nine-spot pattern is the lowest one among the patterns compared here. Extremely low rates clearly indicate that this pattern configuration does not perform well for this particular drainage area and does not improve the CO<sub>2</sub> displacement.

## CHAPTER VII

### CONCLUSIONS

- 1) Recovery from a WAG process is a function of the injection rate as well as WAG ratio and the CO<sub>2</sub> slug.
- 2) WAG injection is effective in increasing the sweep efficiency of the injected CO<sub>2</sub> in the reservoir.
- 3) Simulation showed that Denver Unit tertiary CO<sub>2</sub> flood would have a maximum recovery of 18% at a 1:1 WAG ratio and a CO<sub>2</sub> slug size of 100% HCPV.
- 4) The optimal injection rate for the pattern is 300 RB/D of CO<sub>2</sub> at a WAG 1:1 ratio.
- 5) The injection of viscous water and polymer resulted in a positive production response that yielded an incremental oil recovery of 32% and 20% respectively.
- 6) Modeling suggests that pattern conversion from the typical Denver Unit inverted nine-spot pattern to staggered-line-drive improves the production oil rate in 66%.
- 7) The CO<sub>2</sub> pattern modeling provides guidance in the reservoir management in the Wasson Field, San Andres Formation in the Denver Unit.

## NOMENCLATURE

$Z$  = gas deviation factor

$\phi$  = porosity

$\mu$  = viscosity, cp

$\rho$  = fluid density, lb<sub>m</sub>/ft<sup>3</sup>

$q$  = production rate

FVF= formation volume factor

GOR=Gas-oil ratio

### Subscripts

$g$  = gas

$w$  = water

$o$  = oil

## REFERENCES

1. Fleming, E.A., Brown, L.M. and Cook, R.L.: "Overview of Production Engineering Aspects of Operating the Denver Unit CO<sub>2</sub> flood," paper SPE/DOE 24157 presented at the 1992 SPE/DOE Symposium on Improved Methods for Oil Recovery, Tulsa, OK, 22-24 April
2. Hsu, C.F., Morell, J.I. and Falls, A.H.: "Field Scale CO<sub>2</sub> Flood Simulations and Their Impact on the Performance of the Wasson Denver Unit," paper SPE 29116 presented at the 1995 SPE Symposium on Reservoir Simulation, San Antonio, TX, 12-15 February.
3. Ghauri, W.K.: "Production Technology Experience in a Large Carbonate Waterflood, Denver Unit, Wasson San Andres Field," paper SPE 8406 presented at the 54<sup>th</sup> Annual Technical Conference and Exhibition held in Las Vegas, NV. Sept. 23-26, 1979.
4. Thai, B.N., Hsu, C.F., Bergersen, B.M., Albrecht, S.L., and Richardson, T.W.: "Denver Unir Infill and Pattern Reconfiguration Program," paper SPE 59548 presented at the 2000 SPE Permian Basin Oil and Gas Recovery Conference, Midland, TX, 21-23 March.
5. Mathis, R.L.: "Effect of CO<sub>2</sub> Flooding on Dolomite Reservoir Rock, Denver Unit, Wasson (San Andres) Field, TX," paper SPE 13132 presented at the 59<sup>th</sup> Annual Technical Conference and Exhibition, Houston, TX, 16-19 September.
6. Martin, F.D. and Taber, J.J.: "Carbon Dioxide Flooding," *SPE Technology Today Series* (April 1992) 396 – 400.
7. Jarrel, P.M., Fox, C.E., Stein, M.H. and Webb, S.L.: F.: *Practical Aspects of CO<sub>2</sub> Flooding*, Monograph Series, SPE, Richardson, Texas (2002).
8. Caudle, B.H. and Dyes, A.B.: "Improving Miscible Displacement by Gas-Water Injection", *Transactions of AIME*, (1959) **213**, 281-284.
9. Huang, E.T.S. and Holm, L.W.: "Effect of WAG Injection and Rock Wettability on Oil Recovery During CO<sub>2</sub> Flooding," *SPE* (Feb. 1988) 119-129.
10. Green, D.W. and Willhite, P.: *Enhanced Oil Recovery* SPE Textbook Series, Richardson, Texas (1998).

11. Sanchez, N.L.: "Management of Water Alternating (WAG) Injection Projects," paper SPE 53714 presented at the 1999 Latin American and Caribbean Petroleum Engineering Conference, Caracas, Venezuela, 21-23 April.
12. Christensen, J R, Stenby, E H, and Skauge, A,,: "Review of the WAG Field Experience", paper SPE 71203, presented at the 1998 SPE International Petroleum Conference and Exhibition of Mexico, Villa Hermosa, 3-5 March.
13. Bellavance, J.F.R.: "Dollarhide Devonian CO<sub>2</sub> Flood: Project Performance Review 10 Years Later," paper SPE 35190 presented at the 1996 SPE Permian Basin Oil and Gas Recovery Conference, Midland, TX, 27-29 March.
14. Tanner, C.S. and Baxley, P.T.: "Production Performance of the Wasson Denver Unit CO<sub>2</sub> Flood," paper SPE 24156 presented at the 1992 Enhanced Oil Recovery Symposium, Tulsa, OK, 22-24 April.
15. Kulkarni, M. M. and Rao, D. N.: "Experimental Investigation of Various Methods of Tertiary Gas Injection", SPE 90589, paper presented at the 2004 Society of Petroleum Engineers Annual Technical Conference and Exhibition, Houston, TX, 26 – 29, Sept.
16. Jackson, D.D., Andrews, G.L., and Claridge, E.L.: "Optimum WAG Ratio vs. Rock Wettability in CO<sub>2</sub> Flooding," paper SPE 14303 presented at the 1985 Annual Technical Conference and Exhibition, Las Vegas, NV, 22-25 September.
17. Gorrell, S.B.: "Implications of Water-Alternate-Gas Injection, for Profile Control and Injectivity," paper SPE 20210 presented at the 1990 SPE/DOE Seventh Symposium on Enhanced Oil Recovery, Tulsa, OK, 22-25 April.
18. Rogers, J.D., Reid B. and Grigg, R.B.: "A Literature Analysis of the WAG Injectivity Abnormalities in the CO<sub>2</sub> Process," paper SPE 59329 presented at the 2000 Improved Oil Recovery Symposium, Tulsa, OK, 3-5 April.
19. M.K. Roper Jr., Pope, G.A., and Sepehrnoori, K.: "Analysis of Tertiary Injectivity of Carbon Dioxide," paper SPE 23974, presented at the proceedings of the SPE Permian Basin Oil and Gas Recovery Conference, Midland, TX, March 18-20, 1992.
20. Christman, P.G. and Gorell, S.B.: "A Comparison of Laboratory and Field-Observed CO<sub>2</sub> Tertiary Injectivity," paper SPE/DOE 17335 presented at the 1988 Improved Oil Recovery Symposium., Tulsa, OK, 17-20 April.
21. Bennion, D.B., Thomas, F.B., Jamaluddin, A.K.M. and Ma, T.: "The Effect of Trapped Critical Fluid Saturations on Reservoir Permeability and Conformance,"

paper presented at the 1998 Annual Technical Meeting of the Petroleum Society of CIM, Calgary, Alberta, Canada, 8 -10 June.

22. Harpole, K.J. and Hallenbeck, L.D.: "East Vacuum Grayburg San Andres Unit CO<sub>2</sub> Flood Ten Year Performance Review: Evolution of a Reservoir Management Strategy and Results of WAG Optimization," paper SPE 36710 presented at the 1996 Annual Technical Conference and Exhibition, Denver, CO, 6-9 October.
23. Lemen, M.A., Burlas, T.C., and Roe, L.M.: "Waterflood Pattern Realignment at the McElroy Field: Section 205 Case History," paper SPE 20120 presented at the 1990 Permian Basin Oil and Gas Recovery Conference, Midland, TX, 8-9 March.
24. Pariani, G.J., McColloch, K.A., and Warden, S.L.: "An Approach to Optimize Economics in a West Texas CO<sub>2</sub> Flood," paper SPE 22022 presented at the Hydrocarbon Economics and Evaluation Symposium, Dallas, TX, 11-12 April.
25. Shing-Ming C., Allard, D.R., and Anli, J.: "Factors Affecting Solvent Slug Size Hydrocarbon Miscible Flooding Requirements in Hydrocarbon Miscible Flooding," SPE paper 12636 presented at the 4<sup>th</sup> Symposium on Enhanced Oil Recovery, Tulsa, OK, 15-18, April.
26. Hadlow, R.E.: "Update of Industry Experience with CO<sub>2</sub> Injection," paper SPE 24928 presented at the 1992 SPE Annual Technical Conference and Exhibition, Washington, D.C, 4-7 October.
27. Gharbi-Ridha, B.C., "Integrated Reservoir Simulation Studies to Optimize Recovery from a Carbonate Reservoir," paper SPE 80437 presented at the SPE Asia Pacific Oil and Gas Conference and Exhibition, Jakarta, Indonesia, 9-11 September.
28. Holm, W. L.: "Evolution of the Carbon Dioxide Flooding Processes," *Oil and Gas Journal*, (November 1987) 1337.
29. Seright, R.S.: "Placement of Gels to Modify Injection Profiles," paper SPE/DOE 17332 presented at the 1988 SPE/DOE Enhanced Oil Recovery Symposium, Tulsa, OK, 17-20 April.
30. Vela, S., Peaceman, D.W., and Sandvik, E.I.: "Evaluation of Polymer Flooding in a Layered Reservoir with Crossflow, Retention, and Degradation," *SPEJ* (April 1976) 82.

31. Mathis, R.L.: "Reservoir Geology of the Denver Unit – Wasson San Andres Field, Gaines and Yoakum Counties, Texas," *Permian Basin SEPM Publication* **86-26**, 1986, 43-47.
32. Schneider, W. T.: "Geology of Wasson Field, Yoakum and Gaines Counties, Texas," *Bulletin of the American Association of Petroleum Geologists* (April 1943), **27**.
33. Mathis, R.L.: "Effect of CO<sub>2</sub> Flooding on Dolomite Reservoir Rock, Denver Unit, Wasson (San Andres) Field, TX," paper SPE 13132 presented at the 1984 Annual Technical Conference and Exhibition, Houston, TX, September 16-19.
34. P. E. Cowan and P. M. Harris, "Porosity Distribution in San Andres Formation (Permian), Cochran and Hockley Counties, Texas," *Bulletin of the American Association of Petroleum Geologists* (July 1986), **70**.
35. Galloway, W. E., Ewing, T. E., Garrett, C. M., Jr., Tyler, Noel, and Bebout, D. G., *Atlas of Major Texas Oil Reservoirs*, The University of Texas at Austin, Bureau of Economic Geology, (1983).
36. Purves, W. J., Reservoir Description of the Mobil Oil Bridges State Leases (Upper San Andres reservoir), Vacuum Field, Lea County, New Mexico, in Bebout, D. G., and Harris, P. M., eds., *Geologic and Engineering Approaches in Evaluation of San Andres/Grayburg Hydrocarbon Reservoirs—Permian Basin*, The University of Texas at Austin, Bureau of Economic Geology, (1986) p, 87–112.
37. Loucks, R. G., Mescher, P., Entzminger, D., and Braaten, D, 2003, "Reservoir Geology of the Willard Unit in the San Andres Wasson Field, West Texas," Southwest Section American Association of Petroleum Geologists Convention, Fort Worth, TX, March 1–5.
38. Swift, T.E., Goodrich, J., Kumar, R. and McCoy, R.L; "San Andres Reservoir Pressure Coring Project for Enhanced Oil Recovery Evaluation, Bennett Ranch Unit, Wasson Field, West Texas," paper SPE/DOE 9798 presented at the 1981 SPE/DOE Second Joint Symposium on Enhanced Oil Recovery, Tulsa, OK, 5-8 April.
39. Tanner, C.S., and Baxley, P.T.: "Production Performance of the Wasson Denver Unit CO<sub>2</sub> Flood," paper SPE 24156 presented at the 1992 Enhanced Oil Recovery Symposium, Tulsa, OK, 22-24 April.
40. Kittridge, M.G.: "Quantitative CO<sub>2</sub> Flood Monitoring, Denver Unit, Wasson (San Andres) Field," paper SPE 24644 presented at the 67<sup>th</sup> Annual Technical Conference and Exhibition, Washington, DC, October 4-7, 1992.

41. *ECLIPSE 300 Reference Manual*, 2004A-1 Release, Schlumberger Reservoir Technologies, Houston, TX 77056 (2004).
42. Merrill, R.C., Hartman, K.J. and Creek, J.L.: "A Comparison of Equation of State Tuning Methods," paper SPE 28589 presented at the 69<sup>th</sup> Annual Technical and Exhibition New Orleans, LA, 25-28 September.
43. Khan, S.A., Pope, G.A. and Sepehrnoori, K.: "Fluid Characterization of Three-Phase CO<sub>2</sub>/Oil Mixtures," paper SPE/DOE 24130 presented at the 8<sup>th</sup> Symposium Oil Recovery, Tulsa, OK, 22-24 April, 1992.
44. Peng, D.Y. and Robinson, D.B.: "A New Two-Constant Equation of State," *Ind. & Eng. Chem. Fund.* (1976) **15**, No. 1, 59-64.
45. Lohrenz, J., Bray, B.G. and Clark, C.R.: "Calculating Viscosities of Reservoir Fluids from Their Compositions," *J. Pet. Tech.* (Oct. 1964) **16**, 1171-1176.
46. Whitson, C.H.: "Characterizing Hydrocarbon Plus Fraction," *SPEJ*, **23**, (1983), 683-684.
47. Fevang, O., Singh, K. and Whitson, C.H.: "Guidelines for Choosing Compositional and Black-Oil Models for Volatile Oil and Gas Condensate Reservoirs," paper SPE 63087 presented at the 2000 SPE Annual Technical Conference and Exhibition, Dallas, TX, 1-4 October.
48. Bennion, D.B., Thomas, F.B., Jamaluddin, A.K.M., and Ma, T.: "The Effect of Trapped Critical Fluid Saturations on Reservoir Permeability and Conformance." Presented at the 1998 Annual Technical Meeting of the Petroleum Society of CIM, Calgary, Alberta, Canada, 8 -10 June



**VITA**

Name : Marylena Garcia Quijada  
Permanent Address : 5510 S Rice Avenue # 1614 Houston TX 77081  
Email : marylena@tamu.edu  
Education : B.S., Petroleum Engineering, Universidad de  
Oriente, Barcelona, Venezuela, (November 1998)  
M.S., Petroleum Engineering, Texas A&M  
University, College Station, TX 77843-3116,  
U.S.A. (August 2005)